CHAPTER 3

Analysis of Density, Signal Intensity, and Echogenicity

Christopher Paul Hess and Derk D. Purcell

RADIOGRAPHIC/CT DENSITY

Standard Against Which to Measure Density

Conventional radiography and computed tomography are based on the differential attenuation of photons by tissues as they pass from an x-ray source on one side of the body to a detector on the opposite side. Mathematically, the measurement at the detector is determined by the sum of the values of the *linear attenuation coefficient*, μ, of each individual tissue along the course of the x-ray beam. At each point within an object, μ characterizes the rate at which x-rays are removed by scatter or absorption and thus reflects the biophysical interaction between photons emitted by the x-ray source and the tissue irradiated. For the relatively high photon energies used in diagnostic medical imaging and low atomic numbers of most organic matter, the primary determinant of μ is Compton scatter, which results in a magnitude of photon attenuation that is nearly linearly proportional to tissue density (mass per unit volume).[1] There are several additional contributors to x-ray attenuation that depend both on the x-ray source and the object being imaged, but in practice the primary basis of contrast in both radiography and CT can be considered to be tissue density.[2,3]

Planar projections of linear attenuation, the source of the imaging data depicted on plain films, reliably resolve only five different biologic densities: *air, fat, water, soft tissue,* and *bone.* Before the advent of tomographic imaging modalities such as CT and MRI, neuroradiologists went to great lengths to manipulate contrast in plain film radiography to make diagnoses, for example by purposefully introducing air or iodinated media into the subarachnoid space or blood vessels and thereby identify masses in the skull vault, spinal disc herniations, and intracranial aneurysms. Although important diagnoses can still be made from radiographic density abnormalities (Fig. 3-1), conventional radiographs have only limited application in modern neuroimaging and are commonly used at present for the gross evaluation of integrity of medical devices such as cerebrospinal fluid (CSF) shunts or spinal fusion hardware or in the detection of fractures or malalignment of the skull or spinal column.

Linear attenuation is a useful physical concept for understanding image formation in radiography and CT but is not directly applicable to the visual interpretation of images. Before display and storage, each pixel in a reconstructed CT image is normalized to an integer value termed the *Hounsfield unit* (HU) or *CT number.* This normalized attenuation scale arbitrarily assigns water an attenuation value of zero, such that a difference of 10 HU reflects approximately a 1% difference in linear attenuation. The maximum and minimum values of the Hounsfield scale depend on the numerical storage scheme of the manufacturer, but the range in attenuation that can be discriminated by most modern scanners is 4096 HU (from roughly −1000 HU to 3000 HU). Small numbers correspond to relatively radiolucent structures such as air and fat, and large numbers correspond to radiodense structures such as bone and calcium. There is considerable overlap between CT numbers for different tissues, but certain tissue densities can usually be distinguished based on their typical Hounsfield numbers (Table 3-1).

The dynamic range of the human visual system, which can reliably discriminate fewer than 100 shades of gray, is far less than the range in tissue density represented by the Hounsfield scale. To facilitate visual analysis of images on a digital workstation, different display windows are applied to the raw CT numbers to optimally visualize the different tissues of interest. The effect of windowing is to linearly map a subsegment of the Hounsfield scale to 256 shades of gray, a standard range of gray values between black and white depicted on a computer monitor. The central Hounsfield unit of the window is designated the *window level.* The *window width* determines the overall contrast of the displayed image, translating the values of the standard Hounsfield scale within the window to various shades of gray that are more easily interpreted by the human eye. Typical window parameters used to evaluate different tissues of interest are given in Table 3-2.

The recognition of abnormal density on CT images relies foremost on familiarity with the range of normal densities of the anatomic structures of the central nervous system (CNS) and its supporting structures. Brain regions where neuronal cell bodies are located comprise the gray matter of the cortex and deep gray nuclei, including the basal ganglia and thalami. These structures normally have CT numbers of 20 to 40 HU, which is slightly greater than those of white matter (20-35 HU), where the neuronal axons and their supporting glia are concentrated. As a consequence, optimal examination of the brain parenchyma requires a narrow display window that allows accurate discrimination between the densities of these two types of tissues. Any interruption of the normally homogenous density within a

■ **FIGURE 3-1** Diagnosis based on abnormal radiographic density. **A,** Facial trauma. Frontal radiograph of the face (Waters view) demonstrates low-density orbital emphysema (*arrowheads*) surrounding the right optic nerve (*arrow*) and high-density hemorrhage opacifying the right maxillary sinus. **B,** Calcified sellar mass. Lateral skull radiograph demonstrates enlargement of the sella turcica with ill-defined density (*asterisk*), suggesting the presence of a calcified pituitary tumor or craniopharyngioma. **C,** Hardware failure. Frontal radiograph of the lumbar spine demonstrates discontinuity (*arrow*) of a fusion rod that extends across a vertebral body compression fracture. **D,** Foreign bodies. Radiodense foreign bodies are readily seen on plain films, as in this psychiatric patient who complained of dysphagia after swallowing a safety pin (*arrowhead*).

TABLE 3-1. Typical CT Numbers for Tissues of the CNS and Its Supporting Structures

Air	<–1000 HU
Adipose tissue	–20 to –100 HU
Water	–20-20 HU
White matter	20-35 HU
Gray matter	30-40 HU
Muscle	20-40 HU
Acute hemorrhage	50-100 HU
Calcification	>150 HU
Bone	800-1200 HU

HU, Hounsfield unit.

TABLE 3-2. Typical Window Parameters Used for Interpretation of CT Images

	Window Level	Window Width
Brain	40	80
Subdural	75	150
Bone	500	3500
CT angiography	120	700
Stroke	8	32
Soft tissue	0	225

Note that narrow CT windows, because they result in greater tissue contrast, are useful for displaying gray matter/white matter boundaries. Wider CT windows yield poor soft tissue contrast but allow more accurate delineation of bone/soft tissue interfaces and blood vessels. CT numbers that fall outside the window are displayed as black or white.

discrete white or gray matter structure implies a disruption in its normal physiology. The normal brain has sharp, well-defined boundaries between gray and white matter, and any regions where this distinction is lost should be viewed with suspicion.

CSF within the ventricular system and subarachnoid spaces of the brain and spinal cord normally has uniformly low attenuation that is nearly isodense to water. Inhomogeneity or altered attenuation in these regions is invariably abnormal. Similarly, the blood pool of the intracranial and extracranial vasculature is readily visualized within major arteries and veins and normally has homogeneous density that approximates the density of unclotted blood. Focal intravascular hyperdensity may be the only finding of acute stroke or dural venous thrombosis, and densely calcified vessels suggest atherosclerosis or an underlying disorder in calcium metabolism that could predispose to arterial insufficiency.

Alternate Nomenclature

Because the CT number of a structure may vary[4] among different patients and scanners (and even in the same patient on the same scanner), it is important to interpret density abnormalities relative to an internal standard of reference. This is accomplished according to the type of tissue. The common nomenclature for describing radiodensity used in practice is as follows:

- Lesions within the brain or spinal cord parenchyma proper are described as *hypoattenuating* (*hypodense*), *isoattenuat-*

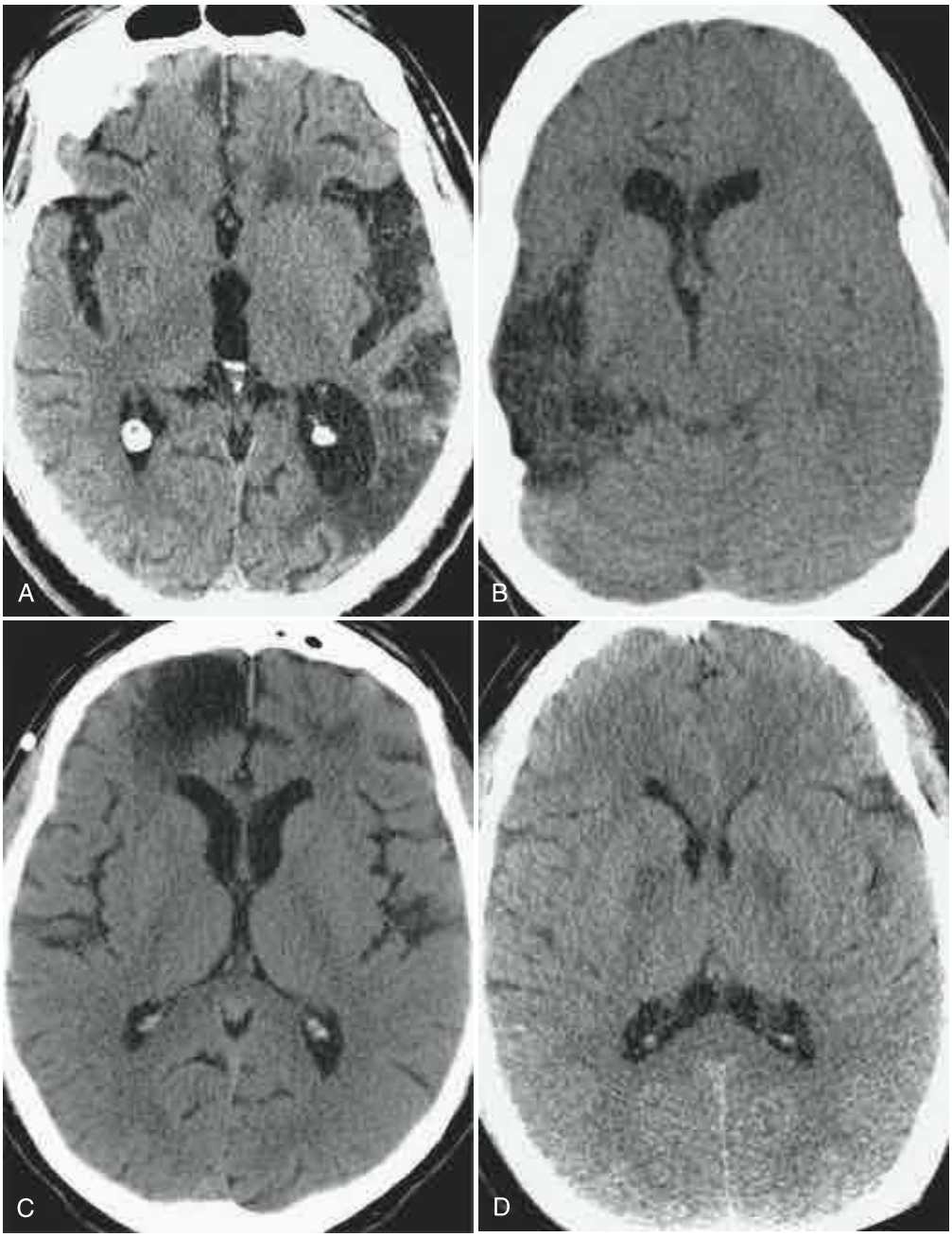

■ **FIGURE 3-2** CT appearance of encephalomalacia. Confluent areas of low density seen in association with focal loss of brain volume representing encephalomalacia and gliosis are nonspecific, but the location of the abnormality often points to an underlying cause. **A,** Remote stroke. Low density with volume loss, seen as ex-vacuo dilation of the left occipital horn, conforms to the territory of the posterior left middle cerebral artery. **B,** Encephalomalacia involving the cortical gray matter in multiple vascular territories can be caused by meningoencephalitis, as in this case of herpes encephalitis. Note ex-vacuo dilation of the frontal horn of the right lateral ventricle. **C,** Bifrontal encephalomalacia is most commonly caused by direct impact of the brain against the noncompliant calvaria years after the trauma. **D,** Chronic and symmetric low density within the deep gray nuclei is characteristic of toxic ingestion or metabolic abnormality, as seen within the globus pallidus of this patient who had previously attempted suicide by inhalation of carbon monoxide.

ing (*isodense*), or *hyperattenuating* (*hyperdense*) relative to normal adjacent structures.

- Soft tissue lesions outside the cranial vault or spinal column are best described in terms of their relative density with respect to muscle.
- Lesions within bone are described as *sclerotic* (*osteoblastic*) or *lucent* (*osteolytic*), depending on whether the density exceeds or is significantly less than that of normal cortical bone.
- Abnormalities that approximate the absolute density of water are characterized as *CSF density* or *water density.*
- Lesions with an attenuation consistent with fat are designated as *fat density.*
- A lesion is said to "enhance" when the difference in CT number between precontrast and postcontrast scans exceeds normal physiologic and technical variability between scans. For CT elsewhere in the body, this threshold has been taken as 10 HU.[5]

Causes of Decreased Density

Low density on CT is the manifestation of any of the acute or chronic pathologic endpoints of disorders that cause edema, necrosis, demyelination, or infarction. When it is chronic, low density usually implies an antecedent insult to the brain. After most serious injuries, there is a loss of tissue with time that results in involution of brain parenchyma, either by direct insult or autolysis of neurons. The process of encephalomalacia affects neurons in both gray and white matter and is characterized by a regional loss of brain volume that is primarily localized to the affected neuronal pathways. The ensuing reaction of the supporting white matter cells in this setting is gliosis, the formation of a dense fibrous network of scar tissue. On the cortical surface, encephalomalacia and gliosis are commonly the result of traumatic, infectious, or ischemic injuries and can be the source of recurrent seizures (Fig. 3-2). Within the structures of the deep gray matter, toxic and metabolic insults, intraparenchymal hemorrhage, infection, demyelinating disease, and lacunar ischemia

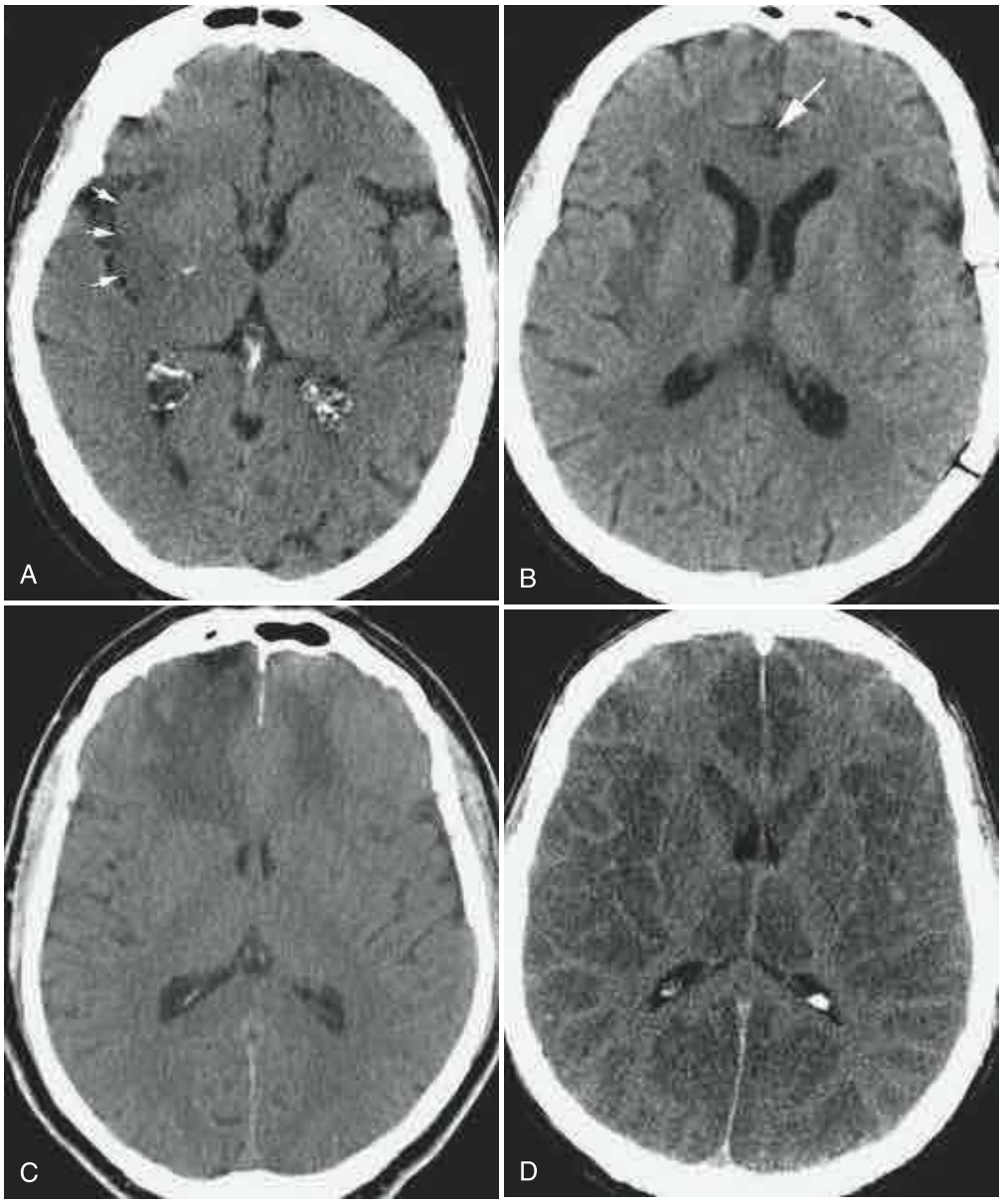

■ **FIGURE 3-3** Cortical low density. The CT finding of cortical low density results in a loss of the normally observed interfaces between gray matter and white matter. **A,** Acute stroke. In this patient with acute onset of left-sided hemiplegia, effacement of the normal subinsular gray matter/white matter interface (*arrows*) results in the "insular ribbon sign" of acute right middle cerebral artery infarction. **B,** Low density of the insular cortices and right cingulate gyrus (*arrow*) caused by herpes encephalitis, a neurologic emergency in this patient with altered mental status and fever. **C,** Bifrontal cortical low density extending into the lobar white matter without volume loss, typical of an acute traumatic injury. **D,** Anoxic encephalopathy. Diffuse cortical low density in this patient who was found unresponsive and hypotensive, giving the false impression of white matter hyperdensity.

are common causes of encephalomalacia. Confluent areas of hypodensity seen on CT thus reflect the end stage of any type of brain injury and can usually be ascribed to a specific insult only in the context of appropriate clinical history or location within the brain.

Diseases that cause net changes in brain water content also give rise to confluent areas of hypodensity. In contrast to encephalomalacia, which is chronic and irreversible, most alterations in tissue water content reflect an acute disturbance in cerebral hemodynamics. Classically, cerebral edema has been categorized as cytotoxic or vasogenic.[6] Cytotoxic edema occurs in both gray and white matter and is the effect of the irreversible intracellular swelling of neurons and glia that occurs with cellular energy depletion. In contradistinction, vasogenic edema predominates in the white matter and reflects the potentially reversible shifts in water within the extracellular space that are due to alterations in the normal blood-brain barrier. Both cytotoxic and vasogenic edema are seen as hypodensity and are not readily distinguished on CT in the early stages of a disease. The identification of edema should prompt a search for its potential primary causes as well as its effects, because edema may secondarily lead to herniation. Edema that involves the entirety of the brain usually reflects hypoxic, traumatic, toxic, or metabolic injury, whereas localized edema suggests either a focal ischemic insult, infection, or a mass lesion inciting changes in the surrounding brain.

Hypodensity localizing to the gray matter of the brain surface (Fig. 3-3) warrants primary consideration of traumatic, infectious, or vascular causes. For example, brain contusion results when rapid acceleration or deceleration causes the cortical surface to come into direct contact with the rigid skull vault or dural reflections. Sources of cerebral infection, such as viral encephalitis and bacterial meningitis, also commonly involve cortical gray matter, usually as the result of direct spread of infection from the subarachnoid spaces. An important infectious cause of gray matter hypodensity that should be considered in the appropriate clinical context is herpes encephalitis. Subtle cortical low attenuation, particularly within the medial temporal lobes and cingulate cortex, can herald this disease and should prompt early treatment with intravenous antiviral chemother-

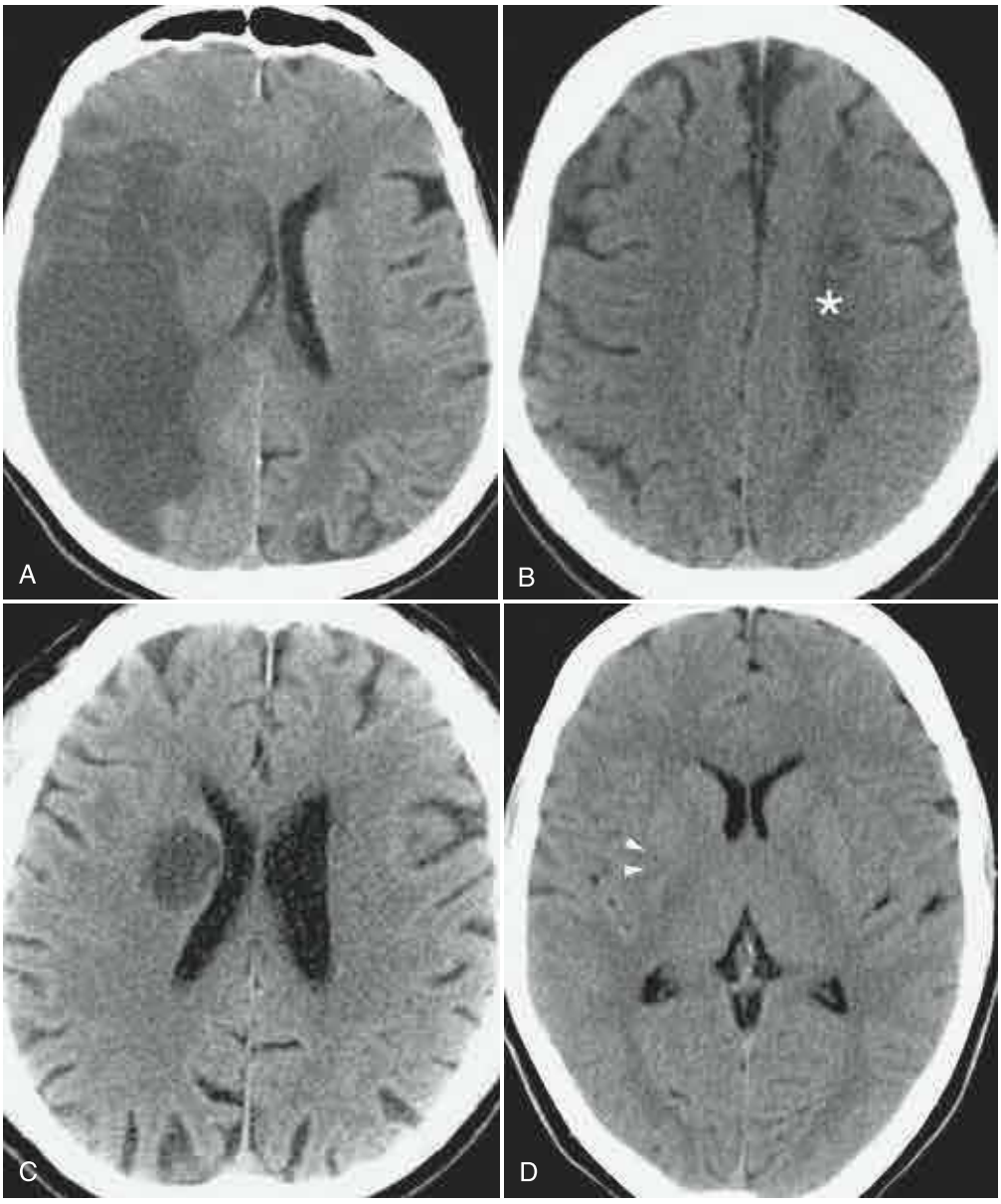

■ **FIGURE 3-4** The manifold appearances of ischemic injury on CT. **A,** Subacute stroke. Cortical and white matter low density in the distribution of the right middle cerebral artery, characteristic of subacute large vessel infarct. Note the accompanying mass effect, as evidenced by effacement of right hemispheric sulci, compression of the right lateral ventricle, and slight shift of the midline toward the left. **B,** Low density area (*asterisk*) conforming to the border zone between the left middle cerebral artery and anterior cerebral artery distributions, typical of watershed infarction. **C,** Low density and enlargement of the globus pallidus and putamen in this patient with altered mental status due to acute lenticulostriate infarct. It is important that this not be mistaken for a tumor, which could lead to unnecessary morbidity or mortality if surgical resection is attempted. **D,** Occlusion of the middle cerebral artery (*arrowheads*), because it also involves the lateral lenticulostriate arteries, may result in the loss of the normal comma-shaped morphology of the posterior putamen. This "comma sign" is a useful early sign of ischemia on noncontrast CT images.

apy. The regions of cortical gray matter hypodensity seen with both traumatic injury and infection are due to acute cellular and interstitial edema and are not infrequently accompanied by hemorrhage and interruption of the blood-brain barrier, the latter manifest by abnormal enhancement on administration of a contrast agent.

Acute interruption of the normal large- or small-vessel arterial supply to the brain and consequent ischemia may also yield hypodensity that involves both gray and white matter. The observation that hypodensity conforms to a vascular territory is central to this diagnosis (Fig. 3-4). In early ischemic injury, the attenuation of acutely ischemic brain parenchyma is inversely proportional to its water content. Specifically, a 1% total increase in tissue water content decreases its CT number by approximately 2.5 HU.[7] Interruption in blood flow causes the highly vascular gray matter to lose the ability to control neuronal permeability. As a result, neurons accumulate water and take on an intrinsic density that approximates that of white matter. This process results in the loss of the normal distinct boundaries between the involved gray matter and subjacent subcortical white matter, as well as local gyral swelling. A similar loss of density within ischemic deep gray matter nuclei also may be recognized only as a change in the normal shape of the nucleus. Infrequently, it is possible to detect acute small-vessel ischemia as a subtle focus of relative low density within white matter. To optimally discern the subtle changes in density that are due to acute ischemia, the level and width of the display window should be selected carefully.[8] With continued vessel occlusion, both gray and white matter hypodensity and swelling progressively increase and become more pronounced. With time, the infarcted brain tissue loses volume, ultimately resulting in encephalomalacia and glial scar within the involved vascular territory on follow-up imaging.

A number of acute and chronic disorders may produce large areas of hypodensity that are localized within the subcortical gray and white matter (Fig. 3-5). Hypodensity in these diseases selectively affects vulnerable brain tissues. For example, cardiopulmonary arrest, drug overdose, and other causes of acute global hypoxic injury preferentially injure tissues that have high metabolic demand. Early findings in this setting can be subtle on CT immediately after the insult, seen only as uniform low attenuation in white matter or effacement of normal gray-white

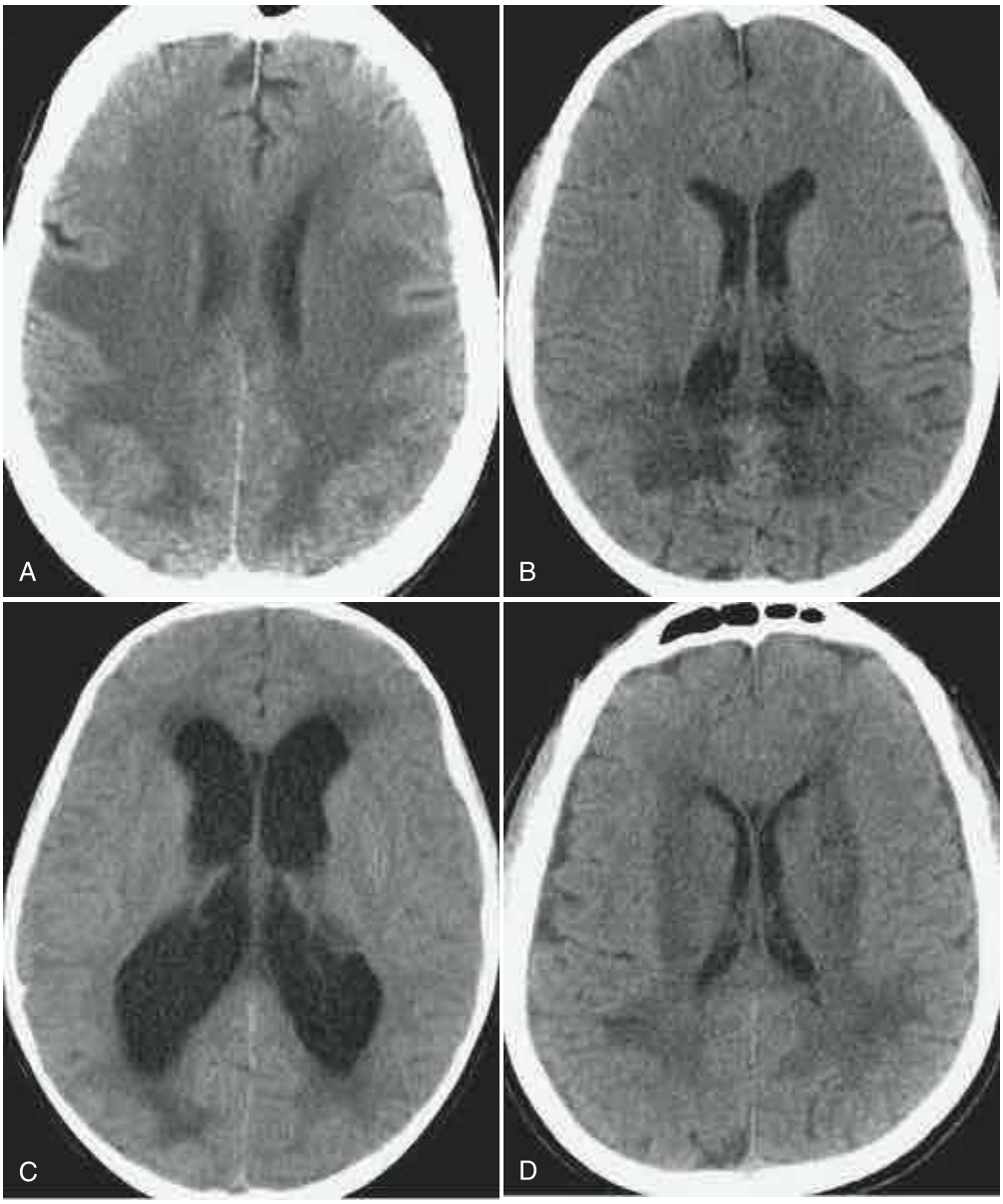

■ **FIGURE 3-5** White matter hypodensity. The relatively common CT finding of white matter hypodensity has a broad differential diagnosis but should be distinguished from hypodensity that involves both gray and white matter. **A,** Global hypoxic-ischemic injury. Uniform low density within the white matter of the supratentorial brain, with involvement of the deep gray nuclei, in a patient after an episode of hemorrhagic shock due to gastrointestinal bleeding. **B,** X-linked adrenoleukodystrophy. In this child there is a classic distribution of low density within the white matter of the occipital lobes and splenium of the corpus callosum. **C,** Transependymal edema. Low density "capping" the ventricular margins, combined with ventriculomegaly, is characteristic of the interstitial white matter edema that results when CSF outflow is obstructed. **D,** Microvascular leukariosis. Low density in the subcortical and periventricular white matter is a common finding in the aging brain and is thought to be due to the chronic ischemic effects of small vessels "pruned" by small vessel vasculopathies such as hypertension or diabetes.

interfaces. Confluent periventricular low density is a common finding in the aging population, where small- and medium-sized vessels supplying the deep white matter of the brain are subject to chronic occlusive disease. In acute hydrocephalus, low density CSF may accumulate within the white matter surrounding the distended ventricles, a phenomenon referred to as *transependymal edema*. Metabolic leukodystrophies represent a broad class of dysmyelinating disorders that characteristically lead to varying distributions of low density within the subcortical white matter and often gray matter.

Benign and malignant tumors are a relatively common cause of altered density within both gray and white matter. Depending on the cell of origin, these may exhibit low or high density relative to normal brain anatomy. Most commonly, intra-axial tumors are seen as low attenuating lesions within white matter or as isoattenuating lesions within a larger region of surrounding vasogenic edema. As discussed later, low density within a tumor suggests necrosis, as may be seen with highly aggressive tumors such as glioblastoma multiforme or after treatment with chemotherapy or radiation. Sometimes mistaken for tumors, gray matter heterotopias may be seen as discrete areas within white matter or along the ventricular margins that are isoattenuating to normal gray matter structures. The rare entity of gliomatosis cerebri should be considered when there are large areas of confluent hypodensity within white matter and clinical history points to an insidious course of cognitive deterioration or pyramidal tract signs. Finally, fat density within a CNS tumor is characteristic of few entities, including lipoma, dermoid, and lipomatous degeneration within certain tumors such as teratomas and rarely meningiomas.

Inflammatory demyelinating diseases such as multiple sclerosis and acute disseminated encephalomyelitis and intracranial infections represent another broad class of disease that should not be overlooked as a potentially reversible causes for low attenuation (Fig. 3-6). Small areas of circumscribed low density in white matter, especially around the margins of the lateral ventricles, may suggest the diagnosis of multiple sclerosis or other autoimmune demyelinating disease given the appropriate clinical history. A cerebral abscess is a cavity that contains pus, necrotic debris, and immune cells due to bacterial, fungal, or

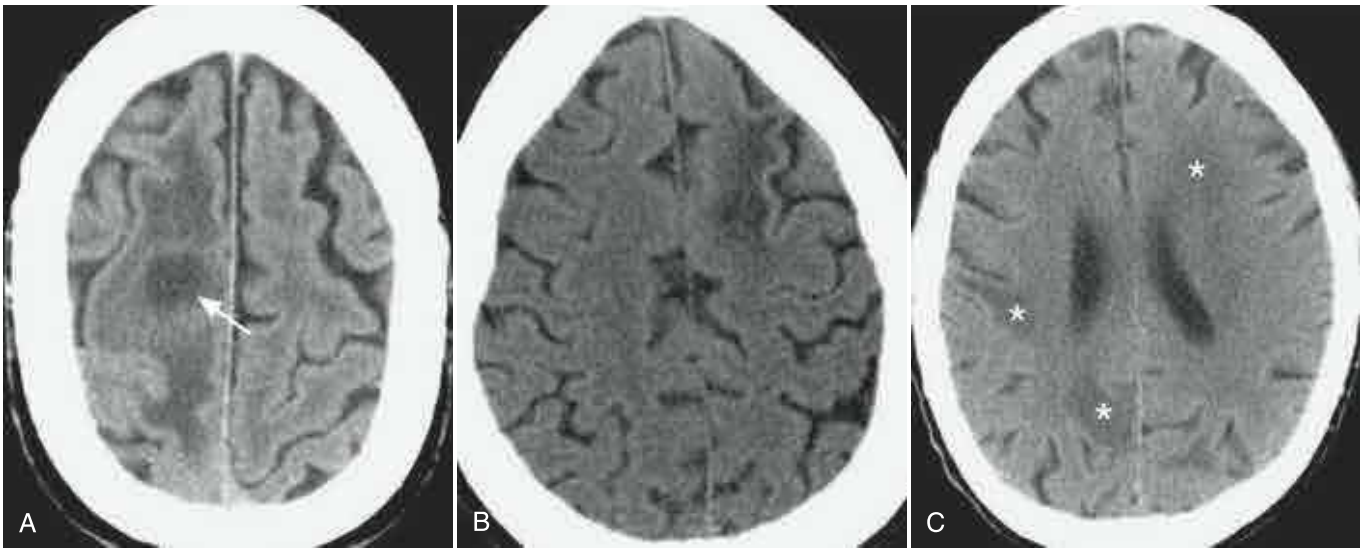

■ **FIGURE 3-6** Low density due to cerebral inflammatory disease. **A,** Typical appearance of a cerebral abscess: round, low-density cavity (*arrow*) surrounded by low-density vasogenic edema. Differentiation from other cavitary lesions such as radionecrotic cysts or cystic neoplasms often requires clinical/laboratory correlation, with help often provided by contrast-enhanced and diffusion weighted MRI. **B,** Progressive multifocal leukoencephalopathy. Whereas white matter low density is nonspecific, involvement of the subcortical U-shaped fibers in the AIDS patient can help differentiate this disorder from HIV encephalitis. **C,** Toxoplasmosis. Patchy white matter low density (*asterisks*) in an immunocompromised patient with altered mental status.

■ **FIGURE 3-7** Tumors of high cellularity. Tumors with densely packed cells and/or high nuclear-to-cytoplasmic ratios can demonstrate intrinsic hyperdensity at CT, even in the absence of calcification or hemorrhage. **A,** CNS lymphoma. Unenhanced CT demonstrating a circumscribed, hyperdense mass in the right hemispheric white matter (*arrowheads*) with surrounding low-density vasogenic edema. **B,** Medulloblastoma. Unenhanced CT demonstrating a lobulated, hyperdense mass in the posterior fossa.

parasitic infection that appears as a focal area of suppurative necrosis within the brain, usually with surrounding low density vasogenic edema. Progressive multifocal leukoencephalopathy, human immunodeficiency virus (HIV) encephalopathy, and infections such as those caused by *Toxoplasma*, cytomegalovirus, and *Cryptococcus* merit special consideration as causes for low density in the immunocompromised population.

Causes of Increased Density

High density on CT has a more limited differential diagnosis than low density. Specifically, high attenuation is characteristic of mineralization, blood products, iodinated contrast media, and certain neoplasms. Calcification is a feature of several primary brain tumors, including oligodendroglioma, ependymoma, and astrocytoma, as well as metastatic tumors such as renal cell carcinoma, neuroblastoma, and mucinous tumors of the gastrointestinal tract. Extra-axial tumors such as meningioma may also calcify. Calcification may be the result of prior infection, such as neurocysticercosis or tuberculosis, or may be the residua of prior hemorrhage. Tumors of high cellularity referred to as "small round blue-cell neoplasms" including lymphoma, medulloblastoma, and primitive neuroectodermal tumors may have high density relative to normal brain parenchyma (Fig. 3-7).

Hemorrhage is a common cause of high density in the brain and extra-axial spaces in the acutely ill patient. Acute blood products have characteristic CT numbers ranging from 50 to 100 HU and often exert mass effect on adjacent structures. Within the brain parenchyma proper, high density due to acute hemorrhage may be the result of trauma, hypertension, hemorrhagic primary or metastatic brain tumor, vascular malformations

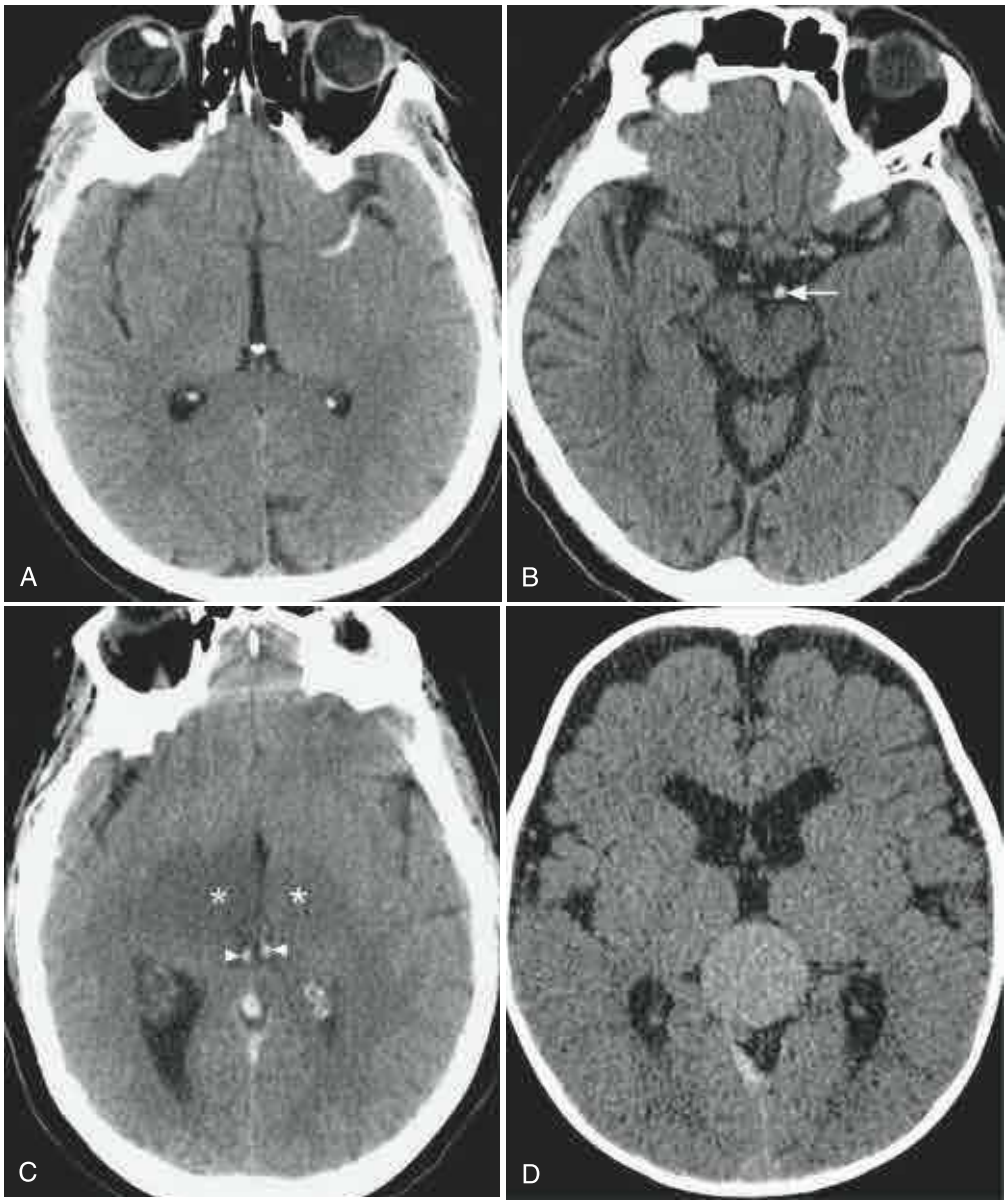

■ **FIGURE 3-8** CT appearance of intravascular hyperdensity. **A,** MCA thrombosis. The "dense MCA sign" is a specific but insensitive finding in acute stroke. **B,** Basilar artery thrombosis. Hyperdense basilar artery (*arrow*); compare with patent branches of the MCA. **C,** Venous thrombosis. Thrombus within the internal cerebral veins (*arrowheads*), resulting in bilateral thalamic ischemia (*asterisks*). **D,** Vascular malformations. Relative hyperdensity in this patent vein of Galen malformation.

including arteriovenous and cavernous malformations, dural sinus thrombosis with venous ischemia, hemorrhagic infection such as from angioinvasive *Aspergillus*, coagulopathy, or amyloidosis. Intravenous administration of a contrast agent may allow discrimination between these causes by the observation of a primary enhancing tumor or vascular malformation or by detection of dural venous sinus occlusion.

High density confined to the lumen of an artery or vein has critical significance in that it suggests the presence of acute thrombosis. Clinical findings of acute hemiplegia, aphasia, visual field changes, or other symptoms of stroke should prompt a careful search for a hyperdense artery. Whereas this is a relatively infrequent finding seen in only approximately 22% of patients presenting with acute middle cerebral artery (MCA) stroke, it portends a poor long-term prognosis and may prompt early thrombolytic treatment.[9] The cause of high attenuation within acute thrombus has been posited to arise from accumulation of erythrocytes, fibrin, and cellular debris.[10] While originally described within the proximal or distal MCA, hyperdense thrombus can also be visualized within the anterior and posterior cerebral and vertebrobasilar systems (Fig. 3-8). In the absence of a leading clinical history, arterial hyperdensity may alternatively suggest atherosclerotic calcification or hemoconcentration due to dehydration or polycythemia. Within the intracranial venous system, hyperdensity may be the only finding in patients with dural venous sinus or internal cerebral venous thrombosis. In patients with headache and venous hyperdensity, contrast-enhanced CT or MRI should be obtained urgently to guide prompt treatment with anticoagulation, because venous thrombosis remains a frequently missed diagnosis that often has disastrous consequences when missed.

The normal CSF spaces of the brain have an attenuation that is nearly that of water (Fig. 3-9). When high density is detected, it is usually caused by subarachnoid hemorrhage. However, meningitis, leptomeningeal tumor, and intrathecal contrast agents are alternative causes for hyperdensity that should be considered in the appropriate clinical setting. Intravenous administration of a contrast agent may help in differentiating among these causes, both for CT angiography in the search for a ruptured intracranial aneurysm and for the observation of enhancement. When hyper-

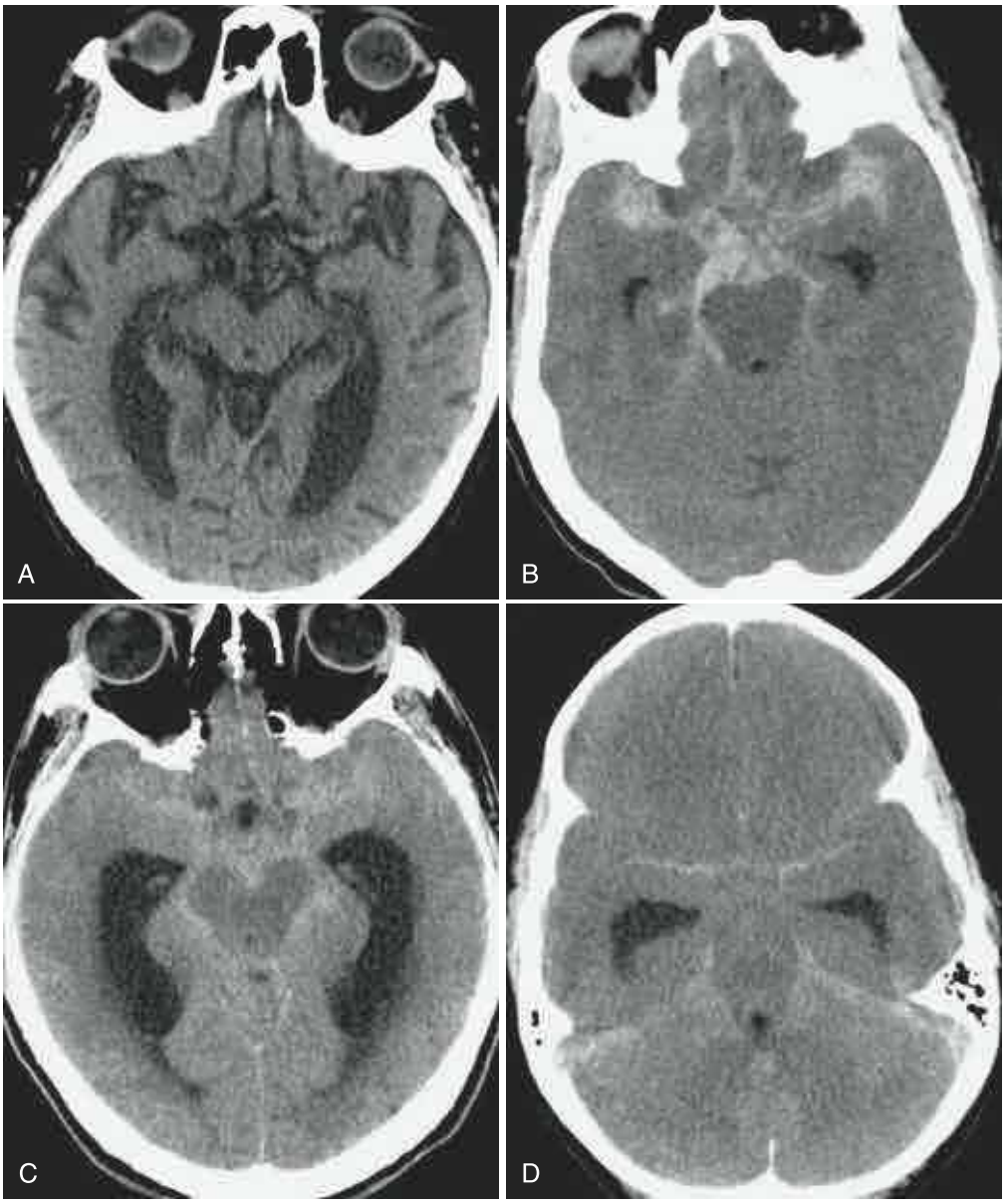

■ **FIGURE 3-9** Hyperdensity within the CSF spaces. The normal low density of normal CSF can be altered by any disease process that increases the protein/cell count. **A,** Normal basilar cisterns. Normal CSF has density that approximates that of water (0 HU). **B,** Subarachnoid hemorrhage. The location of hemorrhage may suggest the site of an aneurysm, although when diffuse the location may not be readily ascertained, as in this case of a ruptured posterior communicating artery aneurysm. **C,** Coccidiomycosis meningitis. High density CSF due to pus in the subarachnoid space is indistinguishable from acute subarachnoid hemorrhage, such that patient presentation and CSF analysis are required to differentiate these disorders. **D,** "Pseudo–subarachnoid hemorrhage." Diffuse cerebral edema displaces the normal hypodense CSF spaces and causes engorgement of pial vasculature that mimics the appearance of hemorrhage.

dense material in the subarachnoid space enhances, primary consideration should be given to bacterial, fungal, or mycobacterial meningitis or to leptomeningeal carcinomatosis. Intrathecal contrast media may be intentionally administered for myelography or for detection of CSF leak or may be present due to renal failure or compromise of the blood-brain barrier due to tumor or infection. The myelographic contrast agent Pantopaque may persist in the CSF many years after an examination.

Analysis of Mixed Patterns of Density

The pattern of mixed density within a lesion or in the structures adjacent to a lesion often provides additional clues as to the cause of a lesion. Low attenuation surrounding a solid lesion with a different dominant density suggests vasogenic edema and is most typical of primary glial tumors and metastases (Fig. 3-10). Variable density may also be due to necrosis, hemorrhage, edema, gliosis, and/or calcification within or incited by a lesion. Necrosis within a tumor is suggested by the presence of areas of low density within a solid lesion, resulting from tumor-induced hypoxia or apoptosis. It is a feature most characteristic of rapidly growing malignancies such as glioblastoma multiforme or metastasis but can also be seen in many other tumors after irradiation or chemotherapy and in the setting of cerebral abscesses and tumefactive demyelinating lesions. Radiation necrosis may be especially difficult to differentiate from recurrent tumor after treatment, because both may demonstrate peripheral enhancement. Calcification may be seen in association with tumors, vascular malformations, and as a sequela of certain infections such as neurocysticercosis. Solid extra-axial tumors, the most common being meningioma, typically have intrinsic high density relative to the brain but also often exhibit some degree of calcification.

Hemorrhage within an intraparenchymal mass is commonly caused by tumors or vascular lesions. Bleeding is more common within metastases than primary brain tumors and may be marginal, diffuse, or heterogeneously scattered throughout different components of a tumor. Extensive tumor vascularity, vascular invasion, and rapid growth with resulting necrosis have all been cited as mechanisms for tumoral bleeding in both primary glioblastoma and metastases.[11] The presence of hemorrhage may

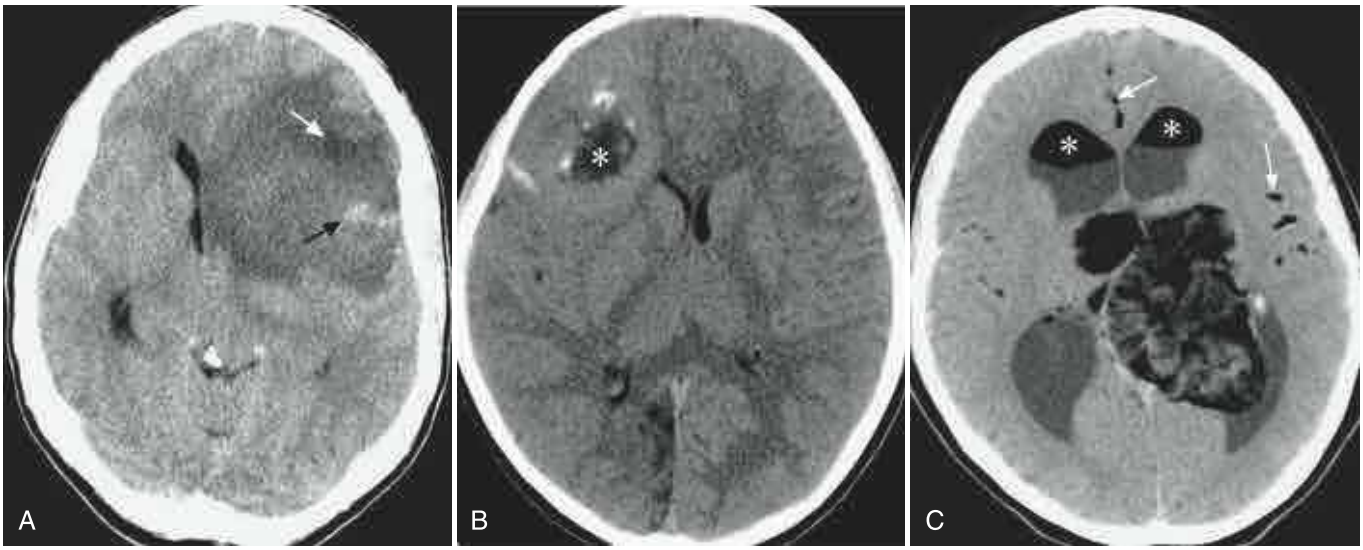

■ **FIGURE 3-10** Variable density due to necrosis, hemorrhage, edema, gliosis, and/or calcification within or incited by a lesion. **A,** Glioblastoma multiforme. Large, heterogeneous mass with peritumoral vasogenic edema. High-density hemorrhage (*black arrow*) and low-density necrosis (*white arrow*) are signature features of this high-grade neoplasm. **B,** Anaplastic ependymoma. Coarse, hyperdense calcium along the periphery of region of central necrosis (*asterisk*). **C,** Ruptured dermoid cyst. Markedly heterogeneous tumor demonstrating densities ranging from fat to calcium. Note fat-fluid levels within the frontal horns (*asterisks*) and fat density within the sylvian and interhemispheric fissures (*arrows*).

suggest the primary origin of metastases, because melanoma, renal cell carcinoma, choriocarcinoma, and bronchogenic carcinoma have a greater propensity for hemorrhage than other metastases. Bleeding may also arise in vascular lesions such as arteriovenous malformations or cavernous angiomas, where adjacent calcifications (seen as focal high density), prominent vessels (seen as isodense to the normal blood pool), or gliosis from ischemic steal (seen as adjacent geographic hypodensity) can suggest the presence of an underlying vascular lesion (Fig. 3-11).

Several extra-axial lesions have characteristic mixed density appearances on CT. Heterogeneity in attenuation within a subdural hematoma may indicate acute or chronic hemorrhage or coagulopathy (Fig. 3-12). Hyperacute hemorrhage is suggested when areas of low density representing uncoagulated blood admix with high-density clotted blood, causing a "swirl sign." When present, fluid levels on CT indicate the presence of fluids of differing densities and can signal the presence of an underlying coagulopathy in patients with acute extra-axial hematomas. Sterile subdural collections should be distinguished from subdural empyema, a subdural collection of pus arising as a complication from meningitis, sinusitis, otitis media, or other infection. Heterogeneity within an extra-axial collection with other findings of infection should prompt primary consideration of subdural empyema.

MRI SIGNAL INTENSITY

Standard Against Which to Measure Signal Intensity

In contrast to the Hounsfield unit scale for CT there is no standard normalization of MR signal intensity that is in common use, and thus there is no absolute reference scale with which to quantify lesion intensity. Intensity is interpreted only through direct visual comparison with surrounding tissues. Such a comparison requires the application of a display window with suitable window width and level, set manually to visually facilitate interpretation rather than on absolute parameters as on CT. Similar to CT, however, the relative T1, T2, and T2* signal intensity of lesions is best described in reference to normal gray or white matter in the brain, CSF in the extra-axial spaces or surrounding the spinal cord, or fat, muscle, or marrow outside the skull or spinal column.

Alternate Nomenclature

The following terms are used to describe MR signal intensity:

- Lesions that are brighter than the tissue of reference are referred to as *T1 hyperintense* or *T2 hyperintense,* depending on the dominant contrast weighting of the image. Because shorter T1 and longer T2 values yield higher signal intensities on T1- (T1W) and T2-weighted (T2W) images, hyperintensity can also be referred to as *T1 shortening* and *T2 prolongation,* respectively.
- Lesions that are less bright than the tissue of reference are designated *T1 hypointense* or *T2 hypointense,* or alternatively as causing relative *T1 prolongation* or *T2 shortening,* respectively.
- Lesions not discerned separately from surrounding structures are termed *T1 isointense* or *T2 isointense*, depending on the image weighting.
- Lesions that characteristically follow the signal intensity of gray matter, white matter, or CSF on all pulse sequences are described as being *isointense to* one of these tissues.

T1 versus T2 versus T2*

MR signal intensity is a complicated function of proton density (PD), T1 relaxation, T2 relaxation, magnetic susceptibility, and scan parameters, including flip angle, echo time (TE), and repetition time (TR). Proton density contributes to the signal intensity with all pulse sequences. Unless explicit water or fat saturating pulses are applied, the highest signal intensities in any MR image arise from proton-rich voxels containing water and/or fat. Air and cortical bone produce the low signal intensities in an image. Images obtained with long TR/short TE sequences are weighted predominantly by PD. However, because the concentration of protons is nearly homogeneous across different soft tissues, PD by itself does not usually provide appreciable tissue contrast. Two notable exceptions are in distinguishing between solid and cystic masses with high T2 signal intensity, where fluid tends to

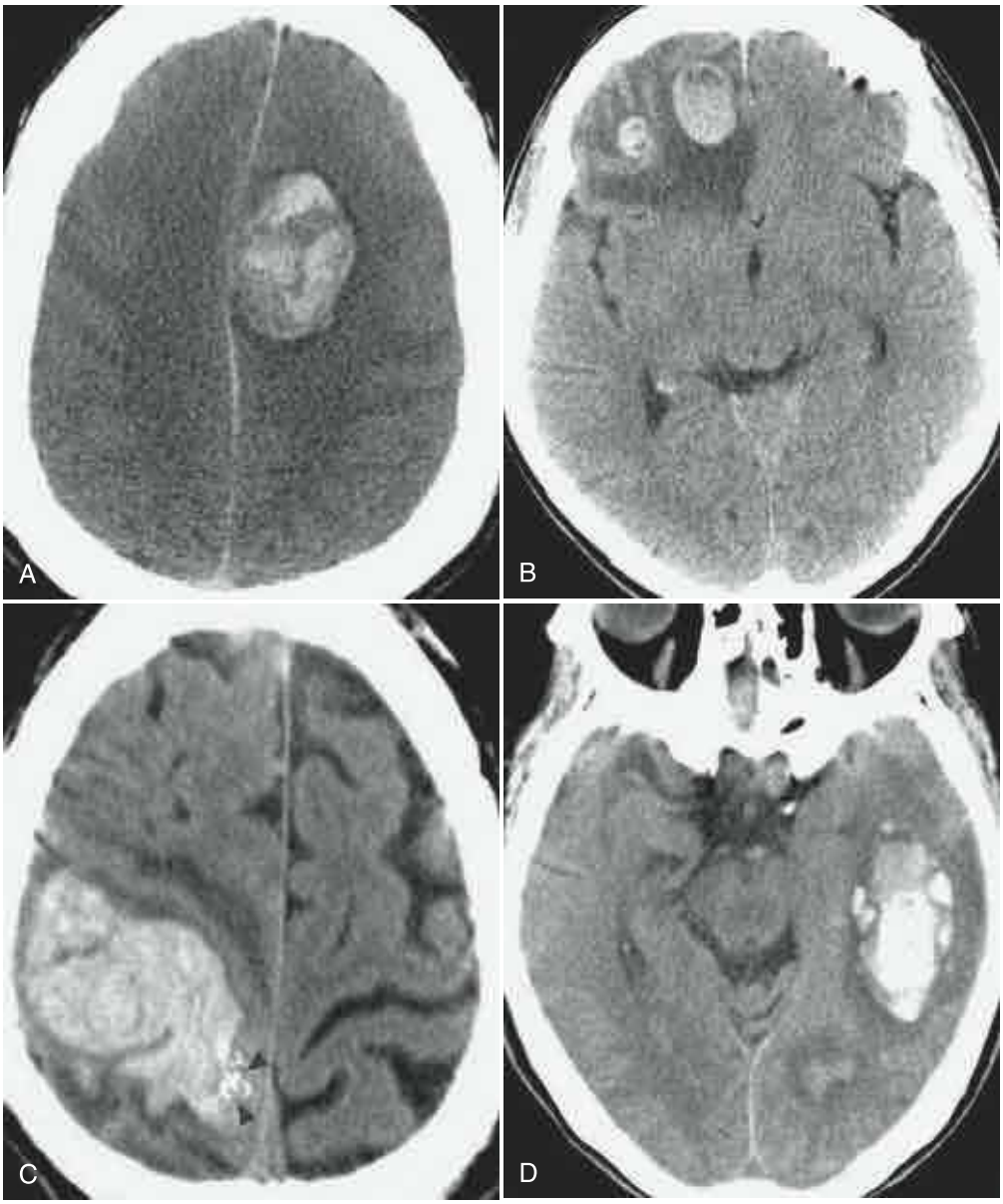

■ **FIGURE 3-11** Hemorrhage within an intraparenchymal mass is most commonly caused by tumors or vascular lesions. **A,** Hemorrhagic glioblastoma multiforme. Extensive hemorrhage and edema within this high-grade neoplasm causes mixed areas of high and low density. **B,** Hemorrhagic metastasis. Unenhanced CT demonstrates multiple intrinsically dense lesions in this patient with metastatic melanoma. **C,** Ruptured arteriovenous malformation. Minimal hyperdense calcium (*arrowheads*) along the medial aspect of this large intraparenchymal hemorrhage suggests an underlying vascular malformation. **D,** Hemorrhagic infarction. The presence of both cortical low density fitting a vascular territory and superimposed parenchymal hemorrhage leads to the diagnosis of middle cerebral artery infarct with hemorrhagic transformation.

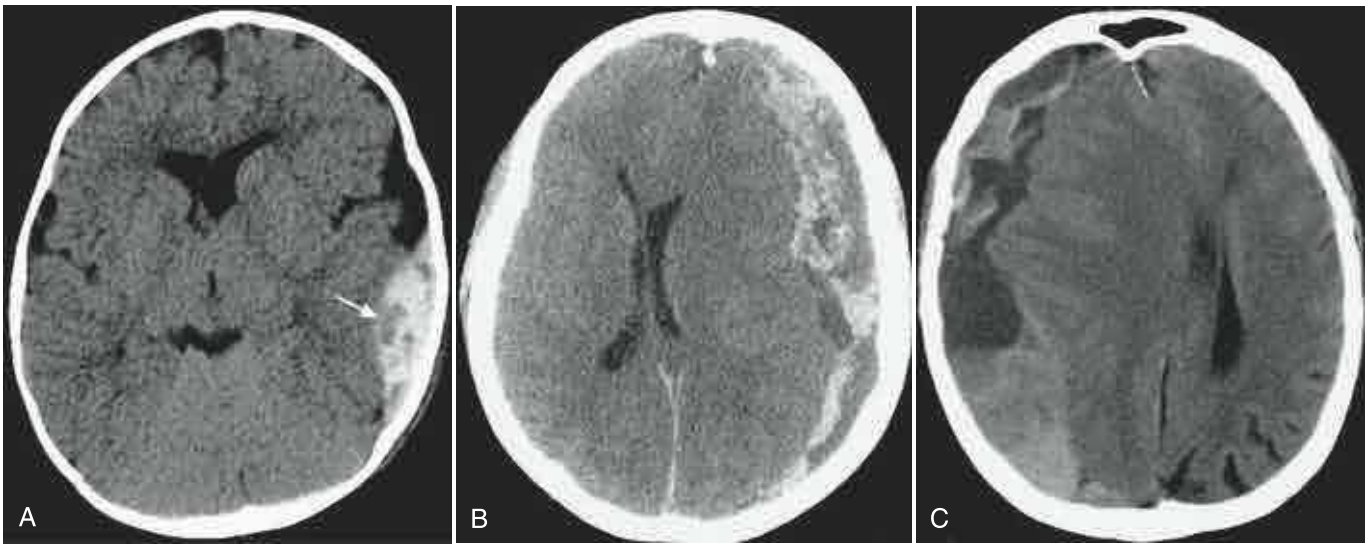

■ **FIGURE 3-12** Mixed attenuation within extra-axial collections. **A,** Acute epidural hematoma. The finding of a "swirl sign" within a lentiform-shaped extra-axial collection should suggest active hemorrhage (*arrow*). **B,** Acute subdural hematoma in a patient with thrombocytopenia. Large hematomas with areas of hypodense unclotted blood may point to an underlying coagulopathy, as in this patient with thrombocytopenia. **C,** Acute on chronic subdural hematoma. Hyperdense blood indicates the presence of acute blood that when superimposed on mixed density suggests hemorrhage of varying ages, especially when there is layering over adhesions from previously clotted blood.

TABLE 3-3. T1 and T2 Values* of Tissues at 1.5 T and 3.0 T

	1.5 T		3.0 T	
Tissue	**T1**	**T2**	**T1**	**T2**
Gray matter	1074-1174	87-103	1706-1934	92-106
White matter	834-934	68-76	1039-1129	66-72
Cerebrospinal fluid	2200-2400	500-1400	2360-2830	480-1200
Fat	240-250	60-80	360-400	64-72
Blood†	1321-1561	260-320	1847-2017	225-325
Muscle	988-1028	38-50	1399-1425	46-54

*Values given in milliseconds.
†Note that the T2 relaxation of whole blood varies according to relative oxygen concentration.

have low intensity on PD-weighted (PDW) images and solid lesions typically have high intensity, and the identification of chemical shift artifact, which signals the presence of fat. Differences in the values of T1 and T2 otherwise provide the dominant mechanism for soft tissue contrast, so that T1W and T2W images play a greater diagnostic role in MRI.

T1 (or spin-lattice) relaxation is the process by which protons return to their normal equilibrium magnetization in a static magnetic field after excitation by a radiofrequency pulse. In their return to the equilibrium state, protons exchange excess energy with the magnetic "lattice" of neighboring molecules. The value of T1 is a measure of the time that is required for spins to return to 63% of their baseline magnetization and is primarily determined by the size of the molecule to which spins are bound. Whereas macromolecules like proteins are subject to greater inertial forces in a magnetic field and thus have short T1 times, small molecules such as unbound water equilibrate rapidly and have long T1 times. On T1W images, tissues with large T1 have *low* signal intensity and tissues with short T1 have *high* signal intensity.

In contradistinction to T1, T2 (spin-spin) relaxation reflects the loss of magnetization that occurs as neighboring excited protons exchange energy not with the lattice but rather with one another. Protons excited by a radiofrequency pulse generate small magnetic fields that interfere with the normally homogeneous magnetic field on the molecular level. The microscopic inhomogeneities in magnetic field induced by differences in neighboring nuclei cause spins that were initially precessing in synchrony to lose coherence. The resulting loss of magnetization is quantified by the value of T2, which determines the length of time in which 37% of the magnetization is lost through this exchange of energy. On T2W images, tissues with large values of T2 have *high* signal intensities and tissues with short values of T2 have *low* signal intensity.

Nominal values for the T1 and T2 relaxation times of different tissues at 1.5 T and at 3.0 T are given in Table 3-3. Because the strength of the magnetic field of the lattice increases with the applied static magnetic field, T1 relaxation times increase gradually with magnetic field strength.[12,13] Normally, T2 values are much smaller than T1 values (and T2* values are much smaller than T2 values). Values of T2 are less dependent on field strength and range from 40 to 120 ms for most tissues, except in fluids with significant numbers of unbound protons such as CSF and blood where T2 values are normally up to 2700 ms.

Quantitative measurement of T1 and T2 can be done using specialized pulse sequences, but the longer imaging times required render these measurements of little value in practice. Instead, the different T1 and T2 characteristics of tissues are inferred by imposing deliberate T1- or T2-weighting on the acquired images. By choosing shorter values for the TR and TE of a spin-echo sequence or through the use of an inversion recovery technique, images with predominantly T1 weighting can be obtained. Long-TR/long-TE spin-echo sequences result in predominantly T2 weighting. Thus, through the judicious choice of scan parameters, the values in Table 3-3 impose characteristic signal intensities in images of the brain. CSF appears dark on T1W images but is very bright on T2W images. Because it has a longer T1 relaxation time in the adult brain, gray matter is normally hypointense relative to white matter on T1W images. In contrast, gray matter typically has greater signal intensity than white matter on T2W images in the adult brain. The signal intensities of gray and white matter depend on the stage of myelination in the developing brain, such that the normal gray matter/white matter relationship is reversed in the newborn. As with CT, inspection of both T1W and T2W images of the brain and spinal cord should show well-defined boundaries between gray and white matter. The identification of abnormalities requires the detection not only of focal variations in signal intensity but also of any effacement of the normal gray matter/white matter interfaces.

In general, T1 and T2 are heavily influenced by the viscosity of tissue. Tissues closer to fluid phase than solid phase have higher values of T1 and T2 and thus lower signal intensity on T1W images and higher signal intensity on T2W images. However, there are several circumstances when lesions on T2W images are solid, and it is not uncommon for lesions with low T2 signal intensity to represent fluid. When protons are bound to large molecules such as lipids or proteins they have short T2 times, and when protons in water molecules are unattached, as in the CSF spaces, they have long T2 times. As noted earlier, PDW images may suggest that a structure is solid or contains fluid, because the former has high signal intensity and the latter usually has lower signal intensity. The intravenous administration of a gadolinium chelate can more reliably make the distinction between solid and liquid phase. Solid tissues that are not composed primarily of bone or calcium usually enhance when the blood-brain barrier is disrupted. Liquids or devitalized tissue such as phlegmon should not enhance except at their margins, where they may be confined by viable vascularized tissue.

As excited protons return to their equilibrium magnetization, they are also subject to a loss of coherence that results from spin dephasing by local inhomogeneities in the main magnetic field. This effect, called magnetic susceptibility, is important when long values of TE are used and provides a third mechanism for image contrast. So-called T2* contrast is superimposed on the underlying T1 or T2 contrast mechanism of the sequence and can be used to detect disruptions in the normally homogeneous main magnetic field by metal, air, blood products, or mineralization. Alterations in magnetic susceptibility are visualized as either focal signal voids within normally homogeneous parenchymal architecture or as geometric distortion of the image. Gradient-echo sequences are especially sensitive to T2* effects, particularly when longer values of TE are used. T2* weighting should be included in any examination in which the detection of small areas of calcification or hemorrhage is necessary.

Causes of Decreased Signal Intensity on T1W, T2W, and T2*W Images

The initial step in the analysis of low MRI signal intensity is to determine the predominant mechanism for tissue contrast through examination of the pulse sequence parameters or relative tissue intensities. Low signal intensity implies that an object has longer T1, shorter T2, or shorter T2* relaxation times than surrounding tissues, depending on the predominant contrast mechanism used to weight the image.

Low T1 signal intensity is by itself nonspecific, because the large majority of pathologic lesions in the brain and spinal cord have long T1 relaxation times. The analysis of T1 hypointensity can be undertaken in a similar fashion to that of CT hypodensity

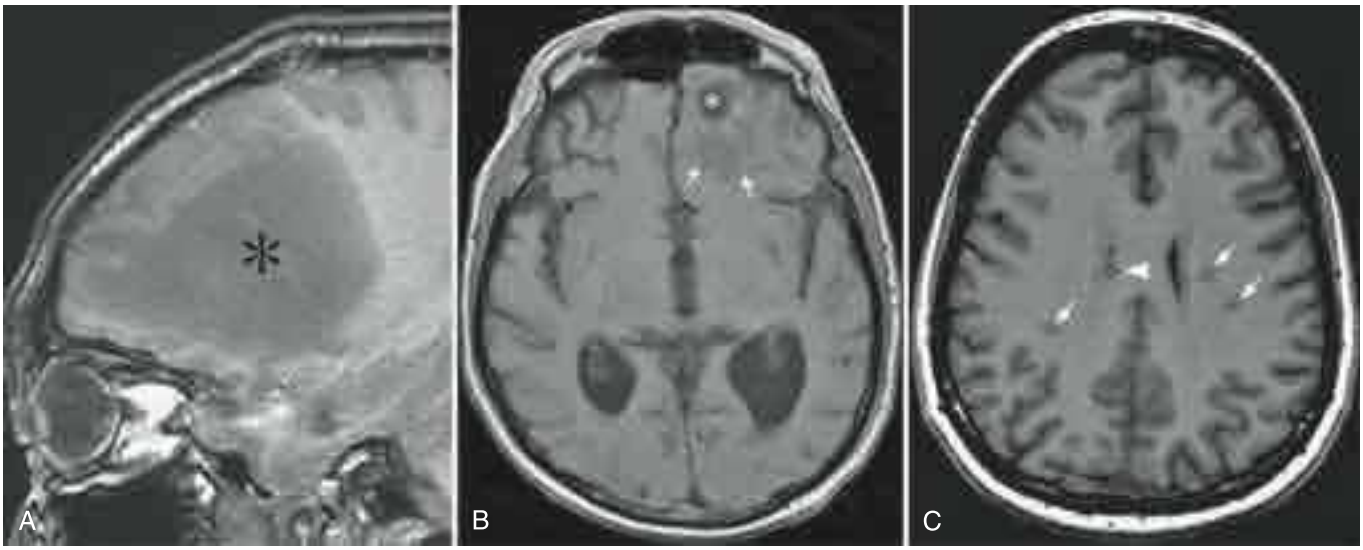

■ **FIGURE 3-13** T1 hypointensity, a nonspecific finding, is found in the large majority of pathologic lesions in the brain and spinal cord. **A,** Peritumoral vasogenic edema. Extensive, confluent white matter T1 hypointensity (*asterisk*) represents vasogenic edema in this patient with left frontal glioblastoma multiforme. **B,** Cerebral abscess. Round, hypointense parenchymal abscess (*asterisk*) with surrounding hypointense vasogenic edema (*arrows*). Contrast-enhanced and diffusion-weighted imaging will help confirm the diagnosis. **C,** Demyelination. Multifocal T1 hypointensity within the lobar white matter (*arrows*) and corpus callosum (*arrowhead*) are characteristic of demyelinating disease, as in this patient with long-standing symptoms of multiple sclerosis.

■ **FIGURE 3-14** Tumors characterized by low T2 signal. **A,** Lymphoma. Relatively T2 hypointense mass in the right frontal lobe white matter (*arrowheads*) with surrounding hyperintense vasogenic edema. **B,** Medulloblastoma. Central T2 hypointensity (*arrow*) within this posterior fossa mass enhanced avidly on postcontrast imaging, excluding the possibility of hemorrhage and/or calcium causing the low T2 signal. **C,** Meningioma. Large extra-axial mass, again demonstrating relative T2 hypointensity. In the case of meningioma, the T2 hypointensity is likely due to a combination of tumor calcification and high fibrous content.

(and, as discussed later, of T2 hyperintensity). Low T1 signal intensity may thus herald a variety of acute and chronic disorders and must be evaluated in conjunction with local mass effect and normal anatomy to determine whether it indicates the presence of edema, fluid collections, demyelination, and solid mass lesions (Fig. 3-13). In general, T1 prolongation is characteristic of fluids, cystic lesions, and solids. Fluid and cystic components of solid lesions commonly have very long T1 relaxation times and are thus seen to have signal intensity that approaches that of CSF on T1W images. Solid lesions including tumors and fibrosis also typically exhibit intermediate T1 signal between that of fluid and normal brain or soft tissue. The T1 signal intensity of protein-containing structures such as mucoceles is low at small protein concentrations and gradually increases with higher concentrations and then falls again at even higher concentrations.[14] Low T1 signal can also be observed with flowing blood, hemosiderin, and calcification.

Low T2 signal intensity is characteristic of fat, tumors, fibrosis, certain blood products, mineralization, and gadolinium chelates in high concentrations. Lipid-containing lesions such as lipomas and dermoid cysts are suggested by relatively low T2 signal intensity in areas that have simultaneously high T1 signal intensity. Other intra-axial tumors are often seen as areas of relatively low T2 signal intensity surrounded by high-intensity vasogenic edema (Fig. 3-14). Tumors of high cellularity that have high density on CT images such as lymphoma, medulloblastoma, and

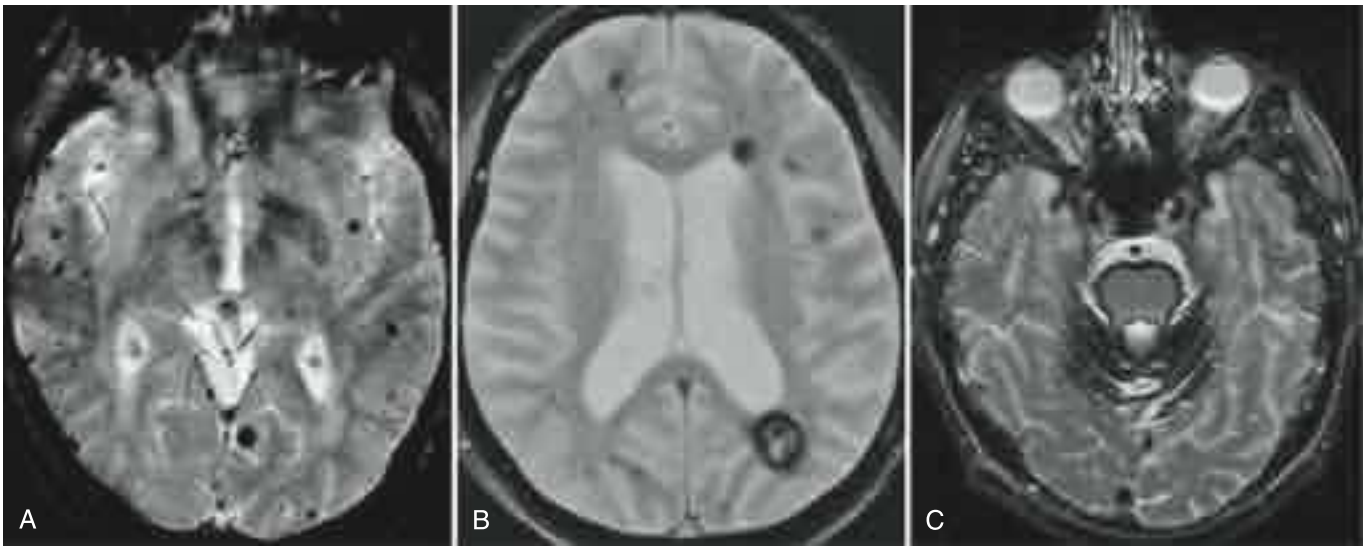

■ **FIGURE 3-15** T2* hypointensity. The appearance of T2* hypointensity is due to magnetic susceptibility, increasing sensitivity to blood products at various stages of evolution. **A,** Amyloid angiopathy. Scattered T2* hypointense foci due to repeated microhemorrhages are characteristic but not diagnostic of this disease. **B,** Multiple cavernomas. Dominant mass centered posterior to the left ventricular trigone with peripheral T2 hypointensity, in conjunction with smaller hypointense lesions within the supratentorial white matter. **C,** Superficial siderosis. Diffuse T2* hypointensity "staining" the leptomeninges of the pons and vermis, owing to repeated hemorrhage in this patient with a spinal cord ependymoma.

other small round blue cell tumors are characterized by a relatively low signal intensity on T2W images. Meningiomas are often T2 hypointense, in part related to calcification and high fibrous content. Mature fibrosis with collagenous tissue, a common host response to prior surgery or trauma of tissue outside the CNS, has characteristic low T1 and T2 signal intensity. In contrast to other causes for T2 hypointensity, mature fibrosis is often seen to enhance in post-gadolinium T1W images. This can be useful, for example, in differentiating between recurrent disc herniation and scarring in the postoperative spine.

Hemorrhage has a complex temporal evolution in both T1 and T2 signal intensity. Both acute and chronic hemorrhage can be T2 hypointense. Shortly after hemorrhage occurs there is a shift in the oxygen dissociation curve of hemoglobin that causes oxyhemoglobin molecules to deoxygenate. Deoxyhemoglobin is highly paramagnetic and leads to a loss of MR signal intensity through its high magnetic susceptibility. Within the first week, however, the host inflammatory response causes deoxyhemoglobin within red blood cells within a hematoma to oxidize to methemoglobin, which has both high T1 and T2 signal intensity. This process typically starts at the margins of the hemorrhage, where phagocytic cells first encounter deoxygenated blood cells. Ultimately, metabolism of the blood cells by phagocytes results in resorption of fluid and protein. In this chronic stage of hematoma evolution, unbound iron released by the phagocytosis of methemoglobin is captured by hemosiderin molecules, which are insoluble in water and unable to cross the blood-brain barrier. The final residual of hemorrhage, the hemosiderin "stain" around the margins of the resorbed hematoma, has high iron content that appears dark on T2W images and gradient-echo images owing to magnetic susceptibility.

Decreased signal intensity on images sensitive to magnetic susceptibility indicates the presence of mineralization, blood products, or gadolinium chelate in high concentrations. These substances produce local disruptions in an otherwise homogeneous main magnetic field and give rise to signal voids on heavily T2*W images. T2*W imaging is especially sensitive for detection of hemosiderin and ferritin, the final products of hemoglobin metabolism that may be the only evidence for prior hemorrhage (Fig. 3-15). The presence of low T2* signal intensity on these images can be especially useful in suggesting the presence of small mineral deposits or blood products that would be otherwise undetectable on standard T1W or T2W imaging. Parenchymal microhemorrhages are most commonly the result of chronic hypertension and amyloid angiopathy, the latter suggested by sparing of the deep gray nuclei and predominant distribution within the subcortical white matter of the frontal and parietal lobes. Cavernous malformations and post-traumatic shear injury can produce a similar pattern of punctate foci of low T2* signal. Less common causes for cerebral microhemorrhage on gradient-echo imaging include cerebral embolism, vasculitis, hemorrhagic micrometastasis, and radiation vasculopathy.[15,16]

Causes of Increased Signal Intensity on T1W, T2W, and T2*W Images

The identification of intrinsic high signal intensity within a lesion on T1W images raises a limited group of diagnostic considerations and usually implies the presence of lipid, methemoglobin, melanin, or proteinaceous fluid.[17] Lipid protons have short T1 relaxation times and may be uniquely identified when T1 hyperintensity is seen in association with chemical-shift artifact (Fig. 3-16). Lipid is characteristic of intracranial and spinal lipomas, dermoid cysts, surgical fat packing, and, rarely, lipomatous degeneration within tumors such as meningioma. Methemoglobin is a common cause of intrinsic T1 shortening that may be seen in the course of extra-axial, intraparenchymal and intraventricular hemorrhage, hemorrhagic infections and tumors, and vessel thrombosis. Gyriform high T1 signal is specific for cortical laminar necrosis, a finding that should suggest subacute infarct when it conforms to a vascular distribution. Interestingly, the mechanism of T1 shortening in laminar necrosis remains unclear. While initially believed to be the result of hemorrhagic infarction, histopathologic studies have failed to confirm the presence of methemoglobin and it is more likely the result of early reactive gliosis and deposition of fat-laden macrophages.[18]

Melanin is thought to reduce parenchymal or leptomeningeal T1 signal through a combination of paramagnetic free radicals in melanin and paramagnetic metal scavenging by melanoma cells. High T1 signal due to melanin is characteristic of melanoma and intracranial deposits of melanin in the phakomatosis neurocutaneous melanosis. Metastatic melanoma, while often hemorrhagic, often demonstrates high T1 signal even in the absence of hemorrhage unless the metastases are amelanotic[18] (Fig. 3-17). Both melanoma metastases and melanin deposits in

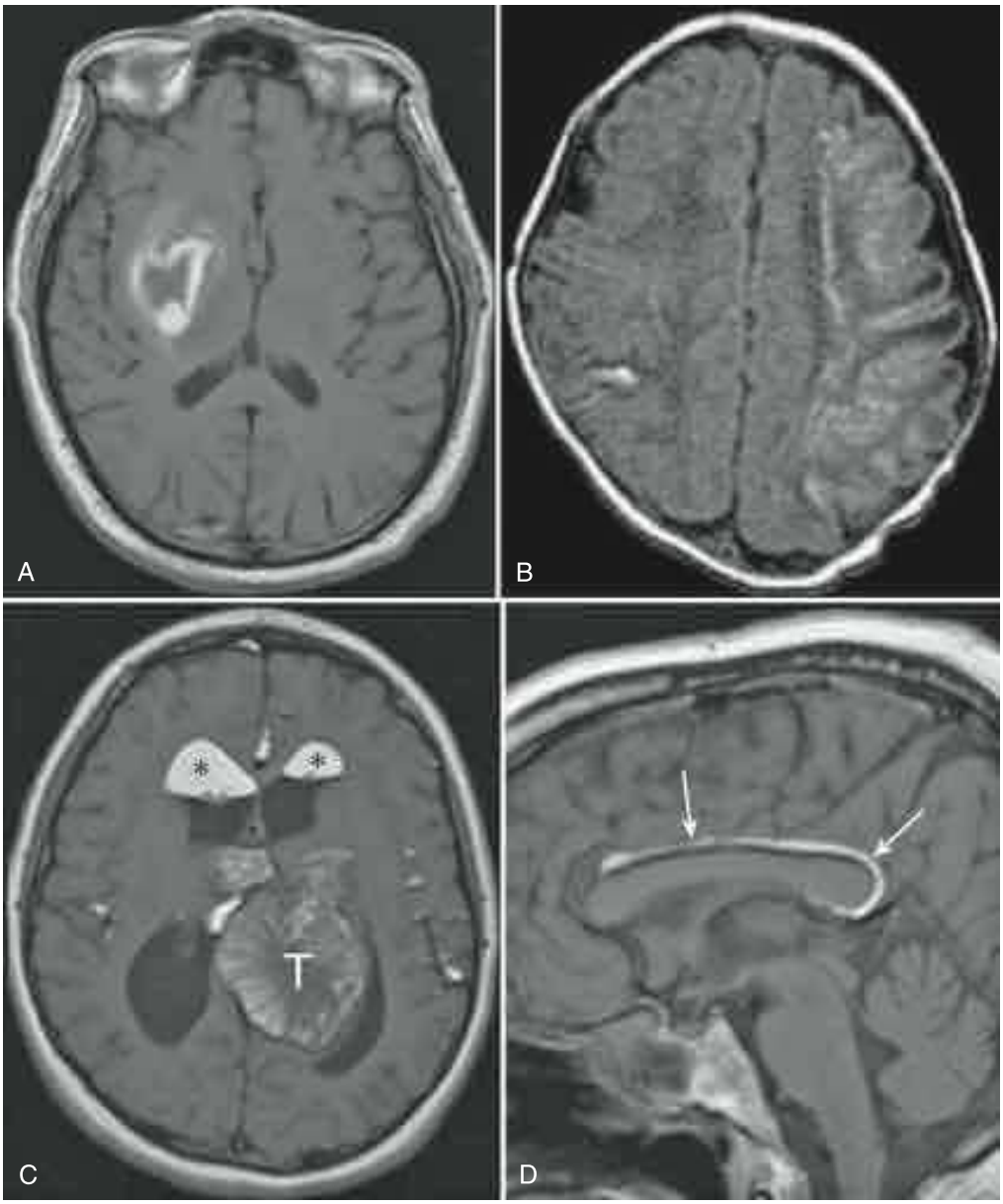

■ **FIGURE 3-16** Intrinsic T1 hyperintensity due to blood and fat. **A,** Intraparenchymal hematoma. Typical appearance of T1 hyperintensity from methemoglobin. **B,** Laminar necrosis. Gyriform T1 hyperintensity secondary to subacute left middle cerebral artery infarct. **C,** Ruptured dermoid cyst. T1 hyperintensity is demonstrated within the mass (T), layering within the ventricles (*asterisks*), and within the sylvian and interhemispheric fissures. **D,** Lipoma. Characteristic T1 hyperintensity along the superior margin of the corpus callosum (*arrows*).

neurocutaneous melanosis may be expected to enhance with administration of gadolinium. T1 shortening can also result from the interaction of water molecules with surrounding macromolecular proteins. Colloid cysts, Rathke's cleft cysts, craniopharyngiomas, and mucoceles may all contain proteinaceous fluids that demonstrate high intrinsic T1 signal. The posterior pituitary normally has intrinsic high T1 signal, most likely the result of proteins or phospholipids concentrated in this portion of the gland.

Flowing blood moves unsaturated spins from outside of a slice into the imaging plane and may result in high T1 signal within vessels. This phenomenon is the basis of flow-related enhancement in time-of-flight MR angiography techniques. Phase artifacts from circulating blood can also give rise to flow ghosts that, when superimposed on normal tissue, produce spurious T1 hyperintensity. Certain paramagnetic cations cause T1 hyperintensity in tissues. Specifically, intravenously administered gadolinium chelates at low concentrations and superparamagnetic iron oxide (SPIO) particle contrast agents deliberately exploit this property to enhance the signal intensity of the blood pool. Concentrations of particulate calcium up to 30% can reduce T1 relaxation times through a surface relaxation mechanism.[19] Finally, manganese deposition from hepatic cirrhosis, parenteral nutrition, or industrial exposure is a rare cause for T1 shortening within the globi pallidi and midbrain.

The differential diagnosis for high T2 signal intensity is exceedingly broad, with a similar range of abnormalities encountered in the analysis of CT hypointensity and T1 hypointensity (Fig. 3-18). Confluent T2 hyperintensity in white matter may indicate edema or gliosis and may thus be a feature of both acute and chronic disease. High T2 signal should thus always be interpreted in conjunction with the presence or absence of local mass effect, because edema is often a secondary phenomenon associated with a mass or hemodynamic changes and gliosis is characterized by regional loss of parenchymal volume. Of note, although characteristic of liquids, T2 hyperintensity is also common to most brain tumors. To determine whether a lesion is truly cystic or necrotic it is necessary to administer gadolinium to document the absence of enhancement. Enhancement in a structure with high T2 signal intensity implies that it is vascular, and thus solid. Solid and cystic lesions with high T2 signal intensity can sometimes be differentiated by comparison with PDW images, where the former are usually bright and the latter are typically dark. Furthermore, "shading" or gravity-dependent

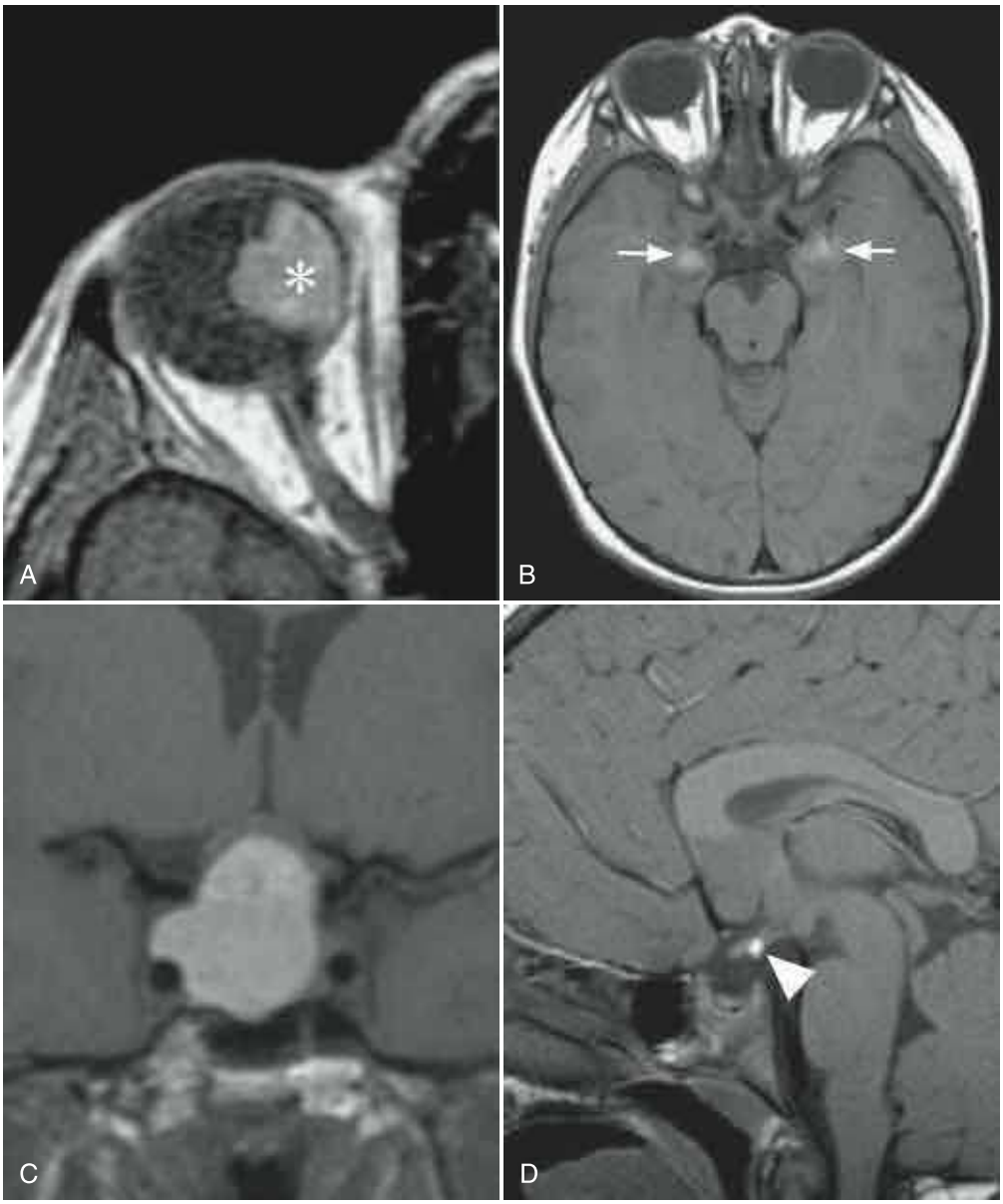

■ **FIGURE 3-17** Intrinsic T1 hyperintensity due to melanin, proteinaceous fluids, and vasopressin. **A,** Orbital melanoma. Homogeneous T1 hyperintensity (*asterisk*) related to high melanin content within the globe in this patient with orbital melanoma. **B,** Neurocutaneous melanosis. T1 shortening within the mesial temporal lobes bilaterally (*arrows*) in a patient with a large dorsal cutaneous nevus on physical examination. **C,** Rathke cleft cyst. Large, cystic mass within the sella turcica. **D,** Ectopic pituitary. Punctate focus of T1 hyperintensity (*arrowhead*) related to storage of the hormone arginine vasopressin.

differentials in T2 signal intensity within a lesion suggest that the lesion is cystic, as may be seen with nodal metastasis of squamous cell carcinoma.[20]

ECHOGENICITY

Standard Against Which to Measure Echogenicity

Echogenicity refers to the ability to return a signal when tissue is in the path of a sound beam and is primarily a function of density and compressibility. Density, as with CT, depends on the mass of the molecules that constitute a tissue and their relative spacing. Compressibility reflects the degree to which molecules are displaced by ultrasonic energy and is the macroscopic correlate to the adherent forces between individual molecules. These intrinsic features of a tissue are characterized together as acoustic impedance, a physical constant that represents the balance of incident acoustic energy that is transmitted through a tissue and scattered back toward the transducer. Tissues with high acoustic impedance attenuate most of the energy of the sound beam, and tissues with low acoustic impedance allow most of the energy to pass through them unhindered. Among biologic tissues, bone has the highest acoustic impedance, followed by muscle, fat, blood, water, and air. Thus, bone blocks the transmission of sound and serves as a poor acoustic window through which to evaluate deeper tissues. Echogenicity can only be adequately assessed for tissues of relatively low impedance such as muscle, blood vessels, and fluid collections. Furthermore, as impedance is proportional to the wavelength of the sound beam, high-frequency transducers are useful only for assessing structures close to the skin surface and it is necessary to use a lower-frequency transducer to interrogate deeper structures.

The relative fraction of energy transmitted and reflected at the interface between two different structures is determined by the transmission coefficient and reflection coefficients for the interface, as calculated from their acoustic impedance. A large difference in the magnitude of the impedance at an interface results in the majority of insonating energy being reflected, and smaller differences allow greater through-transmission of sound. The transmission coefficient is thus greater for air-muscle interfaces than muscle-bone interfaces. The latter produce acoustic shadows, points in the image beyond which there is no visualiza-

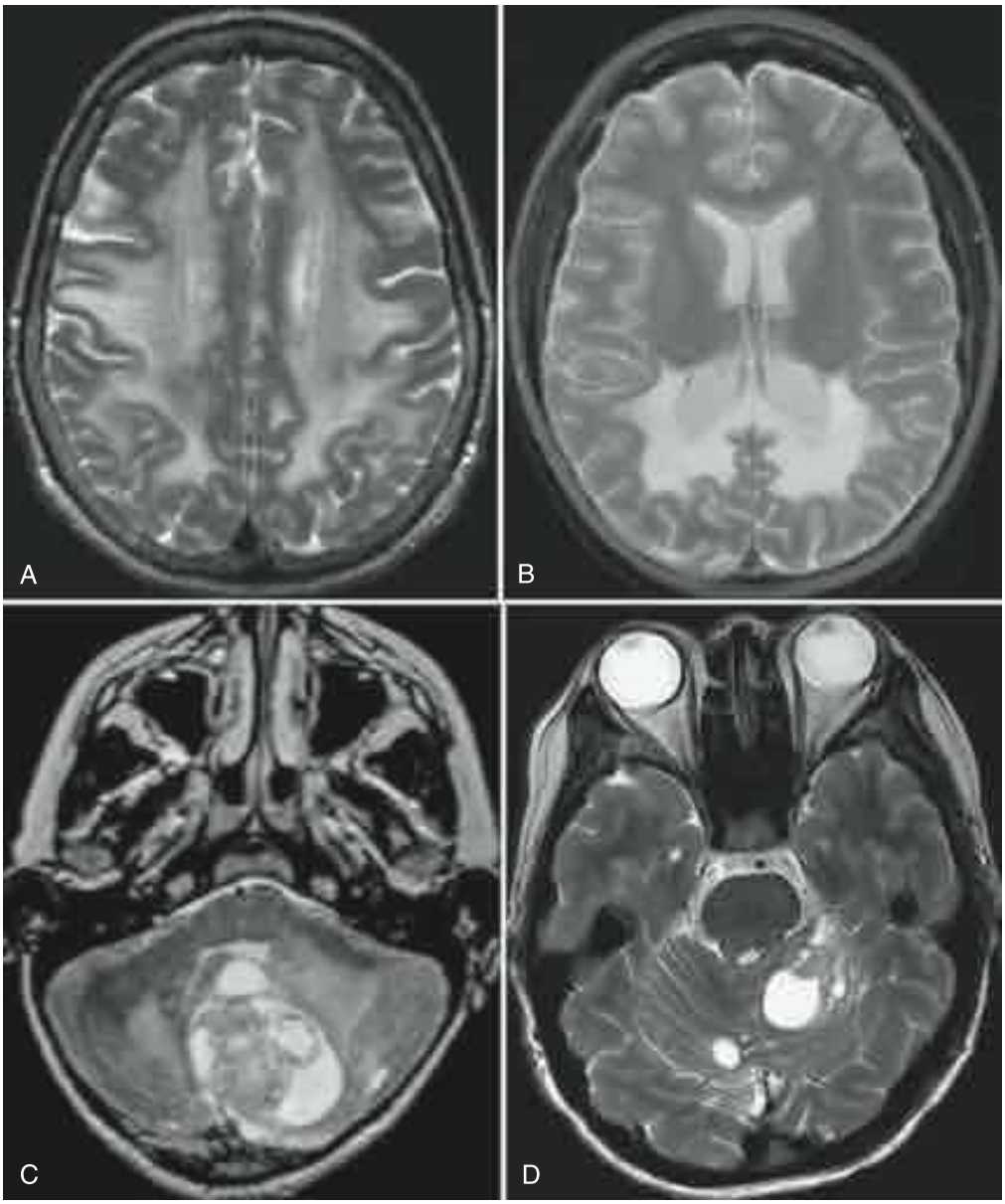

■ **FIGURE 3-18** T2 hyperintensity. Similar to hypodensity with CT, the relatively common MR finding of T2 hyperintensity has a broad differential diagnosis. **A,** Hashimoto's encephalopathy. Diffuse T2 hyperintensity within the supratentorial white matter due to acute inflammation. **B,** Typical distribution of T2 hyperintensity in this patient with X-linked adrenoleukodystrophy. **C,** Juvenile pilocytic astrocytoma. T2 hyperintense tumor cyst favors this diagnosis over that of other posterior fossa tumors in the pediatric population. **D,** Necrotic metastases. Central T2 hyperintensity suggests necrosis and cavitation within these breast cancer metastases.

tion of deeper tissues. Structures in the near field are thus more easily assessed than structures in the far field, which are interrogated by a sound beam of much lower energy that has been successively attenuated as it passes farther from the ultrasound transducer.

While there is some variation in the speed at which ultrasound travels through different tissues, a fixed speed of 1540 m/s is assumed by the scanner to spatially localize the source of reflected sound. As the acoustic beam encounters tissues of different impedance, velocities are altered such that returning echoes are received by the transducer at different times and have different intensities. This information, along with the values for sound wave velocities in different tissues, is synthesized to generate an ultrasound image. The intensities depicted in an ultrasound image should be interpreted as a map of the attenuation of the sound beam, modulated in the far field by the cumulative effects of sound attenuation in the near field.

Anatomic structures respond with characteristic features when insonated with an ultrasound beam. In comparison with neighboring tissues, the echo signature of bone, soft tissue, fluid, muscle, and fat can typically be uniquely distinguished. However, both the echogenicity and echotexture of a lesion are subjective rather than quantitative assessments that depend on the frequency of insonation, acoustic window, angle of insonation, and ultrasound scan parameters. In a similar approach to interpretation of cross-sectional modalities, the intensity (*echogenicity*) and pattern (*echotexture*) of echoes are usually described in reference to adjacent normal tissues.

Alternate Nomenclature

Several descriptive terms are commonly applied to the echogenicity of lesions:

- *Isoechoic* lesions are characterized by echogenicity that is identical to the tissue of reference, such that a lesion is not depicted separately when it is spatially contiguous with normal tissue. For example, subependymal heterotopias may be seen as solid masses along the ventricular margins that are isoechoic to gray matter.
- *Hypoechoic* structures such as infarcted brain appear less bright on ultrasound images than the tissue of reference, and *hyperechoic* (*echogenic*) lesions such as acute hemorrhage

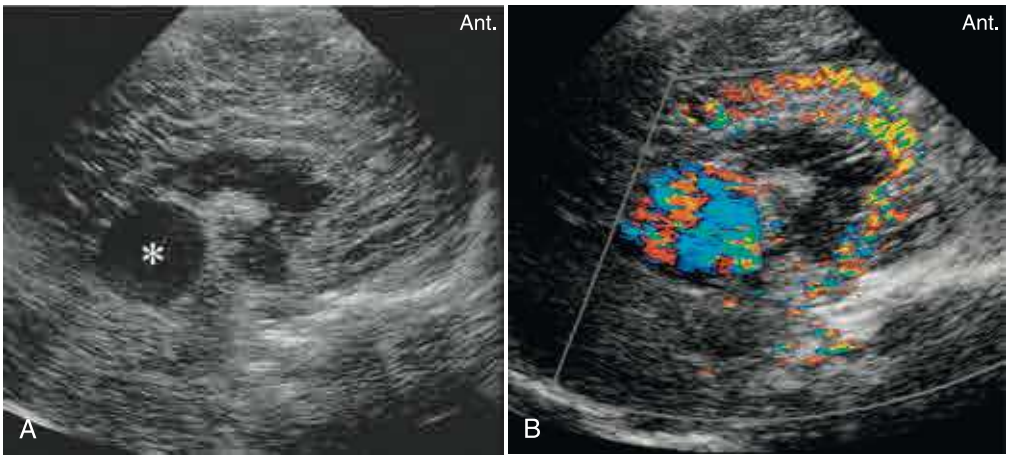

■ **FIGURE 3-19** Vein of Galen malformation. Doppler imaging is used to confirm the vascular nature of hypo/anechoic masses. **A,** Gray-scale ultrasonography of the newborn brain demonstrating an anechoic, cystic-appearing mass (*asterisk*) located posterior to the thalamus. **B,** Color Doppler image demonstrating prominent flow within the "cystic" mass.

are brighter on ultrasound images than the tissue of reference.

- *Anechoic* or *sonolucent* structures such as CSF and cysts are characterized by an absence of internal echoes. The normal ventricular system is anechoic, as are uncomplicated cysts in the posterior fossa in the setting of Dandy-Walker malformations.

Echotexture may also aid in determining whether a lesion is solid or cystic when it is *homogeneous* (containing an internally uniform echo pattern) or *heterogeneous* (containing an internally irregular echo pattern). Homogeneous echotexture is typical of intracranial cysts and normal CSF, and heterogeneous echotexture is often found in intracranial neoplasms such as teratomas or blood products. Finally, the interaction of the sound wave with neighboring tissues is an additional diagnostic feature that may help in determining the nature of a lesion. In particular, the density of a lesion can be inferred from the degree to which it attenuates or enhances sound transmission. Dense structures such as bone and mineralization that dramatically attenuate sound cause *posterior acoustic shadowing,* and less dense structures such as cysts that readily transmit sound lead to *posterior acoustic enhancement* (*enhanced through-transmission*).

Causes of Decreased Echogenicity

Ultrasound imaging has found limited clinical use in routine neuroradiology, in large part due to the poor penetration of sound through the skull and spinal column. However, because bone is less dense in neonates and open fontanelles provide an acoustic window through which to insonate the brain, neurosonography is widely used in the evaluation of the neonatal brain and spine. In this setting, ultrasound is highly sensitive for the detection of intracranial hemorrhage in infants born prematurely. The different echogenicity of normal white matter, basal ganglia, and the choroidal plexus make ultrasonography useful in screening for structural anomalies, periventricular leukomalacia, and hypoxic ischemic injury in the newborn brain, albeit with less sensitivity than MRI or CT. The incompletely ossified or unfused posterior elements of the spine also provide a clinically useful acoustic window, such that ultrasound plays a role in the assessment of the spinal cord in neonates suspected of having a tethered cord or myelomeningocele. Ultrasound imaging is also used in the evaluation of vessels in the neck and skull, the latter via transcranial Doppler ultrasonography. Finally, intraoperative ultrasonography is used in some institutions by surgeons during resection of brain and spinal cord tumors, both in adults and in children.

Decreased echogenicity in the newborn brain is characteristic of intracranial cysts or prior ischemic injury. Interhemispheric cysts and posterior fossa cysts appear as circumscribed regions that are isoechoic to normal CSF and may displace adjacent normal structures. While most often incidental, intracranial cysts are often the first finding in cases of an underlying congenital anomaly, such that their identification should prompt close investigation of the corpus callosum and cerebellum, respectively, to confidently make the diagnosis of callosal agenesis or the Dandy-Walker malformation. Subependymal cysts occur along the walls of the ventricles and reflect germinolysis due to congenital infection. In the late stage of intraparenchymal hemorrhage, hypoechoic areas or cystic cavities remain in areas of hemorrhage within the brain parenchyma, particularly around the margins of the ventricular system. Useful adjunct findings with intracranial cysts include posterior through-transmission and homogeneous echotexture.

Abnormalities primary to the intracranial vasculature are an important differential consideration in the evaluation of intracranial cysts (Fig. 3-19). The echogenicity of the blood pool is determined by the mechanical aggregation of red blood cells, which is directly related to blood flow velocity and inversely related to vessel diameter.[21] The internal echotexture and Doppler flow of hypoechoic or anechoic intracranial lesions should thus be carefully assessed to determine whether an apparently cystic lesion may actually represent a vascular malformation such as a dilated vein. Evaluation of the entirety of the abnormality may show hyperechoic areas that correspond to layering or flowing blood within the lesion.

Decreased echogenicity detected in the dorsum of the lumbar spine may be a subtle finding of myelomeningocele and spina bifida. Nonfusion of the posterior elements in this case allows a portion of the spinal canal to protrude through the defect, leading to the appearance of a rounded hypoechoic lesion within the soft tissues of the back superficial to the opening. A simple myelomeningocele is often associated with characteristic features of the type 2 Chiari malformation in the brain. Sacrococcygeal teratomas may also contain hypoechoic areas and may be included in the differential diagnosis of myelomeningocele.

Causes of Increased Echogenicity

Ultrasonography of the neonatal head has high sensitivity for the diagnosis of intracranial hemorrhage, which typically originates in the germinal matrix and extends into the ventricular system. At most institutions, infants born prematurely are routinely screened for this complication at 4 to 7 days after birth. Hemorrhage confined to the germinal matrix is readily identified as asymmetric increased echogenicity in the region of the

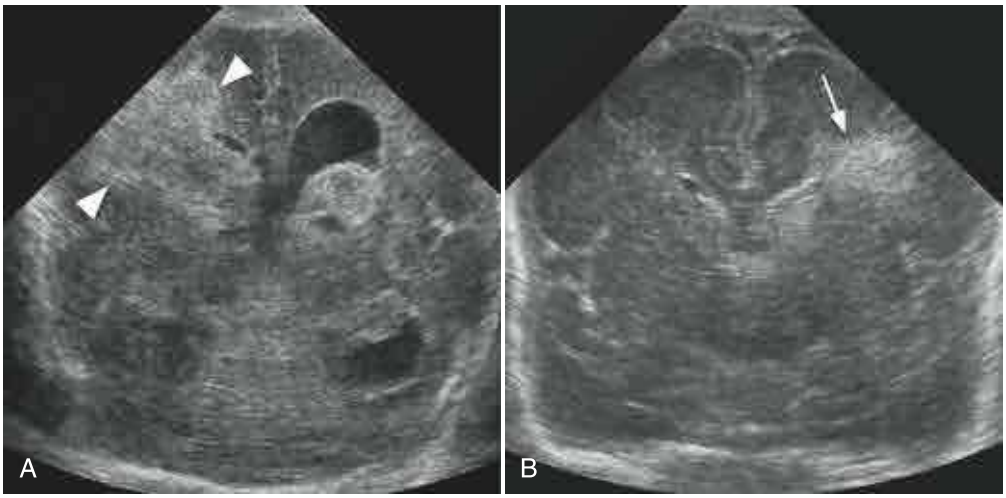

■ **FIGURE 3-20** Hyperechogenicity on neonatal neurosonography. **A,** Grade 4 germinal matrix hemorrhage. Hyperechoic bilateral germinal matrix hemorrhages (*arrowheads*) with parenchymal extension on the right in a newborn born at 28 weeks' gestation. **B,** Acute periventricular leukomalacia. Abnormal echogenic white matter surrounding the ventricles, more pronounced on the left (*arrow*) in a newborn with difficult delivery.

■ **FIGURE 3-21** Multimodality characterization of a sellar mass (craniopharyngioma). **A,** Coronal T2-weighted imaging demonstrating a hyperintense mass with internal hypointense "debris" (*arrowheads*), suggesting the presence of blood and/or calcium. **B,** Sagittal gadolinium-enhanced imaging confirms the cystic nature of the lesion. Irregular enhancement of the cyst wall (*arrowhead*) suggests a neoplastic etiology. **C,** Axial, noncontrast CT confirms the presence of dense mural calcium, consistent with the diagnosis of craniopharyngioma.

caudothalamic notch, where the absence of choroid makes blood stand out from this normal tissue (Fig. 3-20). When blood extends into the ventricular system, ultrasonography is also useful for the detection of ventriculomegaly and accompanying intraventricular hemorrhage, which usually appears as focal areas of echogenicity in close proximity to the ventricular margins. Small subdural hemorrhages, which appear as thin lenticular extra-axial collections, are common after normal vaginal delivery and are usually considered normal incidental findings.

Acute periventricular leukomalacia can be diagnosed on ultrasound evaluation when increased echogenicity is seen within the superolateral periventricular brain parenchyma. When subtle, periventricular leukomalacia may be difficult to distinguish from the normal ring of hyperechoic white matter that surrounds the ventricles caused by the anisotropy effect of sound beam reflection from axons and vessels that emerge centripetally from the ventricles (see Fig. 3-20). When suggested by ultrasonography, this finding can be confirmed by neonatal MRI, which is diagnostic. Hypoxic-ischemic encephalopathy, in contrast, can be suggested by an overall increase in brain echogenicity or focal hyperechoic areas that conform to a vascular territory. The latter may also involve the thalami and lenticular nuclei, giving rise to more linear areas of echogenicity referred to as "thalamostriate vasculopathy." Similar to periventricular leukomalacia, these findings can be exceedingly subtle and are best assessed using MRI.

RELATIVE SPECIFICITY OF DENSITY VERSUS SIGNAL INTENSITY VERSUS REFINING ANALYSIS BY USE OF MULTIPLE TECHNIQUES

There are certain circumstances when the complementary information about image intensity from more than one modality can be used to narrow the differential diagnosis among a longer list of considerations. For example, the MRI appearance of calcium is variable and nonspecific and the presence of calcium within a lesion may not be appreciated a priori on MRI.[22,23] Small particulate calcium seen on CT as fine or punctate may be subsumed by partial volume averaging in MR images and not visualized at all. When sufficiently large, calcium deposits may give rise to signal voids on T1W or T2W imaging, but their signal intensity is sufficiently variable that they may not be readily identified in all cases. CT can be used to increase diagnostic confidence in the differential diagnosis of tumors that commonly calcify, such as meningioma, oligodendroglioma, craniopharyngioma, and choroid plexus papilloma from other noncalcified tumors (Fig. 3-21). CT should also be considered in the workup

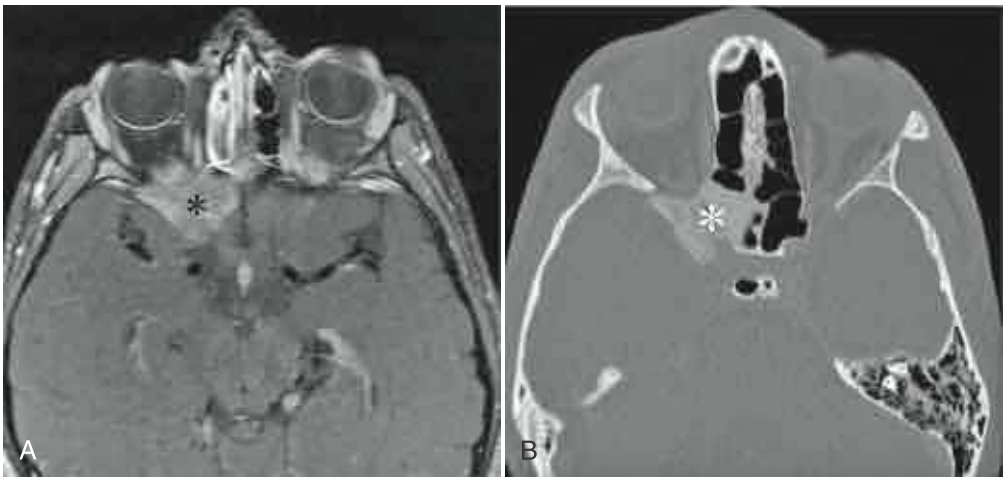

■ **FIGURE 3-22** Fibrous dysplasia. CT versus MRI characterization of bone lesions. **A,** Axial gadolinium-enhanced imaging demonstrating a enhancing lesion at the right orbital apex (*asterisk*). The list of differential considerations would include both neoplastic and inflammatory processes. **B,** Noncontrast CT demonstrates the bony origin of the lesion, with the characteristic "ground-glass" appearance (*asterisk*) of fibrous dysplasia.

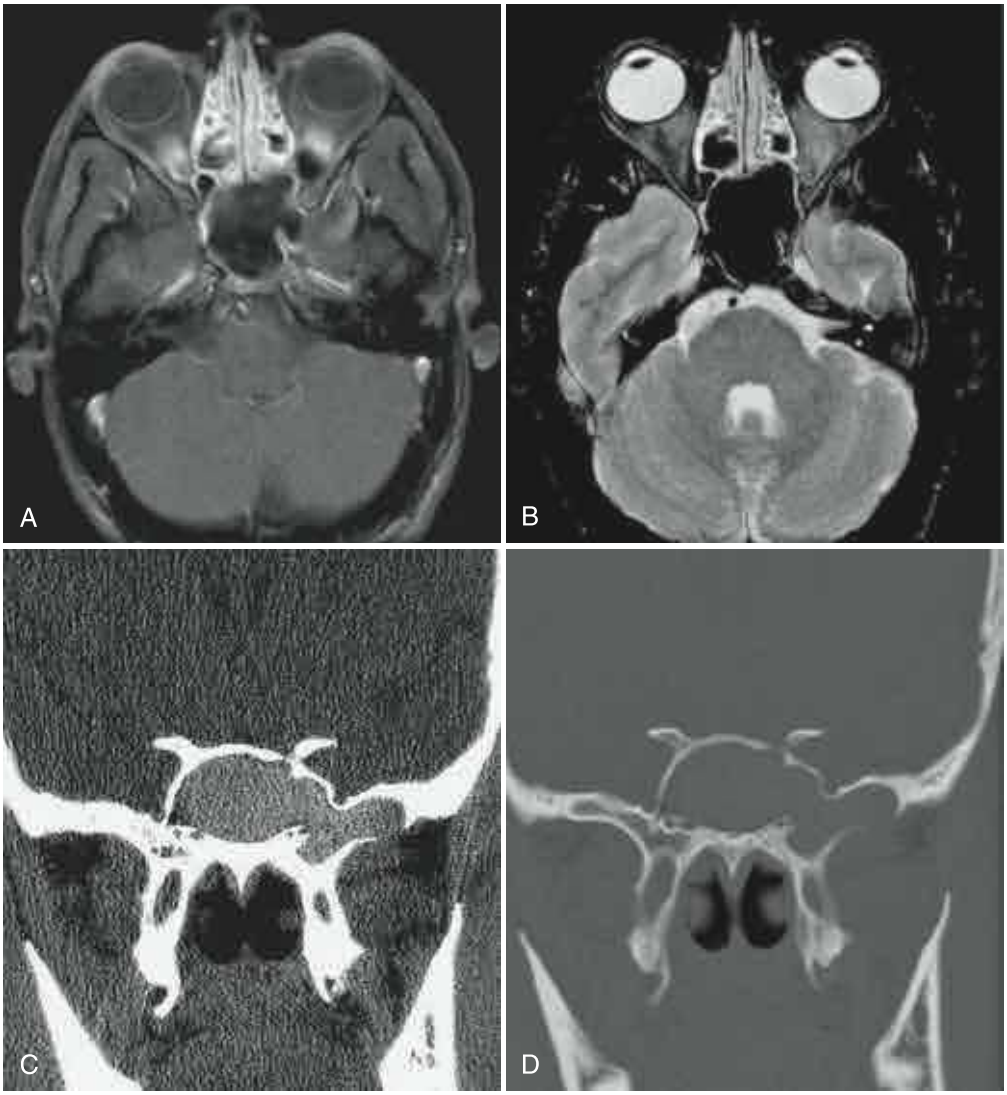

■ **FIGURE 3-23** Dark mucocele. Highly proteinaceous mucus within an obstructed sinus may be hypointense on both gadolinium-enhanced T1W (**A**) and fat-suppressed T2W (**B**) images, such that this mucosal disease of the paranasal sinuses may be overlooked on routine MRI. CT images at bone (**C**) and soft tissue (**D**) windows readily demonstrate relatively hyperdense material within an expanded, remodeled sphenoidal sinus, consistent with a mucocele.

BOX 3-1 Sample Report: MRI of the Brain

PATIENT HISTORY

An 8-year-old boy presented with gradual onset of headaches and loss of vision over a 6-month period.

COMPARISON STUDY

Head CT was done a week earlier.

TECHNIQUE

Axial and sagittal T1W spin-echo, coronal T2W fast spin-echo, axial T2W FLAIR, coronal gradient-echo, and post-gadolinium axial and sagittal T1W spin-echo imaging of the brain performed at 1.5 T.

FINDINGS

There is a 2.4 × 1.2-cm circumscribed mass centered within both the sella and suprasellar cistern that is both solid and cystic. The lesion shows predominantly high T2 and low T1 signal intensity but contains several discrete areas of low T2 and high T1 signal that are consistent with blood products and/or proteinaceous debris. Thin peripheral linear areas of low intensity on T2W images correspond to susceptibility artifact on gradient-echo images, consistent with calcification as demonstrated on recent head CT.

Secondary enlargement of the sella is present, along with upward displacement of the overlying optic chiasm and flattening of an otherwise normal-appearing pituitary gland. The mass does not appear to involve the cavernous sinuses, and the normal flow voids of the internal carotid arteries are preserved. There is no reactive edema within the brain adjacent to the lesion, and although portions of the mass lie just below the foramen of Monroe there is no ventriculomegaly to indicate hydrocephalus.

On administration of gadolinium, the lesion shows several internal nodular areas of enhancement and demonstrates linear enhancement at its periphery. There is no suspicious enhancement of the brain parenchyma or leptomeninges.

IMPRESSION

This suprasellar solid and cystic mass is most consistent with craniopharyngioma, given the presence of internal T1 shortening, cyst wall enhancement, and calcification. Because the lesion is separate from the pituitary gland, this is unlikely to represent a hemorrhagic pituitary adenoma. The presence of calcification and internal solid enhancement also makes Rathke's cleft cyst and simple arachnoid cyst unlikely.

of non-neoplastic CNS disorders in which focal calcification is of diagnostic importance, including certain neoplasms and inflammatory/infectious processes such as granulomatous disease or neurocysticercosis, metabolic derangements such as Fabry's disease, and tuberous sclerosis or Sturge-Weber syndrome.

CT has far greater accuracy than MRI in the evaluation of most disease in or around the bones of the skull or spinal column. When MRI is the first study obtained in a patient with a benign or malignant lesion primary to bone, signal intensity on T1W and T2W images may not be sufficiently specific to arrive at a specific diagnosis. For example, the developmental disorder fibrous dysplasia leads to replacement of normal cancellous bone by immature osseous matrix and fibrous stroma. This has a nearly pathognomonic radiographic or CT appearance but has a variable appearance on MRI that may not be easily recognized (Fig. 3-22).[24] Concomitant T1 and T2 hypointensity, which is characteristic of fibrous tissue, is not usually seen in the entity. Instead, the majority of these lesions are isointense to muscle on T1W images and heterogeneously hyperintense on T2W images. Because identical imaging features can be found in malignant tumors of the brain or surrounding bones, plain film radiographs or CT should be considered when the MRI appearance is equivocal.

MRI may be particularly misleading in the evaluation of fluid collections. For example, the signal intensity of mucus contents within an obstructed paranasal sinus or mucocele depends on the relative protein content. On T1W images, fluid within a sinus is characteristically T1 hypointense. When the protein concentration exceeds roughly 25%, there is a T2-shortening effect that renders these inspissated secretions occult on T2W images. Furthermore, the diagnostic features of sinus expansion and osseous thinning are not easily recognized on MRI. To confidently diagnose the entity of a proteinaceous mucocele, CT should be obtained and correlated with the MRI findings, because the typical bony remodeling is readily visualized on CT (Fig. 3-23).

ANALYSIS

A sample formal imaging report is presented in Box 3-1 in which the description of how signal intensity and density are analyzed should lead the reader to the correct clinical diagnosis of craniopharyngioma. This report refers to the imaging example provided in Figure 3-21.

KEY POINTS

- Density, signal intensity, and echogenicity should be analyzed first in terms of location within gray matter, white matter, CSF spaces, bones, or elsewhere within the brain or spinal cord.
- CT number is an absolute measurement of density, but signal intensity on MRI and echogenicity in ultrasonography are relative and should be interpreted in reference to adjacent tissues.
- A suitable display window should be applied to both CT and MR images to detect subtle changes that may otherwise not be easily discerned.
- The intensity analysis of a lesion should initially focus on the lesion itself to determine its cause, but secondary changes in the intensity of adjacent tissues may provide additional clues.

SUGGESTED READINGS

Babcock DS. Sonography of the brain in infants: role in evaluating neurologic abnormalities. AJR Am J Roentgenol 1995; 165:417-423.

Barnes JE. AAPM Tutorial: characteristics and control of contrast in CT. RadioGraphics 1992; 12:825-837.

Mikulis DJ, Roberts TPL. Neuro MR: protocols. J Magn Reson Imaging 2007; 26:838-847.

Nitz WR, Reimer P. Contrast mechanisms in MR imaging. Eur Radiol 1999; 9:1032-1046.

Roberts TPL, Mikulis DJ. Neuro MR: principles. J Magn Reson Imaging 2007; 26:823-837.

REFERENCES

1. Phelps ME, Hoffman EJ, Ter-Pogossian MM. Attenuation coefficients of various body tissue, fluids, and lesions at photon energies of 18 to 136 keV. Radiology 1975; 117:573-583.
2. Mull RT. Mass estimates by computed tomography: physical density from CT numbers. AJR Am J Roentgenol 1984; 143: 1101-1104.
3. Brooks RA, Mitchell LG, O'Connor CM, Di Chiro G. On the relationship between computed tomography numbers and specific gravity. Phys Med Biol 1981; 26:141-147.
4. Levi C, Gray JE, McCullough EC, Hattery RR. The unreliability of CT numbers as absolute values. AJR Am J Roentgenol 1982; 139:443-447.
5. Bosniak MA. The small (<3.0 cm) renal parenchymal tumor: detection, diagnosis and controversies. Radiology 1991; 179:307-317.
6. Klatzo I. Presidential address: neuropathological aspects of brain edema. J Neuropathol Exp Neurol 1967; 26:1-14.
7. Marks MP, Holmgren EB, Fox AJ, et al. Evaluation of early computed tomographic findings in acute ischemic stroke. Stroke 1999; 30:389-392.
8. Lev MH, Farkas J, Gemmente JJ, et al. Acute stroke: improved nonenhanced CT detection- benefits of soft-copy interpretation by using variable level and center window settings. Radiology 1999; 213:150-155.
9. Somford DM, Nederkoorn PJ, Rutgers DR, et al. Proximal and distal hyperattenuating middle cerebral artery signs at CT: different prognostic implications. Radiology 2002; 223:667-671.
10. Rutgers DR, van der Grond J, Jansen GH, et al. Radiologic-pathologic correlation of the hyperdense middle cerebral artery sign. Acta Radiol 2001; 42:467-469.
11. Zimmerman RA, Bilaniuk LT. Computed tomography of acute intratumoral hemorrhage. Radiology 1980; 135:355-359.
12. Ethofer T, Mader I, Seeger U, et al. Comparison of longitudinal metabolite relaxation times in different regions of the human brain at 1.5 tesla and 3 tesla. Magn Reson Med 2003; 50:1296-1301.
13. Stanisz GJ, Odrobina EE, Pun J, et al. T1, T2 relaxation and magnetization transfer in tissue at 3T. Magn Reson Med 2005; 54: 507-512.
14. Som PM, Dillon WP, Fullerton GD, et al. Chronically obstructed sinonasal secretions: observations on T1 and T2 shortening. Radiology 1989; 172:515-520.
15. Tsushima Y, Aoki J, Endo K. Brain microhemorrhages detected on T2*-weighted gradient echo MR images. AJNR Am J Neuroradiol 2003; 24:88-96.
16. Blitstein MK, Tung GA. MRI of cerebral microhemorrhages. AJR Am J Roentgenol 2007; 189:720-725.
17. Cakirer S, Karaarslan E, Arslan A. Spontaneously T1-hyperintense lesions of the brain on MRI: a pictorial review. Curr Probl Diagn Radiol 2003; 32:194-217.
18. Boyko OB, Burger PC, Shelburne JD, Ingram P. Non-heme mechanisms for T1 shortening: pathologic, MR and CT elucidation. AJNR Am J Neuroradiol 1992; 13:1439-1445.
19. Henkelman RM, Watts JF, Kucharczyk W. High signal intensity in MR images of calcified brain tissue. Radiology 1991; 179:199-206.
20. Hetts SW, Urban JP, Quinones-Hinojosa A, et al. The shading sign in cerebral squamous cell metastases. AJR Am J Roentgenol 2004; 182:1087-1088.
21. Machi J, Sigel B, Beitler JC, et al. Relation of in vivo blood flow to ultrasound echogenicity. J Clin Ultrasound 1983; 11:3-10.
22. Holland BA, Kucharcyzk W, Brant-Zawadzki M. MR imaging of calcified intracranial lesions. Radiology 1985; 157:353-356.
23. Tsuchiya K, Makita K, Furui S, Nitta K. MRI appearance of calcified lesions within intracranial tumors. Neuroradiology 1993; 35:341-344.
24. Shah ZK, Peh WCG, Koh WL, Shek TWH. Magnetic resonance imaging appearance of fibrous dysplasia. Br J Radiol 2005; 78:1104-1115.

CHAPTER 4

Analysis of Mass Effect

Ellen E. Parker

Lesions or processes that cause *compression, distortion,* and/or *displacement* of intracranial contents may be said to have "mass effect." One important concept to understand is that mass effect is a manifestation on imaging of various intracranial processes (including tumor, hemorrhage, ischemia, and trauma) and not a diagnosis in itself. An analogy to clinical medicine is that vertigo is not a diagnosis in itself but rather a symptom with multiple possible underlying causes (such as posterior fossa infarct or vestibular abnormality). Detection and characterization of mass effect is a fundamental skill of neuroradiology. Accurate characterization of mass effect helps to precisely define the location of a lesion, which is crucial to forming an accurate differential diagnosis. In addition to diagnostic value, detection and prompt reporting of mass effect is also of great importance to the care of patients, especially those with life-threatening herniation. The goal of this chapter is to introduce key concepts and methods of analysis of mass effect to the beginning radiologist.

Prior to the advent of cross-sectional imaging, intracranial masses were localized and characterized by catheter angiography or other invasive techniques such as pneumoventriculography, pneumocisternography, and metrizamide ventriculography/cisternography.[1,2] CT and MRI are now the modalities of choice for evaluation of intracranial space-occupying lesions. Catheter angiography is now largely reserved for further characterization of and therapy for vascular intracranial lesions (e.g., preoperative evaluation and embolization of meningioma).

Although analysis of mass effect may be quantitative (e.g., measurement in centimeters of midline subfalcine herniation), mass effect is usually described in qualitative terms (e.g., severity of ventricular compression, hydrocephalus, sulcal effacement, obliteration of basal cisterns, or local tissue pressure effects).

Mass effect may be due to direct displacement of intracranial contents by discrete space-occupying lesions, such as benign and malignant neoplasms, non-neoplastic masses (e.g., arachnoid cyst), localized hemorrhage, or abscess. Mass effect may also be caused by brain swelling or *edema.* The pathophysiology of abnormal accumulation of fluid within the brain parenchyma is complex.[3] Edema may be described in terms of etiology (osmotic, hydrostatic, hyperemic), microscopic location (extracellular or intracellular), or macroscopic anatomic location (e.g., gray matter vs. white matter). In simple terms based on physical location with regard to cell membranes, brain edema may be classified as *vasogenic* (extracellular) or *cytotoxic* (intracellular). Although these two descriptors of edema in reality often coexist and are not mutually exclusive, cerebral edema, on imaging, is often described as one or the other. In simple terms, cytotoxic edema demonstrates reduced diffusion (reduced apparent diffusion coefficient [ADC]) whereas vasogenic edema does not (normal or increased ADC). Cytotoxic edema is more prominently found in gray matter, whereas vasogenic edema is more prominent in white matter. The causes of cerebral edema are myriad. Examples include regional cytotoxic edema due to ischemic infarct, local or regional vasogenic edema associated with tumor or infection, post-traumatic edema, and generalized cerebral edema due to diffuse insult such as hypoxia/ischemia.[4]

According to the Monro-Kellie hypothesis, the intact calvaria creates a fixed intracranial space[5] that under normal conditions contains (1) *brain* (and its meningeal coverings), (2) *blood* (within vessels and dural venous sinuses), and (3) *cerebrospinal fluid* (within the subarachnoid space and ventricles).[6] Although the pathophysiology of intracranial pressure/volume relationships is indeed much more complex,[7] this basic understanding of the Monro-Kellie hypothesis is sufficient for the beginning radiologist. A corollary to this hypothesis for the radiologist is that under normal conditions the intracranial contents demonstrate a clearly defined midline with bilateral symmetry. Any disruption of this normal equilibrium (e.g., a space-occupying lesion and/or edema) may change the appearance of the contents of the intracranial space.

There are many factors contributing to mass effect. Some slow-growing large lesions may exhibit virtually no mass effect, whereas some small lesions may incite a surprisingly dramatic response.

ANATOMY

The discussion of analysis of mass effect may begin with a review of basic anatomic principles. Figure 4-1 presents a diagrammatic representation of the principles discussed here.

Brain Parenchyma: Gray and White Matter

The parenchyma of the brain may be divided into *gray matter,* consisting of unmyelinated neurons, and *white matter,* consisting of myelinated axons. The cortical mantles as well as deep nuclei of the cerebrum and cerebellum are composed of gray matter. White matter is characteristically located deep to the cortex and may be further described by location:

■ **FIGURE 4-1** Key anatomic concepts for discussion of mass effect.

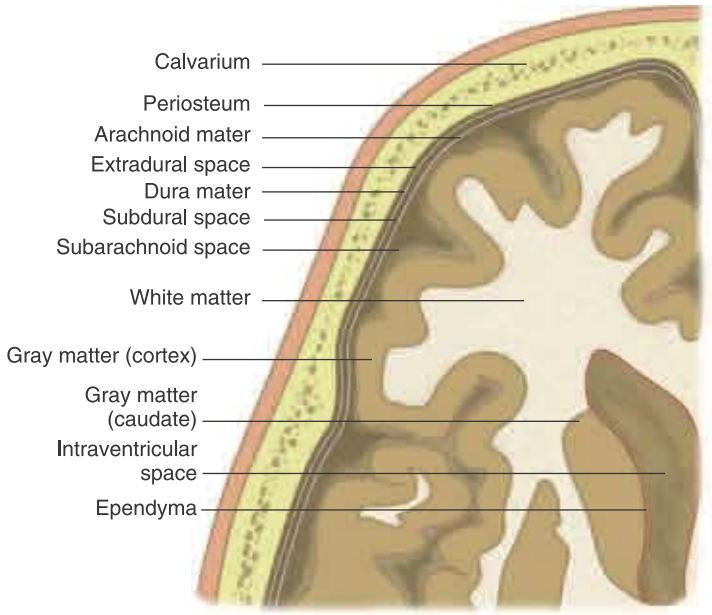

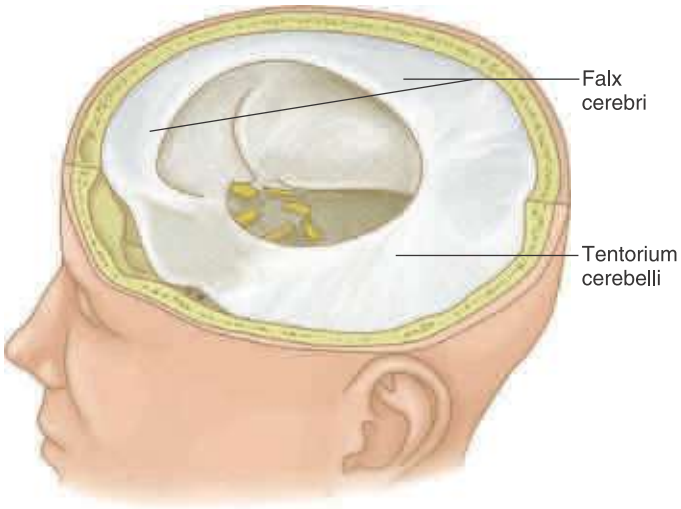

■ **FIGURE 4-2** Gross specimen with dura retained in place to illustrate the falx cerebri and tentorium cerebelli. *(From Thibodeau GA, Patton KT. Anatomy and Physiology, 4th ed. St. Louis, Mosby, 1999, p 376.)*

subcortical, deep, and *periventricular.* The ventricles are lined by *ependyma*.

Meninges

The brain is held in place by the tough inelastic *dura mater* (also called *meninx fibrosa* or *pachymeninx* [plural, *pachymeninges*]), which under normal conditions is adherent to the periosteum of the inner surface of the calvaria. Reflections of the dura mater create fixed compartments within the intracranial space (Fig. 4-2). Named for its crescentic shape (L. *falx*, "sickle"), the *falx cerebri* separates the cerebral hemispheres along the interhemispheric fissure. The cerebrum and cerebellum are separated by the *tentorium cerebelli* (L. *tentorium,* "a shelter made of stretched skins"). The brain stem traverses an opening of the tentorium called the *tentorial incisura* (or *hiatus*).

The delicate *pia mater* and *arachnoid mater* comprise the *leptomeninges,* which cover the superficial cortical surfaces of the brain. The pia mater, adherent to the brain surface, follows the convolutions of the sulci and gyri. The arachnoid mater, external to the pia mater, covers the brain surface but follows the dural contours (i.e., it does not extend into the gyri and sulci). The reticulated inner surface of the arachnoid mater has fibers that intermingle with the surface of the pia. Free-flowing cerebrospinal fluid (CSF) is found in the *subarachnoid* space between the arachnoid mater and pia mater. Under normal conditions, the smooth outer surface of the arachnoid mater, overlying dura mater, and calvarial periosteum are in close approximation to each other with no discernible separation (i.e., the "subdural space" and "epidural space" are collapsed potential spaces).[8]

Localization as intra-axial or extra-axial is arguably the critical first step in evaluation of intracranial lesions.

Intra-axial versus Extra-axial

Lesions located within the brain parenchyma are termed *intraparenchymal* or *intra-axial.* It may be helpful for purposes of forming a differential diagnosis to further localize lesions with respect to gray and white matter. Lesions located external to the brain parenchyma are termed *extra-axial.*

Clues to the extra-axial location of a tumor (Fig. 4-3) may include displacement of pial vessels subjacent to the mass, buckling of the gray matter/white matter junction, widening of the adjacent subarachnoid space, a "cleft" of CSF between the brain parenchyma and the mass, a wide base along the dural or calvarial surface, and changes within the adjacent bone such as hyperostosis associated with meningioma (Fig. 4-4) or smooth scalloping associated with epidermoid (Fig. 4-5).[9,10]

Extra-axial lesions may be further characterized by their relationship to the meninges. Depending on the nature of the pathology, different descriptions for subdivisions of the extra-axial space may be used. Extra-axial intracranial *hemorrhage* may be described as subarachnoid, subdural, epidural, or intraventricular. Extra-axial intracranial *masses* are often described as intradural (rarely are they subdivided into subdural or subarachnoid categories), extradural, or intraventricular.

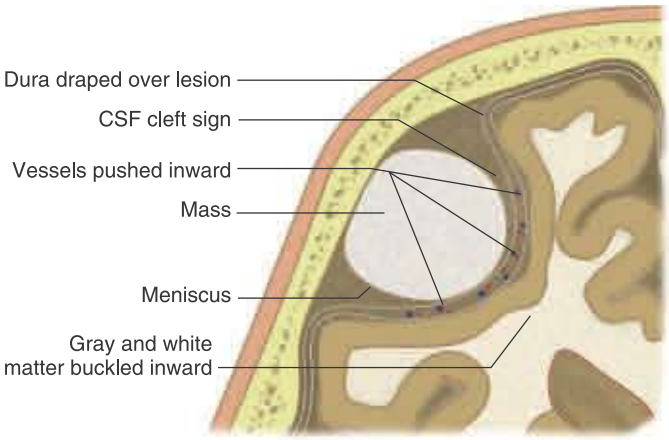

■ **FIGURE 4-3** Clues to extra-axial location of a mass. *(From Grossman RI, Yousem DM [eds]. Neuroradiology Requisites. St. Louis, Mosby, 2004, p 275.)*

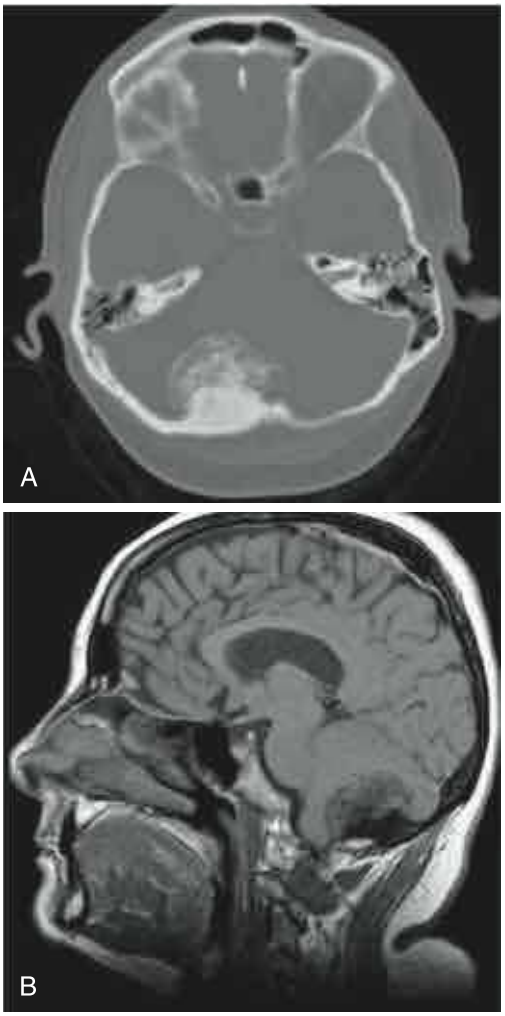

■ **FIGURE 4-4** Posterior fossa meningioma in a 45-year-old woman with chronic headaches. **A,** Noncontrast CT (NCCT) demonstrates hyperostosis of the adjacent right occipital bone as well as calcification/ossification of the mass. **B,** Suggestion of hyperostosis and calcification (T1 lengthening) is evident on sagittal T1W precontrast MR image.

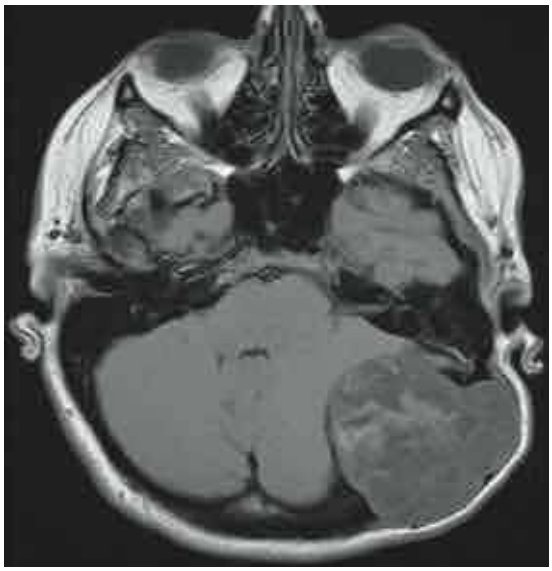

■ **FIGURE 4-5** Posterior fossa epidermoid in a 40-year-old woman with palpable left occipital mass. Axial T1W noncontrast image demonstrates a heterogeneous extra-axial mass extending through the calvaria, with smooth scalloping of bone margins.

■ **FIGURE 4-6** Acute subarachnoid hemorrhage in a 61-year-old woman with acute onset of headache and neck pain. NCCT demonstrates high density within the subarachnoid space, generalized cerebral edema with effacement of sulci, and early hydrocephalus with prominence of the temporal horns.

The *subarachnoid* space, between arachnoid and pia, normally contains CSF. The subarachnoid space (SAS) may be subdivided into the peripheral SAS and the basal cisterns. Subarachnoid hemorrhage may present as high density within these CSF spaces (Fig. 4-6). The *subdural* space, between dura and arachnoid, is normally a potential (collapsed) space. Subdural hematoma results from accumulation of blood products between the dura and arachnoid (Fig. 4-7). The dura is normally adherent to the periosteum of the inner table. Hematomas accumulating between the dura and periosteum are termed *epidural* or *extradural* (Fig. 4-8).

The *intraventricular space* (IVS) may also be considered a subdivision of the extra-axial compartment. The IVS contains CSF and choroid plexus and is lined by ependyma (in contrast

to the peripheral SAS, which is lined by pia and arachnoid). Figure 4-9 demonstrates an intraventricular meningioma. CSF communicates between the IVS and SAS via the foramen of Luschka and choroid fissures.

TYPES OF HERNIATION

Under normal conditions, the brain rests within various compartments created by the rigid dural reflections just described. Brain swelling (cerebral edema) and/or discrete space-occupying lesions (e.g., tumor, hemorrhage) can cause parts of the brain at the margins of these dural reflections to be forced into another compartment. Damage to brain tissue may occur as a result of direct pressure of the herniating part against the dura, as a result of the herniating part causing pressure on another brain part (e.g., brain stem), or as a result of vascular damage as vessels are compressed.[10-12] Prompt reporting of herniation may literally save a patient's life.

■ **FIGURE 4-7** Subdural hematoma in a 63-year-old man with altered mental status. NCCT demonstrates left holohemispheric crescentic mixed density fluid collection with compression and displacement of subjacent brain and effacement of sulci. On the right there is minimal dural thickening, but the dura is closely approximated to the calvarial periosteum.

There are five classic descriptive patterns of herniation[10] (Fig. 4-10). Although these patterns are described as separate entities, different types of herniation may coexist in any given patient. In addition, please note that descriptions of these herniation syndromes slightly vary among authors.

1. *Subfalcine herniation* occurs when supratentorial mass effect is directed medially, causing the cingulate gyrus to shift below the falx cerebri. This is often reported as "midline shift" on CT examinations. The anterior cerebral arteries and internal cerebral veins may be compressed, causing infarcts. If the foramen of Monro is compressed, obstructive hydrocephalus involving one or both lateral ventricles may occur. This is often referred to as "entrapment" of the lateral ventricle(s). The lateral ventricle ipsilateral to the mass effect may be compressed (Fig. 4-11).
2. *Central caudal transtentorial herniation* occurs when supratentorial mass effect displaces the structures of the diencephalon (including the thalamus) and midbrain inferomedially. Obstructive hydrocephalus of the lateral and third ventricles may occur. *Duret's hemorrhage,* almost invariably an ominous sign, may occur within the midbrain and pontine tegmentum, presumably due to compression and shearing of perforating arterioles (Fig. 4-12).[13] Caudal transtentorial herniation usually occurs in the setting of bilateral uncal herniation.
3. *Temporal lobe (uncal) herniation* occurs when supratentorial mass effect displaces the temporal lobe medially and inferiorly over the medial free edge of the tentorium. (Note that some authors refer to this displacement of the uncus as "descending transtentorial herniation," not to be confused with central caudal transtentorial herniation of the thalamus and midbrain.) Uncal herniation may cause compression of the oculomotor nerve (cranial nerve III) with resultant ipsilateral pupillary dilatation, compression or occlusion of the posterior cerebral and anterior choroidal arteries leading to ischemic infarct in these territories, and midbrain compression. The suprasellar and perimesencephalic cisterns may be effaced (Fig. 4-13).
4. *Superior vermian transtentorial herniation* occurs when mass effect within the posterior fossa causes superior

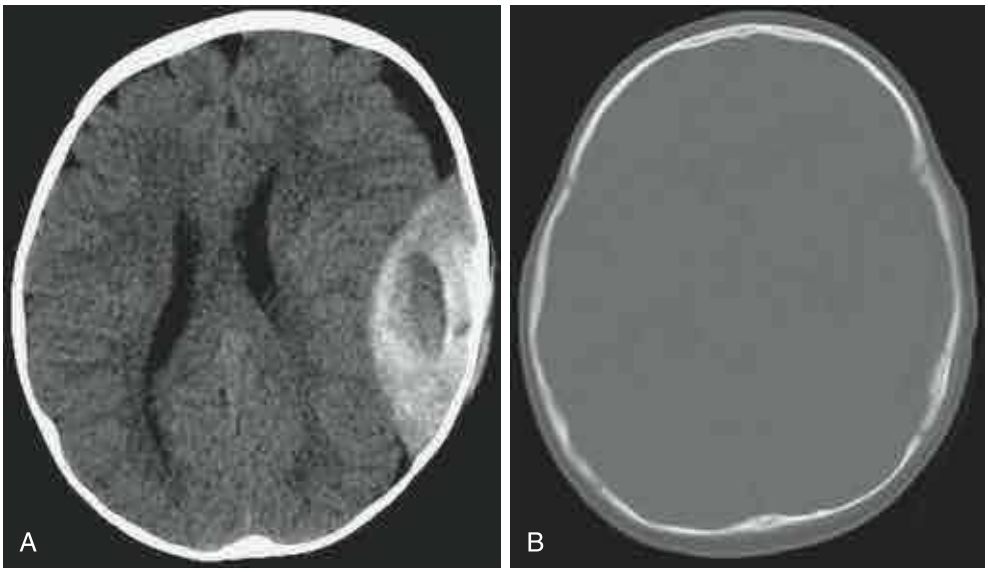

■ **FIGURE 4-8** Acute epidural hematoma in a 6-month-old male infant with vomiting after a fall from a bed. **A** and **B,** NCCT of the brain reveals biconvex hyperdense hematoma with central low density overlying a subtle nondisplaced fracture of the squamous portion of the left temporal bone. Note normal appearance of the patent coronal and lambdoid sutures.

■ **FIGURE 4-9** Intraventricular meningioma in a 73-year-old woman with headache. Preoperative 3D FSPGR post-gadolinium MR image demonstrates an enhancing intraventricular mass, with subtle expansion of the trigone of the left lateral ventricle. Note subtle anterior displacement and enhancement of the choroid plexus.

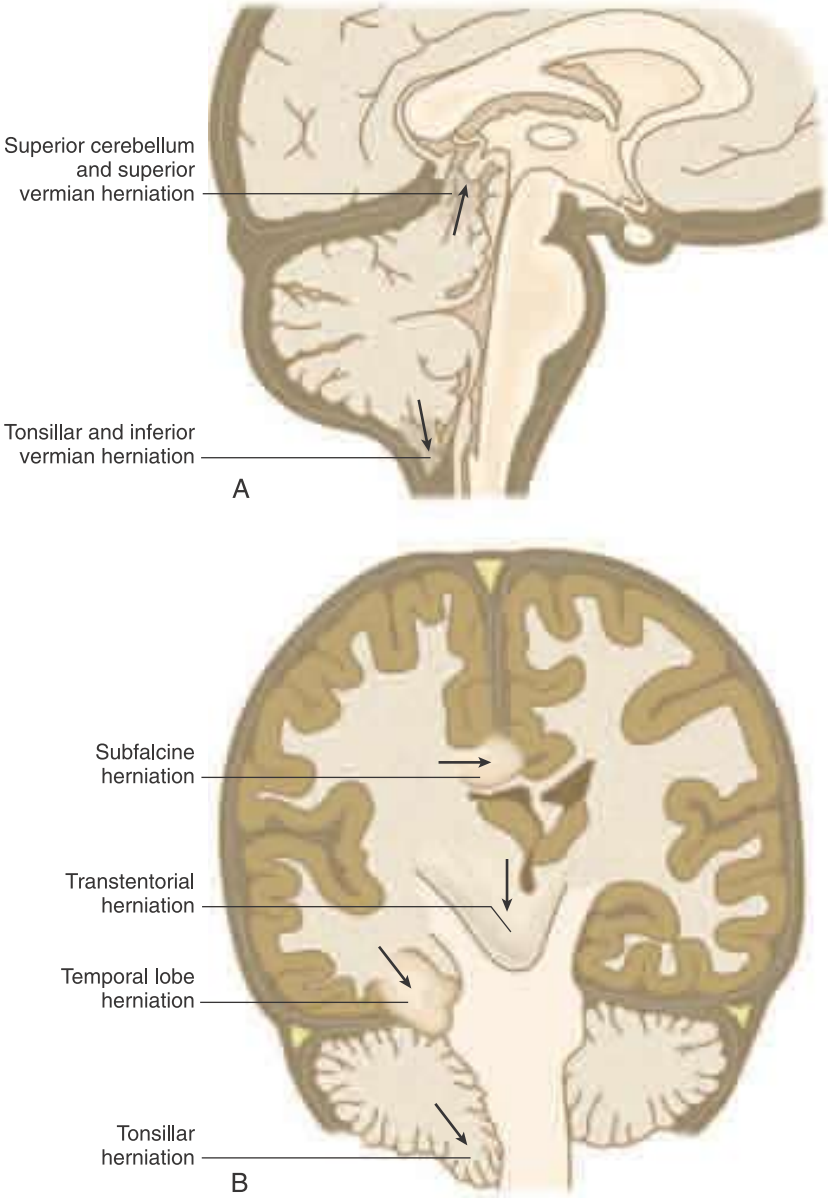

■ **FIGURE 4-10** Herniations of the brain. **A,** Sagittal diagram of cerebellar herniation with the *upper arrow* demonstrating upward herniation of the superior cerebellum and superior vermis and the *lower arrow* demonstrating tonsillar and inferior vermian herniation. **B,** Coronal diagram, from the top downward, subfalcine herniation, central transtentorial herniation, downward transtentorial temporal lobe herniation and tonsillar herniation. Lines of force are demonstrated by the *arrows*. Note the pressure on the brain stem from these herniation patterns. *(From Grossman RI, Yousem DM. Neuroradiology Requisites. St. Louis, Mosby, 2004, p 261.)*

■ **FIGURE 4-11** Subfalcine herniation due to right middle cerebral artery infarct with hemorrhagic transformation in a 34-year-old man. Note compression of ipsilateral lateral ventricle and dilatation of the contralateral lateral ventricle due to entrapment.

■ **FIGURE 4-12** Duret's hemorrhage, due to compression or shearing of perforating arterioles with caudal transtentorial herniation, in an 80-year-old woman with altered mental status and blown right pupil. Also note traumatic left subdural hematoma and obstructive hydrocephalus.

■ **FIGURE 4-13** Isolated left uncal herniation due to glioblastoma multiforme in a 57-year-old man initially presenting with seizure. Effacement of the left perimesencephalic cistern and left aspect of the suprasellar cistern is apparent on NCCT (**A**) but is more conspicuous on MRI (**B** and **C**). Axial T2 MR image (**B**) more clearly shows the extent of mass-like T2 prolongation. Axial T1 FSPGR postcontrast image (**C**) shows the relatively small focus of enhancement in the setting of a much larger nonenhancing abnormality.

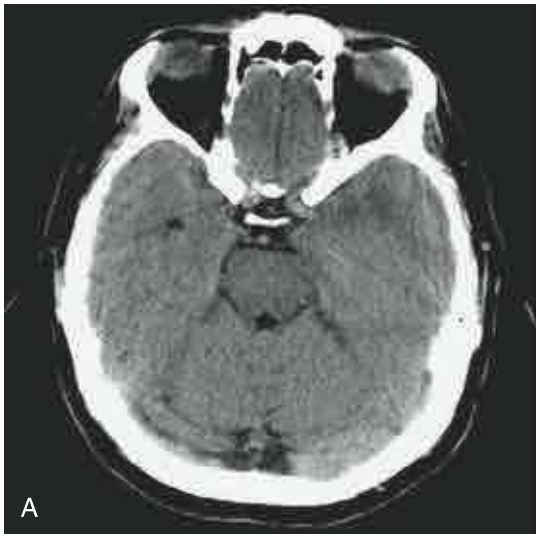

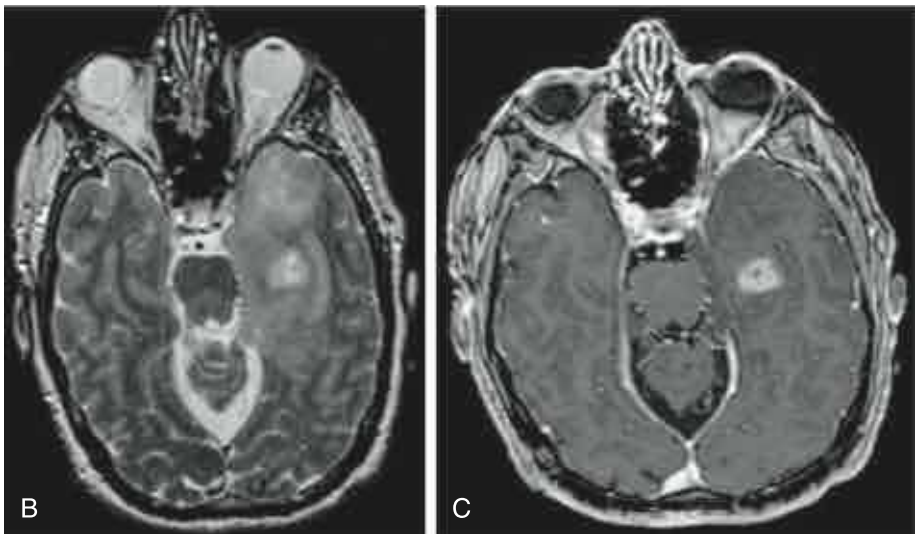

displacement of the vermis through the tentorial incisura, obliterating the superior vermian and quadrigeminal cisterns (Fig. 4-14). The midbrain and pons may be compressed. Obstructive hydrocephalus (typically involving the lateral and third ventricles) may occur if the cerebral aqueduct or fourth ventricle is compressed.[14,15]

5. Cerebellar (inferior tonsillar) herniation most commonly occurs when mass effect within the posterior fossa causes inferior displacement of the cerebellar tonsils through the foramen magnum (Fig. 4-15). This may cause compression of the cervicomedullary junction.[16] Mass effect within the posterior fossa may also cause compression of the fourth ventricle, with resultant obstructive hydrocephalus (typically involving the lateral and third ventricles). If the posterior inferior cerebellar arteries are compressed, cerebellar infarcts may occur.

Other types of herniation include *transalar* herniation and *transcalvarial* herniation.[12] Transalar (L. for "across the wing") refers to displacement of brain across the sphenoid wing or ridge. Transalar herniation may be "descending," involving posteroinferior displacement of the frontal lobe, with possible compromise of the middle cerebral artery, or "ascending," involving anterosuperior displacement of the temporal lobe, with possible compromise of the supraclinoid internal carotid artery. *Transcalvarial* (also known as *external calvarial, extracranial,* or *extracalvarial)* herniation occurs in the presence of an acquired, or much less commonly congenital, cranial defect, usually in the setting of a decompressive craniectomy (Fig. 4-16).

TECHNIQUES

Numerous techniques are available for detection and characterization of mass effect. The two primary imaging modalities, CT

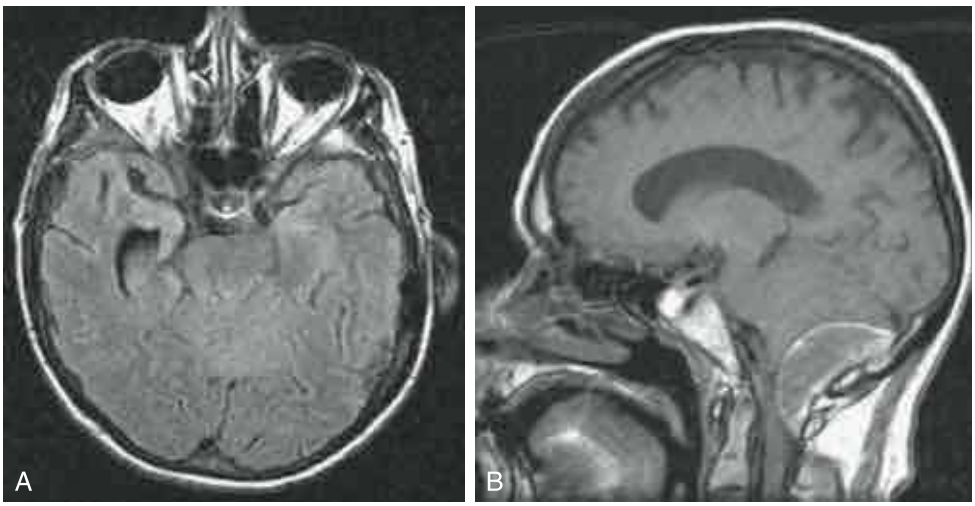

■ **FIGURE 4-14** Superior vermian transtentorial herniation due to posterior fossa epidural hematoma in a 57-year-old woman with new-onset somnolence and remote history of breast cancer. **A,** Axial FLAIR image demonstrates effacement of the superior vermian and quadrigeminal cisterns, with compression of the dorsal pons. **B,** Sagittal T1W MR image demonstrates the epidural hematoma as well as the cisternal effacement.

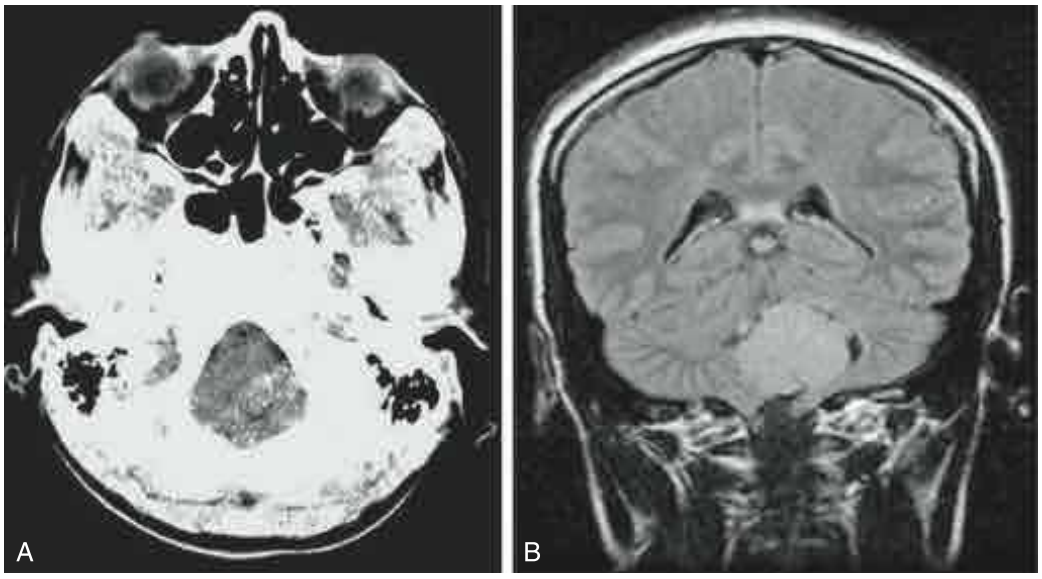

■ **FIGURE 4-15** Bilateral cerebellar tonsillar herniation due to choroid plexus papilloma in a 20-year-old woman presenting to the emergency department with headache. **A,** NCCT demonstrates crowding of the foramen magnum. **B,** Coronal FLAIR image shows downward displacement of the cerebellar tonsils due to a mass within the fourth ventricle.

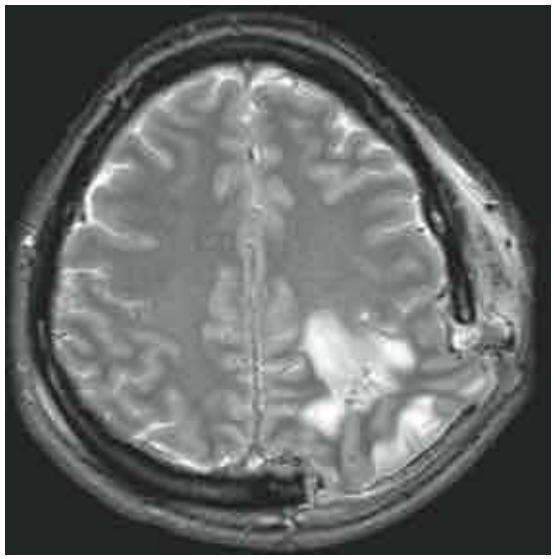

■ **FIGURE 4-16** Transcalvarial herniation after decompressive craniectomy to relieve increased intracranial pressure due to left parietal venous infarct in a 19-year-old woman with postpartum dural venous sinus thrombosis. This type of herniation has sometimes been described as "fungal" owing to its mushroom-like appearance.

and MRI, are discussed here. Each modality has benefits as well as disadvantages. Selection of imaging studies for the care of any particular patient involves weighing risks and benefits in the context of that patient's needs.

CT

Noncontrast CT (NCCT) of the brain is an indispensable tool for neuroradiology. It is often the first examination performed for patients presenting with symptoms of increased intracranial pressure, such as nausea, vomiting, headache, and ataxia. NCCT is useful for detecting (or excluding) the "3 Hs": herniation, hemorrhage, and hydrocephalus. The ready availability and the rapidity of CT are very useful in critically ill patients, who may not tolerate either the wait for or duration of an MRI examination. In addition, CT is the study of choice for evaluation of features such as hyperostosis, bony erosion, and calcification.[17] NCCT is a useful tool for initial detection as well as for follow-up of certain pathologic processes.

Benefits of NCCT include relatively low cost, wide availability, rapid examination and interpretation, high sensitivity for acute intracranial hemorrhage, and excellent bone detail. Drawbacks to NCCT include the use of ionizing radiation, relatively poor soft tissue contrast compared with MRI, and artifacts within the posterior fossa.

In the setting of a negative NCCT of the brain, contrast-enhanced CT (CECT) is rarely indicated.[18,19] However, in patients with an abnormal brain NCCT, or a normal NCCT in certain clinical contexts, further investigation is usually required. Many indications for CECT of the brain have largely been replaced by MRI. However, CECT of the brain may be useful in the acute setting or for patients with contraindications to MRI. The utility of CECT must be weighed against the risks of ionizing radiation and iodinated contrast material.

MRI

With its excellent tissue contrast and characterization and multiplanar ability, MRI is superior to CT for precise intraparenchymal localization and is often superior to CT in defining extra-axial lesions as well. Lack of ionizing radiation is another benefit.

Gadolinium-diethylenetetraminepentaacetic acid (Gd-DTPA)–enhanced MRI has become the study of choice for evaluation of most space-occupying intracranial lesions. Gadolinium-enhanced MRI has been shown to be more sensitive for detection of metastases than enhanced CT, with multiple-dose gadolinium more sensitive than single-dose gadolinium.[20,21] However, recent recognition of a relationship of Gd-DTPA administration to an increased risk of development of nephrogenic systemic fibrosis presents a new challenge for imaging patients with impaired renal function.[22]

In addition to potential gadolinium complications, disadvantages of MRI (both contrast enhanced and noncontrast) include its relatively high cost, lesser availability, and longer acquisition time. The magnetic field presents a contraindication for patients with certain implants and pacemakers, as well as poses a safety hazard when ferromagnetic objects are introduced into the MRI suite.[23,24] A combination of these factors typically makes monitoring of critically ill patients more difficult during MRI than during CT.

ANALYSIS

One of the greatest challenges for the beginning radiologist is developing a comprehensive yet efficient search pattern for any particular study. A checklist of features that should be evaluated on every scan (CT and MRI) is provided. Although not inclusive of everything necessary to interpret studies, it provides a framework for developing a search pattern:

- Herniation
- Midline shift
- Effacement of ventricles, sulci, basilar cisterns, foramen magnum
- Hydrocephalus
- Hemorrhage
- Edema
- Bony changes

Noncontrast CT

Under normal conditions, axial NCCT images of the brain demonstrate a clearly defined midline with bilateral symmetry. The higher density of gray matter is easily differentiated from the lower density of white matter. CSF spaces (ventricles, sulci, basilar cisterns) demonstrate no effacement.

Manifestations of mass effect discernible on NCCT include displacement of brain parenchyma, low-density white matter edema, and effacement of sulci, ventricles, and basilar cisterns. Various herniation syndromes and their complications, such as ischemic infarct, may be diagnosed by NCCT. CT is the study of choice for evaluation of fine bony detail. Hyperostosis (e.g., meningioma) as well as scalloping and thinning (e.g., epidermoid) are usually better demonstrated on CT than MRI (see Fig. 4-4).

Contrast-Enhanced CT

Although indications for CECT have largely been supplanted by MRI, CECT is still commonly performed. Abnormal contrast enhancement of intracranial lesions increases their conspicuity. In addition, *normal* contrast enhancement of vascular structures may increase conspicuity of otherwise subtle or confusing intracranial lesions. For example, subdural hematoma may be more easily differentiated from brain parenchyma when the cortical veins are opacified (Fig. 4-17).

MRI

With its multiplanar capability and superior soft tissue contrast, MRI has largely replaced CT as the imaging modality of choice for evaluation of intracranial mass lesions.

The superior soft tissue contrast of MRI allows for more precise localization of both intra-axial and extra-axial lesions. In addition, the relationships of intracranial masses to vital structures (e.g., the relationship of parasagittal meningioma to the dural venous sinuses) are usually better evaluated on MRI. Herniation and hydrocephalus are readily identified and evaluated. Extent of edema (manifest as FLAIR and T2 hyperintensity) is also well demonstrated. Although also sometimes discernible on CT, different degrees of mass effect (focal, local, and regional) are optimally evaluated by MRI (Figs. 4-18 to 4-20).

Sample reports are presented in Boxes 4-1 and 4-2.

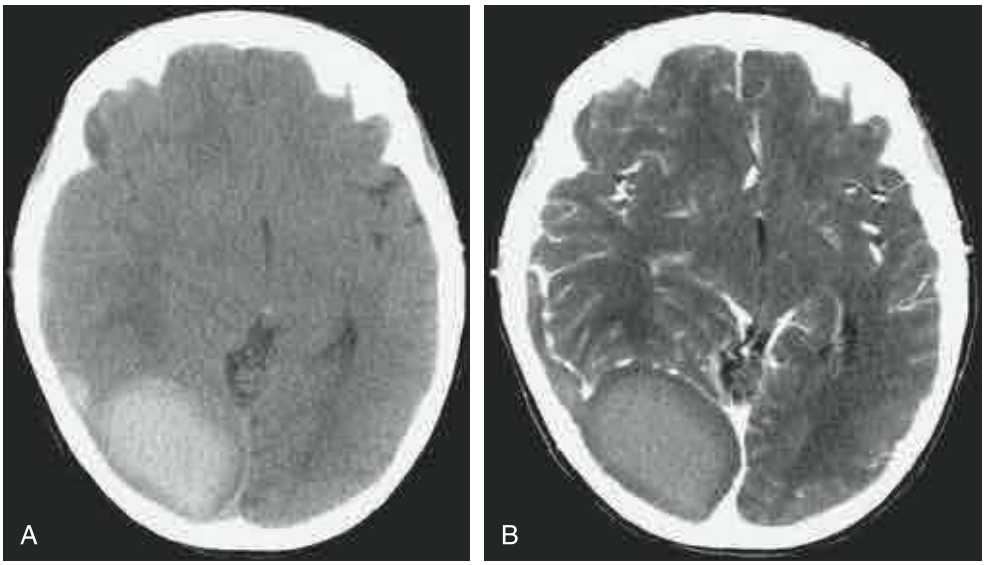

■ **FIGURE 4-17** Right parieto-occipital hematoma in a 20-year-old coagulopathic comatose woman with multisystem organ failure. **A,** NCCT reveals high density consistent with blood products. Localization of the hematoma as intra-axial or extra-axial is difficult on NCCT. **B,** CECT demonstrates displacement of cortical veins and buckling of cortex, clearly identifying the hematoma as extra-axial. Also note subfalcine herniation and generalized cerebral edema with sulcal effacement.

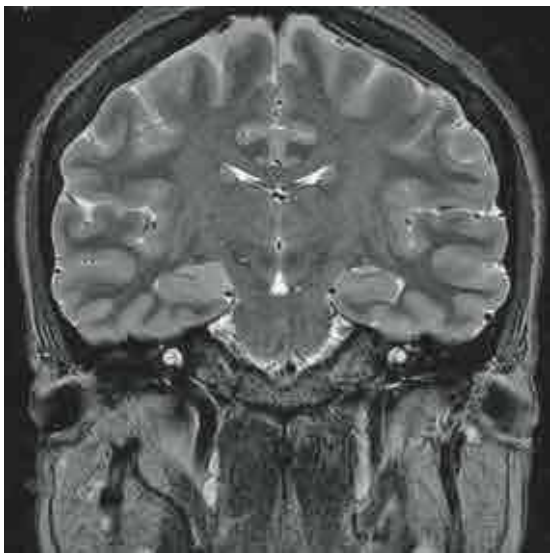

■ **FIGURE 4-18** Focal mass effect in a 30-year-old woman with seizures. Coronal T2W inversion recovery image reveals a focal mass, isointense to cortex, arising from the fimbria of the right hippocampus, with focal mass effect effacing the right choroid fissure. This mass was stable over 18 months of follow-up and is presumed to represent a low-grade glioma or hamartoma. Note lack of edema and lack of displacement of adjacent brain parenchyma.

BOX 4-1 Sample Report: Noncontrast CT of the Brain

PATIENT HISTORY

A 6-month-old presented after a fall.

COMPARISON STUDIES

None was available.

TECHNIQUE

CT with 5-mm contiguous transaxial images was performed from the skull base to the vertex without intravenous administration of a contrast agent (see Fig. 4-8).

FINDINGS

A left convexity extra-axial hemorrhagic collection, with lentiform shape, was found, suggestive of epidural hematoma. The hematoma demonstrates mixed densities, consistent with acute to subacute stage. There is an associated nondisplaced left temporal bone fracture involving the squamous portion. No other areas of hemorrhage are seen. The epidural hematoma exerts mass effect on the adjacent brain parenchyma. One centimeter of left-to-right midline shift is present. No areas of vascular infarct are evident. The gray matter/white matter differentiation is preserved.

IMPRESSION

A left convexity epidural hematoma measuring 3 cm transverse, with associated nondisplaced left temporal bone fracture involving the squamous portion, exerts mass effect on the adjacent frontotemporal lobe, with 1 cm of left-to-right subfalcine herniation.

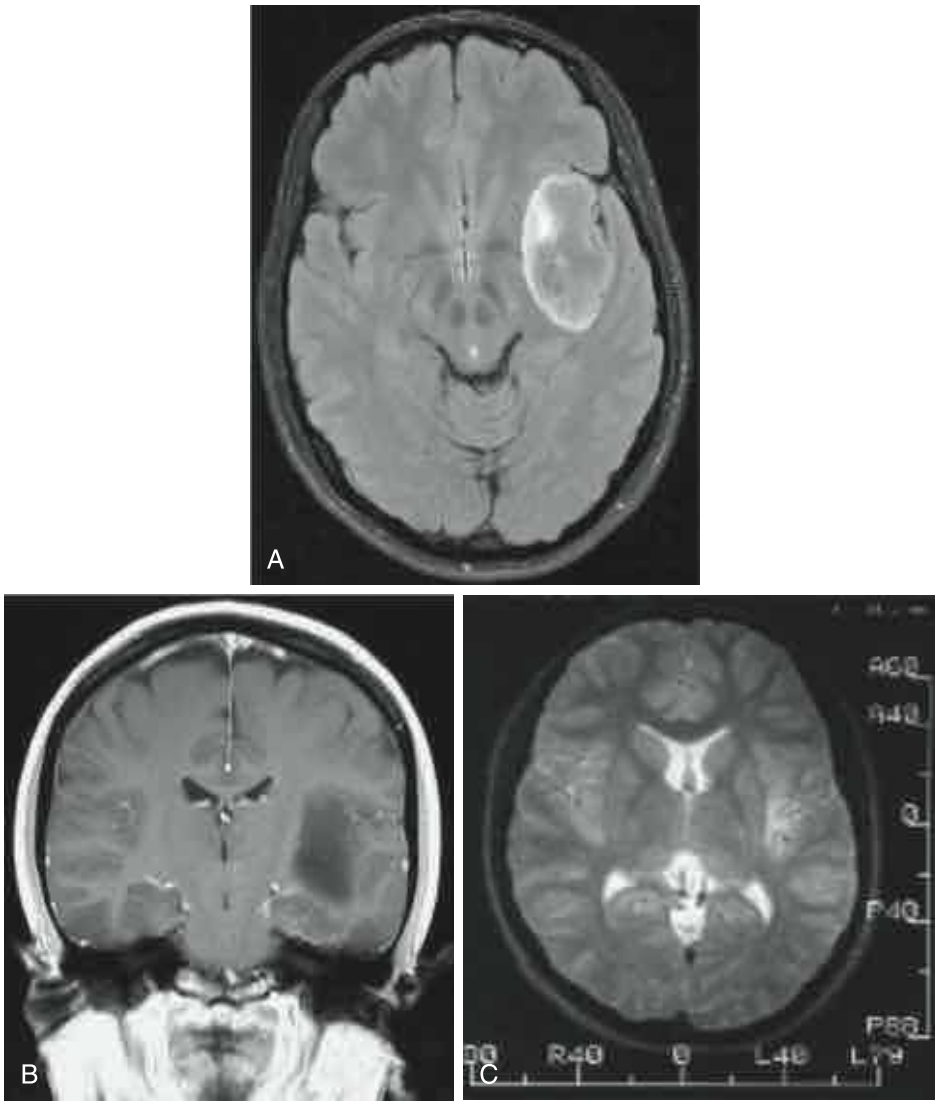

■ **FIGURE 4-19** A 32-year-old woman presented with left-sided weakness. Axial FLAIR (**A**) and coronal T1W postcontrast (**B**) MR images demonstrate an expansile mass centered within the left insula, with minimal if any enhancement. At surgery, pathologic process was grade 2 astrocytoma. Note subtle local mass effect on the adjacent brain parenchyma but no edema and no subfalcine, uncal, or descending transtentorial herniation (compare with patient in Fig. 4-20). **C,** Axial T2W MR image from the same patient 19 years earlier; she underwent MRI at 13 years old for workup of dizziness. Note the subtle asymmetric T2 prolongation within the left insular cortex and subinsular white matter.

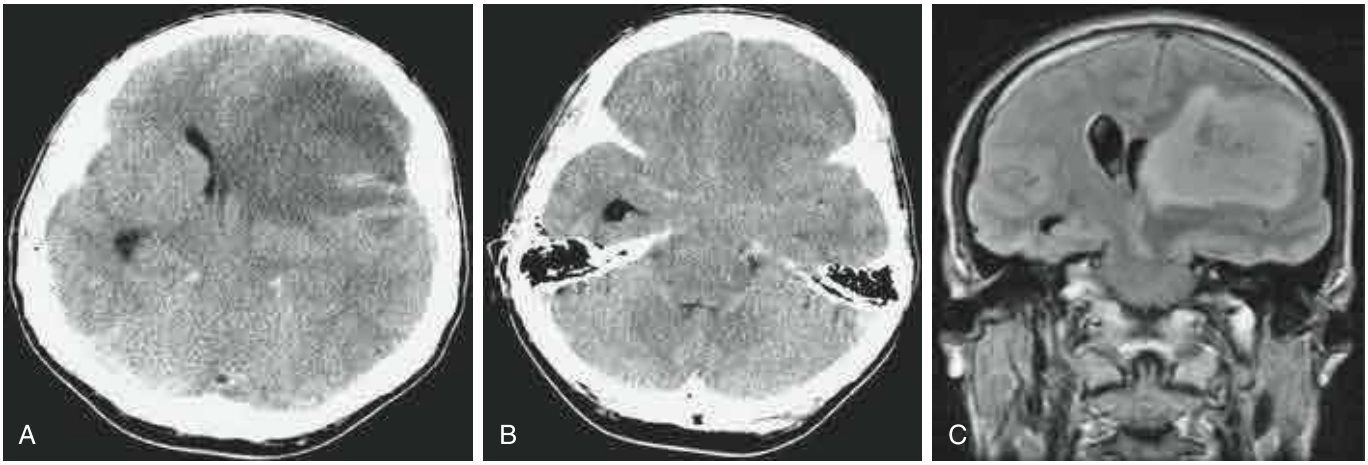

■ **FIGURE 4-20** Regional mass effect due to left frontal glioblastoma multiforme. A 31-year-old man presented to the emergency department with headache. NCCT images (**A** and **B**) and coronal FLAIR MR image (**C**) demonstrate a heterogeneous left frontal mass with subfalcine, uncal, and descending transtentorial herniation as well as entrapment of the left lateral ventricle.

BOX 4-2 Sample Report: MRI of the Brain

PATIENT HISTORY

A 53-year-old man presented with seizure and abnormal NCCT.

COMPARISON STUDY

NCCT of brain was done, but there was no previous MRI.

TECHNIQUE

The following sequences were used to image the brain on a 1.5-T magnet with fiducial markers in position: sagittal FSPGR, axial diffusion, axial FLAIR, axial 3D SPGR postcontrast and postcontrast axial 3D FSE T2 (see Fig. 4-13).

CONTRAST AGENT

Magnevist, 14 mL (0.1 mmol/kg; 0.2 mL/kg)

FINDINGS

An extensive amount of abnormal T2 prolongation and associated mass effect are identified within the mesial left temporal lobe with involvement of the left hippocampus and extension into the left parahippocampal gyrus. A more focal area of slightly less T2 prolongation is centered in the left hippocampus where irregular enhancement is noted after administration of the contrast agent. The remainder of the T2 abnormality is nonenhancing. This abnormal enhancement extends along the ependymal surface of the adjacent left temporal horn. There is associated uncal herniation and midbrain compression without evidence of transtentorial herniation. The ventricles are normal in size without hydrocephalus.

Several scattered foci of subcortical T2 prolongation are noted bilaterally, most likely representing small vessel ischemic disease. There are no areas of reduced diffusion to suggest acute ischemia. The major intracranial vessels are patent.

IMPRESSION

There is extensive abnormal T2 prolongation and associated mass effect within the left mesiotemporal lobe consistent with an infiltrative neoplasm. A more focal area of slightly less T2 prolongation centered in the left hippocampus is associated with irregular enhancement and is highly suggestive of an area of anaplastic transformation. Abnormal enhancement also extends along the ependyma of the adjacent right temporal horn.

KEY POINTS

- Mass effect causes compression, displacement, or distortion of intracranial structures.
- NCCT is a useful tool for screening or follow-up of mass effect.
- CE MRI is the imaging study of choice for definitive characterization of intracranial masses.

SUGGESTED READINGS

Andrews PJ, Citerio G. Intracranial pressure: I. Historical overview and basic concepts. Intensive Care Med 2004; 30:1730-1733.

Citerio G, Andrews PJ. Intracranial pressure: II. Clinical applications and technology. Intensive Care Med 2004; 30:1882-1885.

Fisher CM. Brain herniation: a revision of classical concepts. Can J Neurol Sci 1995; 22:83-91.

Johnson PL, Eckard DA, et al. Imaging of acquired cerebral herniations. Neuroimaging Clin North Am 2002; 12:217-228.

Neff S, Subramaniam RP. Monro-Kellie doctrine. J Neurosurg 1996; 85:1195.

REFERENCES

1. Haddad FS, Hajjar J. [Pneumoventriculography in the localization of intracranial tumors]. Rev Med Moyen Orient 1956; 13:77-78.
2. Roberson GH, Taveras JM, Tadmor R, et al. Computed tomography in metrizamide cisternography—importance of coronal and axial views. J Comput Assist Tomogr 1977; 1:241-245.
3. Marmarou A, Signoretti S, Aygok G, et al. Traumatic brain edema in diffuse and focal injury: cellular or vasogenic? Acta Neurochir Suppl 2006; 96:24-29.
4. Marmarou A. A review of progress in understanding the pathophysiology and treatment of brain edema. Neurosurg Focus 2007; 22:E1.
5. Monro A. Observations on Structure and Functions of the Nervous System. Edinburgh, Creech and Johnson, 1783.
6. Mokri B. The Monro-Kellie hypothesis: applications in CSF volume depletion. Neurology 2001; 56:1746-1748.
7. Lakin WD, Stevens SA, Tranmer BI, Penar PL. A whole-body mathematical model for intracranial pressure dynamics. J Math Biol 2003; 46:347-383.
8. Greenberg RW, Lane EL, Cinnamon J, et al. The cranial meninges: anatomic considerations. Semin Ultrasound CT MR 1994; 15:454-465
9. Young RJ, Knopp EA. Brain MRI: tumor evaluation. J Magn Reson Imaging 2006; 24:709-724.
10. Grossman RI, Yousem DM. Neuroradiology: The Requisites, 2nd ed. Philadelphia, Mosby, 2003.
11. Castillo M. Neuroradiology: Core Curriculum. Philadelphia, Lippincott Williams & Wilkins, 2002.
12. Laine FJ, Shedden AI, Dunn MM, Ghatak NR. Acquired intracranial herniations: MR imaging findings. AJR Am J Roentgenol 1995; 165:967-973.
13. Parizel PM, Makkat S, Jorens PG, et al. Brainstem hemorrhage in descending transtentorial herniation (Duret hemorrhage). Intensive Care Med 2002; 28:85-88.
14. Hahn FJ, Witte RJ. CT signs of ascending transtentorial cerebellar herniation. J Comput Assist Tomogr 1989; 13:1091-1092.
15. Cuneo RA, Caronna JJ, Pitts L, et al. Upward transtentorial herniation: seven cases and a literature review. Arch Neurol 1979; 36:618-623.
16. Ishikawa M, Kikuchi H, Fujisawa I, Yonekawa Y. Tonsillar herniation on magnetic resonance imaging. Neurosurgery 1988; 22:77-81.

17. Loevner LA. Imaging features of posterior fossa neoplasms in children and adults. Semin Roentgenol 1999; 34:84-101.
18. Chishti FA, Al Saeed OM, Al-Khawari H, Shaikh M. Contrast-enhanced cranial computed tomography in magnetic resonance imaging era. Med Princ Pract 2003; 12:248-251.
19. Branson HM, Doria AS, Moineddin R, Shroff MM. The brain in children: is contrast enhancement really needed after obtaining normal unenhanced CT results? Radiology 2007; 244:838-844.
20. Kuhn MJ, Hammer GM, Swenson LC, et al. MRI evaluation of "solitary" brain metastases with triple-dose gadoteridol: comparison with contrast-enhanced CT and conventional-dose gadopentetate dimeglumine MRI studies in the same patients. Comput Med Imaging Graph 1994; 18:391-399.
21. Akeson P, Larsson EM, Kristoffersen DT, et al. Brain metastases—comparison of gadodiamide injection–enhanced MR imaging at standard and high dose, contrast-enhanced CT and non-contrast-enhanced MR imaging. Acta Radiol 1995; 36:300-306.
22. Broome DR, Girguis MS, Baron PW, et al. Gadodiamide-associated nephrogenic systemic fibrosis: why radiologists should be concerned. AJR Am J Roentgenol 2007; 188:586-592.
23. Price RR. The AAPM/RSNA physics tutorial for residents. MR imaging safety considerations. Radiological Society of North America. RadioGraphics 1999; 19:1641-1651.
24. Colletti PM. Size "H" oxygen cylinder: accidental MR projectile at 1.5 Tesla. J Magn Reson Imaging 2004; 19:141-143.

CHAPTER 5

Patterns of Contrast Enhancement

James G. Smirniotopoulos, Alice B. Smith, John H. Rees, and Frances M. Murphy

Contrast material has been essential to cross-sectional neuroimaging for almost 4 decades. The first intravascular contrast agents were U.S. Food and Drug Administration (FDA)–approved urographic and angiographic iodine-based compounds for parenteral injection. Modern iodine-based agents for CT are now usually low- and iso-osmolar compounds designed to lower the frequency of side effects and provide a higher safety margin. Multiple gadolinium-based contrast agents have been developed, and six have been approved by the FDA for intravascular injection for contrast-enhanced MRI: Vasovist Injection; Magnevist; MultiHance; Omniscan; OptiMARK; and ProHance.

In the central nervous system (CNS) contrast enhancement is produced by two related, yet independent, processes: interstitial (extravascular) enhancement and vascular (intravascular) enhancement.[1,2] The brain, spinal cord, and nerves are supplied by capillaries that have a selectively permeable membrane that creates a "blood-brain barrier." This selective barrier protects the nervous system from certain plasma proteins and limits inflammation by blocking inflammatory cells from entering the tissue. The primary structure of the blood-brain barrier is from endothelial cell specialization produced by cooperation between these cells and the astrocyte foot processes. The normal blood-brain barrier includes a continuous basement membrane, narrow intercellular gaps with junctional complexes, and only rare pinocytosis. The normal intact blood-brain barrier is far more permeable to lipophilic compounds (as measured by octanol/water partition fraction), and the blood-brain barrier retards lipophobic compounds. Some "desirable" compounds, such as glucose, are facilitated to cross the vessel wall or are actively transported out of the vessel and into the tissue compartment. Vascular enhancement is a combined product of blood volume, blood flow (delivery of contrast agent or "wash-in"), and "mean transit time" or time needed for "washout" of a contrast agent. In addition to neovascularity, which increases both blood volume and blood flow, vasodilatation of existing normal vessels (hyperemia) produces increased intravascular enhancement.

Parenteral contrast material is usually injected into a large peripheral vein, either slowly by a drip infusion or more rapidly by a short duration or bolus injection. A pressure injector may be used. When a contrast agent is injected as a bolus, the blood level rapidly rises to a peak concentration that pushes the contrast agent against the capillary endothelial membrane. If that capillary membrane is permeable to the contrast agent, it will rapidly leave the vessel and diffuse into the perivascular interstitial fluid space, driven by the concentration gradient. The higher the gradient, the greater the diffusion out of the vessel; thus, giving a double or triple dose of a contrast agent will increase enhancement. The spinal cord, brain, and spinal nerves have specialized capillary vessels with a blood-brain barrier, giving them special properties of selective permeability. Extravascular or interstitial enhancement will also depend on the permeability of these capillaries to the chosen agent. If you "choose wisely," enhancement will occur only in tissues without an intact blood-brain barrier. Interstitial enhancement is related to alterations in the permeability of the blood-brain barrier, whereas intravascular enhancement is proportional to increases in blood flow or blood volume. On CT, intravascular and interstitial enhancement may be seen simultaneously. When rapid dynamic CT images are obtained, as in CT angiography, most of the observed enhancement is intravascular. When CT is delayed for 10 to 15 minutes after a bolus infusion, most of the observed enhancement is interstitial. At intermediate times, or with a continuous drip infusion of contrast material, enhancement is a composite variable mixture of both intravascular and interstitial compartments.

MRI after administration of a contrast agent has several important differences, as compared with CT enhancement. Many MR pulse sequences create a "flow void phenomena"; thus, high-flow lesions such as aneurysms and vascular shunts (e.g., arteriovenous malformations) will have very low signal intensity.[3] The aneurysmal dilation of the vein of Galen, dural and pial fistulas, and the more common arteriovenous malformations will show as spherical, tubular, or serpentine signal voids.

The enhancement on MRI from blood-brain barrier breakdown and leakage of gadolinium out of the vessel requires a substrate of mobile water. Relative "dry" tissues, such as bone and normal dura, have very little interstitial free water. These tissues do not enhance well with gadolinium on routine T1-weighted (T1W) MR images—the gadolinium is in the tissues, but we cannot see a signal change without the water. This can be confusing, for example, when comparing an enhanced CT scan in which the falx and tentorium are brightly enhanced with an MR image in which there is only patchy and discontinuous enhancement.

Many different physiologic and pathologic conditions demonstrate contrast enhancement. Angiogenesis and neovascularity in neoplastic masses, breakdown of the blood-brain barrier in both infectious and noninfectious inflammation, physiologic changes from cerebral ischemia, and capillary pressure overload (eclampsia and hypertension) will all affect the blood-brain barrier and increase permeability. A paralysis of autoregulation—the primary cause of "malignant brain edema"—is actually a reactive hyperemia and will enhance on MRI, CT, and even at angiography. The newly created vessels from tumor angiogenesis will increase both blood volume and blood flow as compared with contralateral normal brain tissue. There will also be a short mean transit time.

All of these processes can produce enhancement on conventional angiograms, conventional T1W gadolinium-enhanced MR images, and iodine-enhanced CT scans. The old-fashioned "early draining vein" on the arteriogram is a direct correlate of the shortened mean transit time that can be calculated on perfusion MR and CT examinations.

EXTRA-AXIAL ENHANCEMENT

Extra-axial enhancement in the CNS may be classified as either pachymeningeal or leptomeningeal. The pachymeninges (from the Greek for "thick" meninges) are the dura mater, which comprises two fused membranes derived from the embryonic meninx primativa: the periosteum of the inner table of the skull and a meningeal layer. Pachymeningeal enhancement may be manifested up against the bone, or it may involve the dural reflections of the falx cerebri, tentorium cerebelli, falx cerebelli, and cavernous sinus. The leptomeninges (Greek for "skinny" meninges) are the pia and arachnoid. Leptomeningeal enhancement may occur on the surface of the brain or in the subarachnoid space. Because the normal, thin arachnoid membrane is attached to the inner surface of the dura mater, the pachymeningeal pattern of enhancement is also described as *dura-arachnoid enhancement* (Fig. 5-1). In comparison, enhancement on the surface of the brain is called pial or *pia-arachnoid enhancement.* The enhancement follows along the pial surface of the brain and fills the subarachnoid spaces of the sulci and cisterns. This pattern is often referred to as leptomeningeal enhancement and is usually described as having a "gyriform" or "serpentine" appearance.

Pachymeningeal or Dura-Arachnoid Enhancement

Because the vessels supplying the dura do not have a blood-brain barrier, both endogenous and exogenous compounds (e.g., albumin, hemosiderin, contrast agents) readily leak into the interstitial space. Enhancement of the dura is normal on CT, typically uniform in the falx and tentorium. Enhancement of the dura against the skull is not readily noticed because of the adjacent dense white line of the cortical bone of the inner table of the skull. In contrast, on contrast-enhanced T1W MR images, the normal dura shows only thin, linear, and discontinuous enhancement.[4]

A variety of processes may accentuate dural enhancement, including vasocongestion and intradural edema, both of which may be nonspecific reactions to a wide variety of benign or malignant processes, including transient postoperative changes, intracranial hypotension (Fig. 5-2), neoplasms such as meningiomas, metastatic disease (from breast and prostate cancer), secondary CNS lymphoma, and granulomatous disease. Because of the Monro-Kellie doctrine,[5] when the cerebrospinal fluid pressure drops, there may be secondary fluid shifts that increase the volume of capacitance veins in the subarachnoid space. After neurosurgical intervention, even the placement of a shunt catheter or intracranial pressure bolt, meningeal enhancement is very frequent and occurs in a majority of patients. The postoperative enhancement may be pachymeningeal (dura-arachnoid) or leptomeningeal (pia-arachnoid)[6] and can be localized to the side of the procedure or diffuse (bilateral, supratentorial and infratentorial). Extra-axial enhancement may also occur after uncomplicated lumbar puncture in about 5% of patients.[7] Patients with spontaneous intracranial hypotension, with or

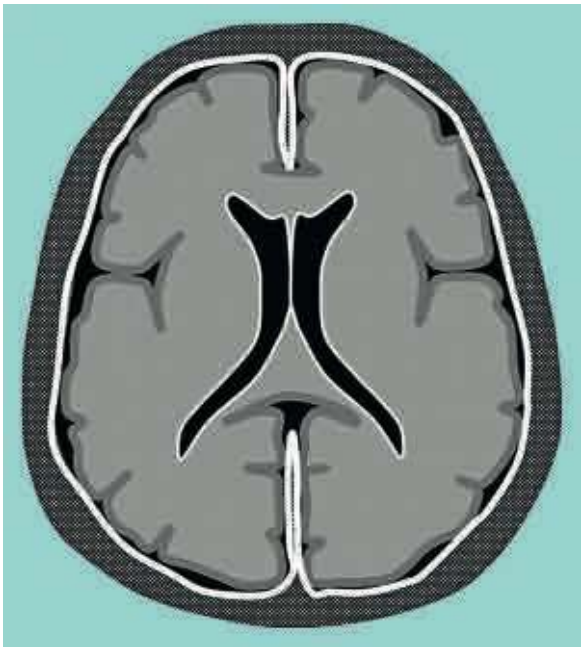

■ **FIGURE 5-1** Schematic diagram of dura-arachnoid enhancement on MRI. This is also called pachymeningeal enhancement. *(From Smirniotopoulos JG, Murphy FM, Rushing EJ, et al. Patterns of contrast enhancement in the brain and meninges. RadioGraphics 2007; 27:525-551.)*

■ **FIGURE 5-2** Coronal T1W MR gadolinium-enhanced image of idiopathic intracranial hypotension. There is diffuse, smooth, and linear dura-arachnoid enhancement. Although veins may also enhance normally, there should be no other subarachnoid enhancement.

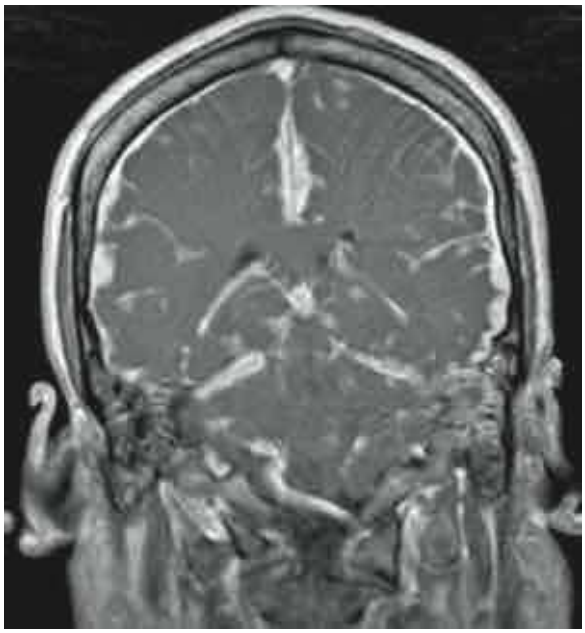

■ **FIGURE 5-3** Coronal T1W MR gadolinium-enhanced image of dural sarcoid. There is grossly abnormal diffuse thickening and enhancement of the dura including both the falx and the tentorium.

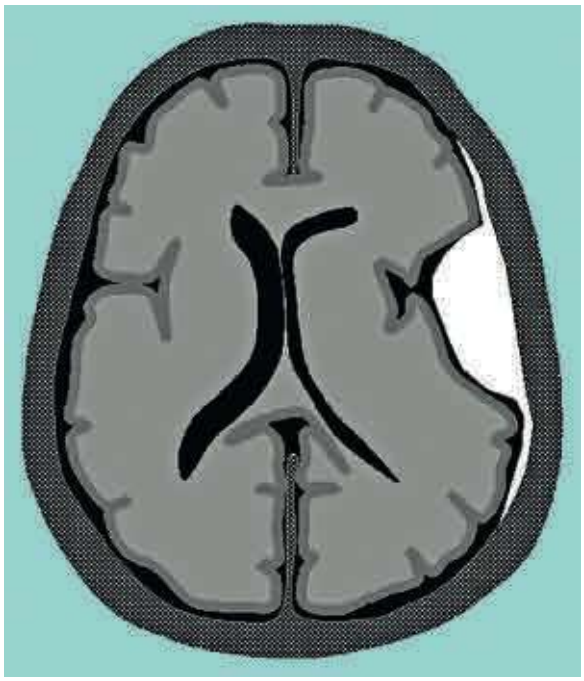

■ **FIGURE 5-4** Schematic diagram of dural-based enhancement limited to a mass growing against the inner table of the skull. This is a typical pattern for a meningioma, with linear tapering enhancement from the "dural tail." *(From Smirniotopoulos JG, Murphy FM, Rushing EJ, et al. Patterns of contrast enhancement in the brain and meninges. RadioGraphics 2007; 27:525-551.)*

without a cerebrospinal fluid leak, may show generalized diffuse pachymeningeal enhancement.[4,8,9] Prolonged intracranial hypotension may lead to vasocongestion and interstitial edema in the dura mater, findings similar to those seen in the dural tail of a meningioma. Rarely, a skull fracture may cause a cerebrospinal fluid leak and intracranial hypotension. More often intracranial hypotension may be related to a (seemingly) uncomplicated lumbar puncture. However, in most cases no definitive cause is ever found, and it is described as "idiopathic" intracranial hypotension.

MRI is relatively sensitive and specific in the detection of benign or spontaneous intracranial hypotension. A typical clinical feature of spontaneous intracranial hypotension is a headache that is orthostatic (postural) and worse when the patient is upright. Imaging findings include thickened dura with linear enhancement of the pachymeninges both above and below the tentorium, no enhancement of the sulci or brain surface, enlargement of the pituitary gland, and descent of the brain (low cerebellar tonsils and downward displacement of the iter of the third ventricle below the tentorial incisura line).[9] Some patients may have additional features of subdural effusions or even subdural hemorrhage. Other features of intracranial hypotension include dural thickening and an enlarged pituitary gland. Leptomeningeal enhancement (within the sulci) may be seen postoperatively but is not common with spontaneous intracranial hypotension and could suggest leptomeningitis, either inflammatory or neoplastic.

Extra-axial neoplasms may produce pachymeningeal enhancement. The most common primary dural neoplasm is meningioma, a benign tumor of meningothelial cells (Figs. 5-3 and 5-4). Meningiomas are slow-growing, well-localized, World Health Organization (WHO) grade 1 lesions that are usually resectable for cure.[10-12] They typically manifest in patients in the fourth to sixth decades of life, and they are roughly twice as common in women as in men. The typical meningioma is a localized lesion with a broad base of dural attachment (see Fig. 5-5B). This neoplasm actually arises from the arachnoid membrane that is attached to the inner layer of the dura mater. Even in the early days of CT, the accuracy of cross-sectional imaging in the detection and characterization of meningioma was very good.[13] Contrast-enhanced MRI demonstrates a new finding (one not observed at CT): the dural tail or "dural flare." The dural tail is a curvilinear region of dural enhancement adjacent to the bulky hemispheric tumor (Figs. 5-5 to 5-7; see also Fig. 5-4).[14-16] The finding was originally thought to represent dural infiltration by tumor, and resection of all enhancing dura mater was thought to be appropriate.[17] Several studies have confirmed that in most cases of meningioma, linear dural enhancement is most likely a reactive process[18] rather than neoplastic, especially when it was more than a centimeter away from the bulky part of the tumor. The dural reaction may include a combination of increased extravascular spaces as well as small vessel vasocongestion. Both will thicken the dura, and the increased interstitial water allows visualization of contrast enhancement (see Fig. 5-5) because even normal dural capillaries do not form a blood-brain barrier. In addition to primary dural neoplasms, such as meningioma, hemangiopericytoma, and solitary fibrous tumor, metastases are possible. In women, breast carcinoma can cause a solitary dural metastasis; and in men, prostate cancer can do the same. Secondary CNS lymphoma is usually extra-axial and may be dural based or fill the subarachnoid space. Granulomatous inflammatory and infectious diseases including sarcoid, tuberculosis, Wegener's granulomatosus, luetic gummas, rheumatoid nodules, and fungal disease produce pachymeningeal enhancement usually involving the basilar meninges, including the suprasellar cistern and vessels of the circle of Willis. Sarcoid may produce focal or diffuse dural thickening (see Fig. 5-3).

Leptomeningeal or Pia-Arachnoid Enhancement

When the abnormal enhancement extends into the subarachnoid spaces of the sulci and cisterns it is called leptomeningeal or "pia-arachnoid" enhancement. Bacterial, viral, and even fungal meningitides may cause leptomeningeal enhancement (Fig. 5-8). The primary mechanism for this enhancement is a breakdown

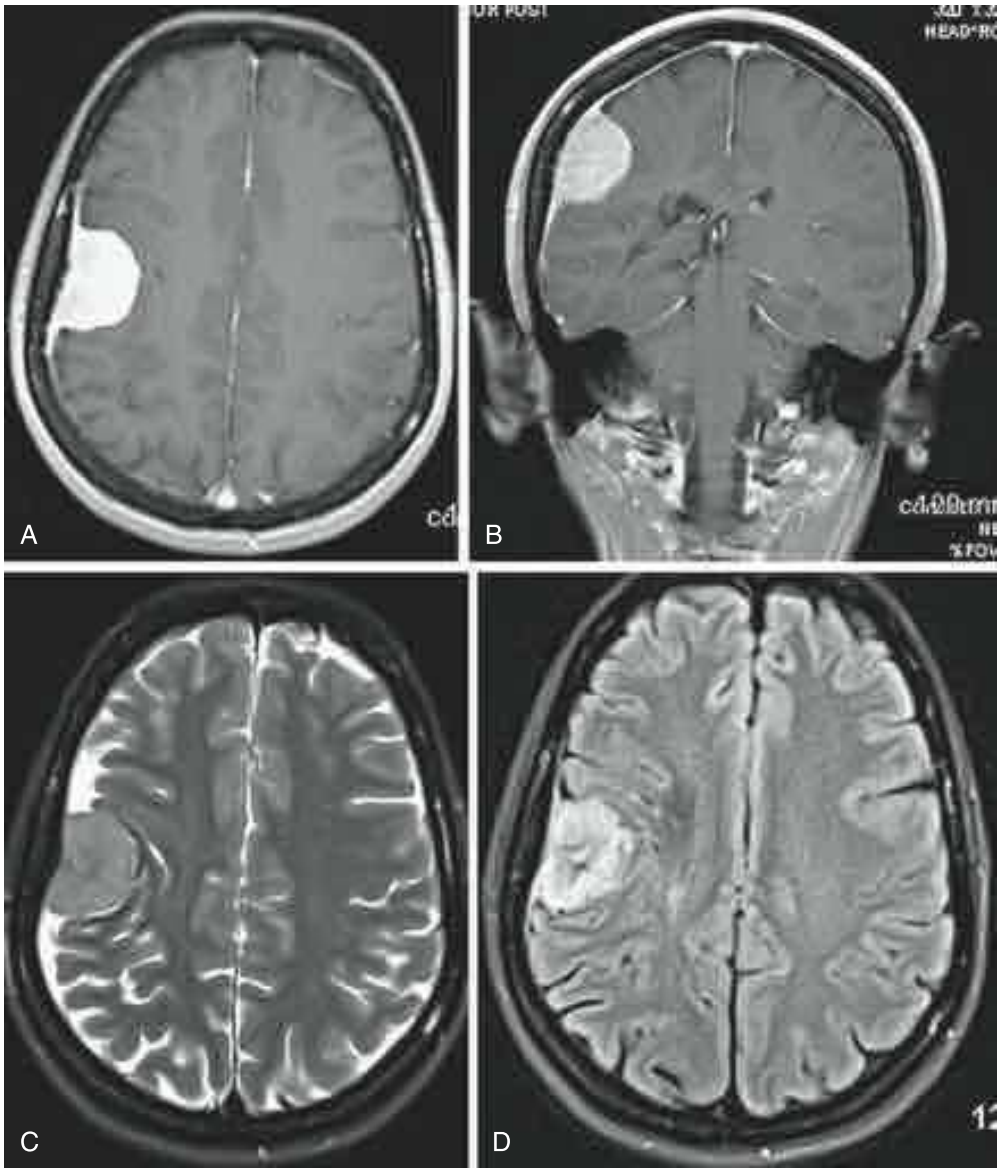

■ **FIGURE 5-5** Axial (A) and coronal (B) T1W MR gadolinium-enhanced images of a meningioma. There is a brightly enhancing dural-based mass with a hemispheric shape. A long area of tapering linear enhancement—"dural tail"—extends away from the central bulky mass. Most of this linear enhancement is reactive rather than neoplastic. Axial T2W (C) and FLAIR (D) images show clearly that the lesion is extra-axial.

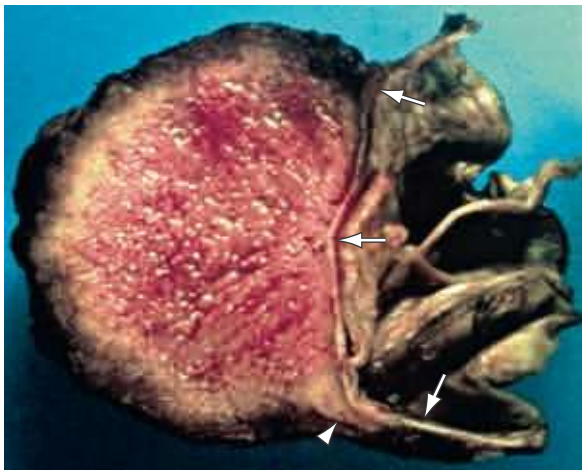

■ **FIGURE 5-6** Meningioma. The specimen has been cut in half, showing a hemispheric mass affixed to the underlying dura (*arrows*). There is a "claw" of tumor growing along the dura (*arrowhead*). However, the enhancement seen on MRI was far more extensive. *(From Smirniotopoulos JG, Murphy FM, Rushing EJ, et al. Patterns of contrast enhancement in the brain and meninges. RadioGraphics 2007; 27:525-551.)*

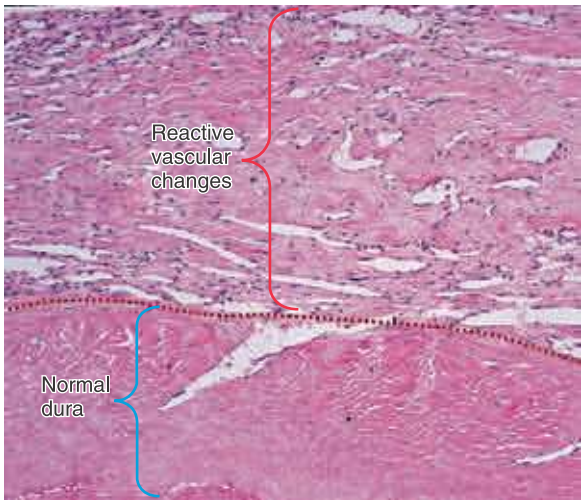

■ **FIGURE 5-7** Meningioma. Dural tail (H&E, original magnification, ×250). The lower half shows normal dura mater—mostly collagen. Vascular reactive changes and venous congestion, along with interstitial edema, contribute to contrast enhancement. *(From Smirniotopoulos JG, Murphy FM, Rushing EJ, et al. Patterns of contrast enhancement in the brain and meninges. RadioGraphics 2007; 27:525-551.)*

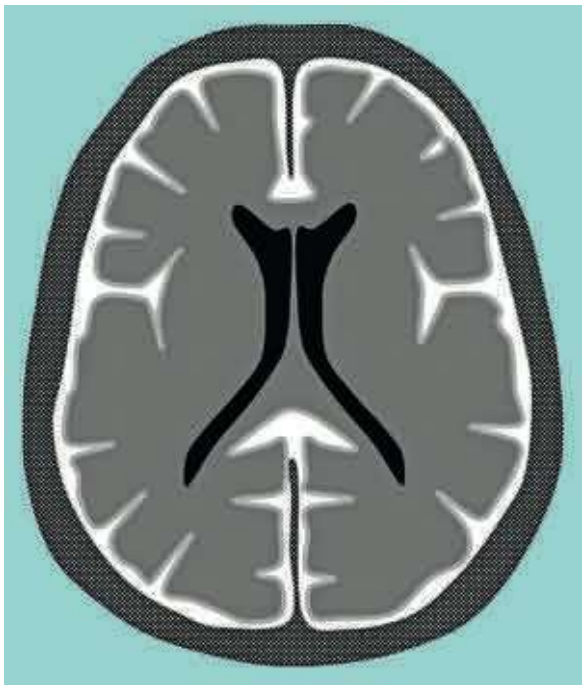

■ **FIGURE 5-8** Schematic of pia-arachnoid (subarachnoid) enhancement. The contrast material fills the subarachnoid space and enters the sulci between the cerebral and cerebellar gyri. This pattern occurs in both bacterial meningitis and cerebrospinal fluid dissemination of neoplasms—"carcinomatous" meningitis. *(From Smirniotopoulos JG, Murphy FM, Rushing EJ, et al. Patterns of contrast enhancement in the brain and meninges. RadioGraphics 2007; 27:525-551.)*

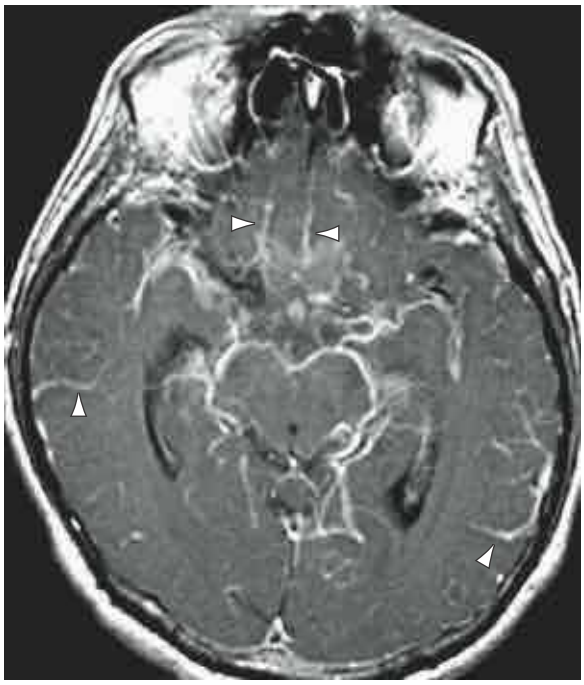

■ **FIGURE 5-9** Axial T1W MR gadolinium-enhanced image of bacterial meningitis. There is diffuse linear superficial (pial) enhancement in the subarachnoid space, extending into sulci (*arrowheads*) and along the surface of the midbrain. *(From Smirniotopoulos JG, Murphy FM, Rushing EJ, et al. Patterns of contrast enhancement in the brain and meninges. RadioGraphics 2007; 27:525-551.)*

of the blood-brain barrier of the pial vessels themselves. In bacterial meningitis, glycoproteins released by bacteria cause breakdown of the blood-brain barrier and allow contrast material to leak from vessels into the cerebrospinal fluid. Bacterial and viral meningitis exhibit enhancement that is typically thin and linear (Figs. 5-9 and 5-10).[19] Some cases of fungal meningitis may produce nodular or "lumpy" enhancement.

Neoplasms that disseminate by spreading into the subarachnoid space—"carcinomatous meningitis"—also produce enhancement of the brain surface and subarachnoid space (Fig. 5-11). Primary brain tumors that reach the ventricular or pial surface may spread this way, including medulloblastoma, ependymoma, choroid plexus papilloma/carcinoma, glioblastoma, germinoma, and oligodendroglioma, as well as secondary tumors (e.g., lymphoma and breast cancer. We expect neoplastic disease in the subarachnoid space to produce thicker, lumpy, or nodular enhancement, similar to that of fungal disease. However, despite this logic, neoplastic meningitis can appear surprisingly thin and linear.

The clinical presentation should suggest an infectious cause with fever and meningismus. Spinal tap and cerebrospinal fluid sampling may reveal a reactive pleocytosis, and cerebrospinal fluid cultures may demonstrate the organism. Viral meningitis may be "culture negative," "aseptic," or "sterile." Normal cranial nerves never enhance within the subarachnoid space, and such enhancement is always abnormal. Viral encephalitis (as well as sarcoidosis) may also produce linear enhancement of the cranial nerves. Primary nerve sheath tumors (e.g., schwannoma) may show nerve enhancement in the subarachnoid space, but in the form of a lump or mass enlarging the nerve.

INTRA-AXIAL ENHANCEMENT

Intra-axial enhancement of the brain and spinal cord is never normal. There must be a vascular structure or a breakdown in the blood-brain barrier. An abnormal increase in permeability may be reactive (gliosis), inflammatory (multiple sclerosis), infectious (encephalitis or abscess), and neoplastic. Intravascular enhancement may occur with developmental venous anomalies and cavernous malformations. Intravascular enhancement requires special MR pulse sequences, because of the "flow-void" effect of moving blood.

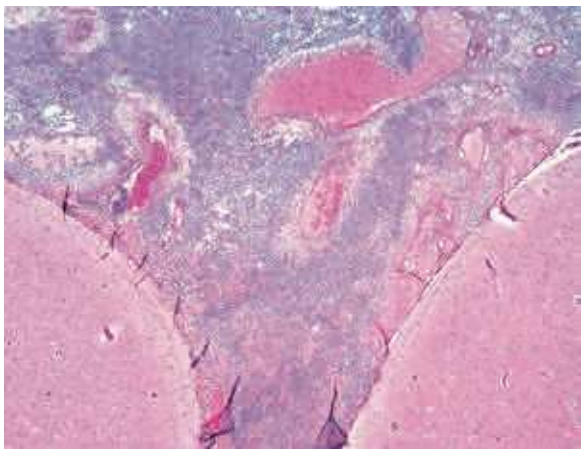

■ **FIGURE 5-10** *Streptococcus pneumoniae* meningitis (H&E, original magnification, ×400). There is a dense inflammatory infiltrate along the surface of the brain that fills the subarachnoid space. *(From Smirniotopoulos JG, Murphy FM, Rushing EJ, et al. Patterns of contrast enhancement in the brain and meninges. RadioGraphics 2007; 27:525-551.)*

Gyral Enhancement

Gyral enhancement—along the surface of the brain—is almost always vascular or inflammatory and only rarely neoplastic

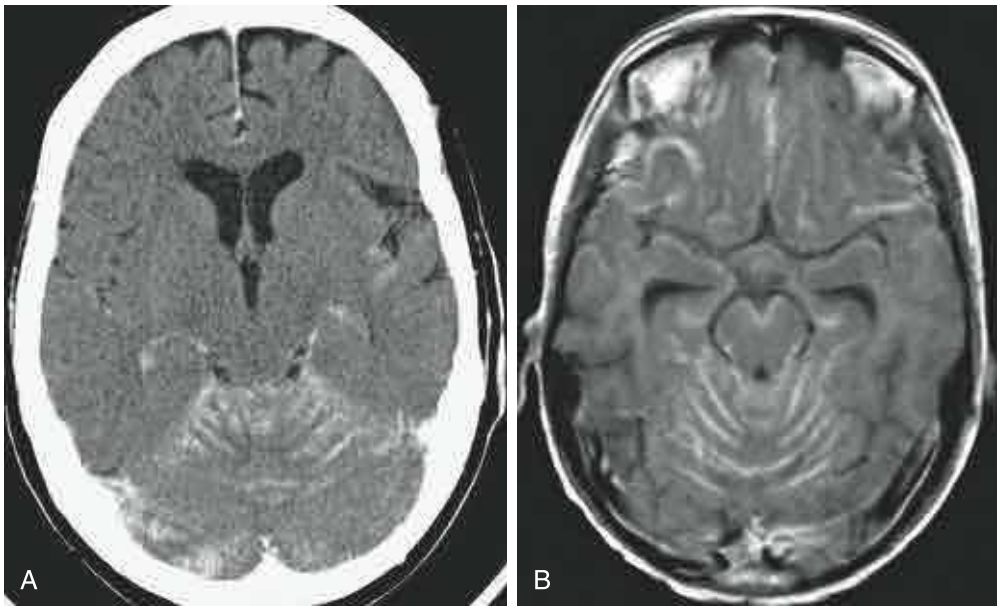

■ **FIGURE 5-11** Carcinomatous meningitis. This patient has diffuse subarachnoid spread of medulloblastoma. Axial contrast-enhanced CT scan (**A**) and axial T1W MR gadolinium-enhanced image (**B**) both show abnormal yet linear enhancement in the sulci of the cerebellum, forming a coating around the brain stem. *(From Smirniotopoulos JG, Murphy FM, Rushing EJ, et al. Patterns of contrast enhancement in the brain and meninges. RadioGraphics 2007; 27:525-551.)*

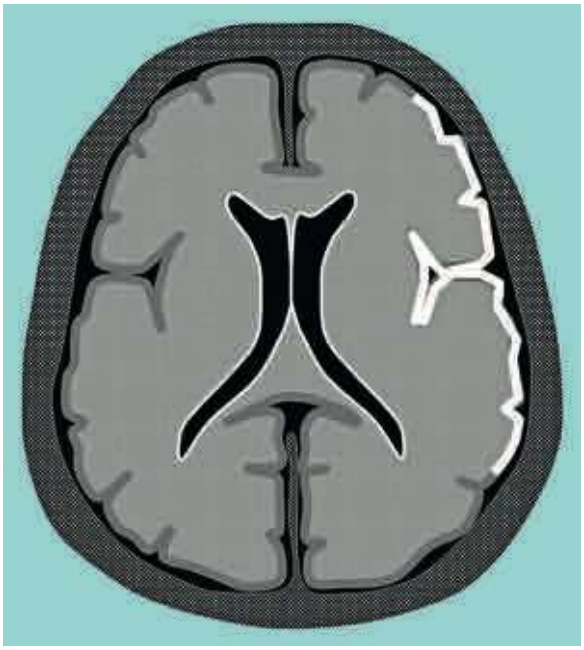

■ **FIGURE 5-12** Schematic of gyral gray matter enhancement. The cortical gray matter enhances while the underlying white matter does not. *(From Smirniotopoulos JG, Murphy FM, Rushing EJ, et al. Patterns of contrast enhancement in the brain and meninges. RadioGraphics 2007; 27:525-551.)*

(Fig. 5-12). Vascular causes of brain parenchymal gyral enhancement include causes of vasoactive hyperemia: migraine, loss of autoregulation, posterior-reversible encephalopathy syndrome, and reperfusion after thrombolysis or spontaneous clot lysis/migration. Gyral enhancement due to blood-brain barrier breakdown is also seen with reperfusion, during the subacute "healing" phase after cerebral infarction, and with vasculitis and encephalitis. Enhancement from hyperperfusion can be seen after seizures. The differential diagnosis between vascular and inflammatory causes of a superficial and serpentine pattern of enhancement requires clinical correlation and analysis of the enhancement topography. Embolic events and most thrombotic strokes have an abrupt onset of symptoms and involve regions that map to vascular territories. Migraine headache has a characteristic aura and throbbing pain. Fever, indolent history, and nonspecific headache or lethargy may suggest an encephalitis. Gyral lesions affecting the territory of a single artery are often vascular, whereas inflammatory lesions may affect multiple territories. The most common vascular processes affect the middle cerebral artery territory (up to 60% of cases). The lesions of posterior-reversible encephalopathy syndrome usually localize in the posterior cerebral artery territory, perhaps due to a deficiency in the sympathetic innervations (vaso nervorum).

Inflammatory Gyral Enhancement

The most common brain infection is caused by members of the herpesvirus family of viruses. Herpes encephalitis usually begins in the gray matter, causing swelling and altered signal intensity. Later, inflammatory breakdown of the blood-brain barrier will allow contrast enhancement in a cortical gyral pattern. The most common site of herpes encephalitis is the uncus of the medial temporal lobe and involvement of the cingulate gyrus of the medial frontal and parietal lobes (Fig. 5-13).[20,21] This distribution of lesions supports a route of infection from the nasal cavity, along the olfactory pathways to the brain. Because enhancement may be a lagging indicator of disease and because enhancement may be reduced by corticosteroids, the absence of enhancement cannot be used to rule out encephalitis.

Vascular Gyral Enhancement

Vascular gyral enhancement results from various mechanisms with variable time courses. The earliest enhancement can be caused by reversible blood-brain barrier changes when ischemia lasts for only several hours before reperfusion occurs.[22] Early reperfusion may also produce vasodilatation, with increased blood volume and shortened mean transit time. These features were first observed at conventional angiography; they were described as dynamic changes and were called "luxury perfusion" because of the increased blood flow.[23] The increased blood flow is caused by autoregulation mechanisms, which are "tricked" by the increased tissue Pco_2 that accumulates before reperfusion occurs. Ischemia or infarction may demonstrate gyral enhancement on both CT and MR images within minutes

(with early reperfusion) (Fig. 5-14). In the healing phases of cerebral infarction, from several days (5 to 7 days) to several weeks after the event, there will be vascular proliferation or hypertrophy. Contrast enhancement usually fades away between 4 weeks and 4 months after the stroke, and enhancement is usually replaced by brain volume loss and encephalomalacia (Fig. 5-15).[24] The vascular changes facilitate the breakdown and removal of the dead brain tissue and lead to the encephalomalacia and atrophy characteristic of old "healed" infarction. The imaging appearance of postictal states may mimic the findings of cerebral infarction in several features, including gyral swelling, increased signal intensity on T2-weighted (T2W) images, and decreased signal intensity on T1W images, sulcal effacement, and gyral enhancement.[25] Reperfusion, whether acute (e.g., after thrombolysis) or subacute to chronic ("healing" infarction), is required to deliver contrast material to produce enhancement.

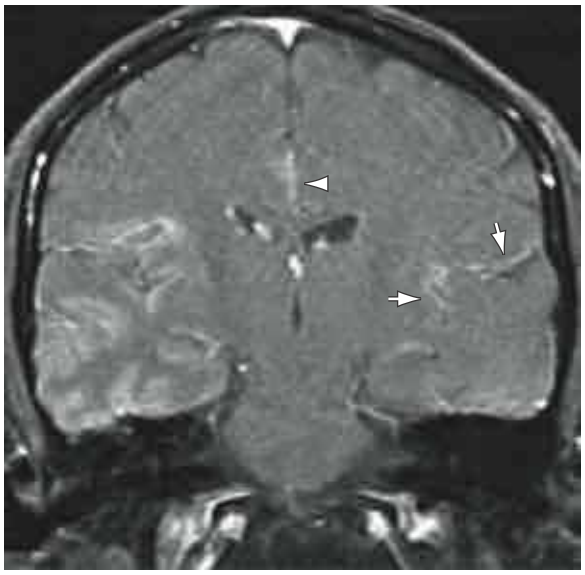

■ **FIGURE 5-13** Coronal T1W gadolinium-enhanced MR image of herpes type 2 encephalitis. Herpesvirus replicates within neurons, causing cortical destruction, inflammatory enhancement, and eventually destruction and atrophy. Ascending infection from the nasopharynx commonly affects the temporal lobes (*arrows*). However, involvement of the cingulate gyrus (*arrowhead*) is also frequent. *(From Smirniotopoulos JG, Murphy FM, Rushing EJ, et al. Patterns of contrast enhancement in the brain and meninges. RadioGraphics 2007; 27:525-551.)*

Nodular Cortical and Subcortical Enhancement

Metastatic lesions are often small (<2 cm) circumscribed nodular lesions near the corticomedullary (gray matter/white matter) junction (Fig. 5-16). Metastatic disease usually reaches the brain hematogenously through the arteries and less commonly via the venous system. Metastatic deposits are distributed by blood flow. The majority of lesions are supratentorial in the cerebral hemispheres, often in the territory of the middle cerebral artery,[26] which has the widest distribution. Venous metastatic disease to the CNS is most often related to a primary pelvic malignancy (e.g., of the prostate or uterus) and travels through the prevertebral veins of the Batson venous plexus. This venous pathway connecting to the retroclival venous plexus partially accounts for the preferential distribution of some pelvic metastases to the posterior fossa (cerebellum and brain stem).

Metastatic lesions are typically juxtacortical, occurring in or near the gray matter/white matter (corticomedullary) junction. In contrast, most primary glial tumors arise deeper in the periventricular white matter. This peripheral dominant pattern of nodule distribution reflects where vessels branch and taper, acting as a sieve to filter intravascular tumor. Dissemination is only the beginning; the tumor emboli must establish themselves to grow into a macroscopic deposit. On gross pathologic inspection, as on imaging, metastatic nodules are circumscribed and have a "pushing margin," usually with significant surrounding perilesional vasogenic edema. Even small cortical or juxtacortical lesions may present as early symptoms, because of their ability to cause disruption of the sensory and motor cortex, and seizures are common. This early clinical presentation allows detection of small solid nodular lesions, often 0.5 to 2.5 cm in diameter (see Fig. 5-16). Primary glial tumors, both low-grade and high-grade astrocytomas, arise outside the cortex and deep in the white matter. They may infiltrate extensively without destruction or disruption and will usually present as much larger (2.5 to 5.0 cm in diameter) lesions by the time symptoms are reported.

We usually imagine that hematogenous metastasis is almost invariably multiple. However, in reality, roughly one half (40% to 60%) of patients will have only a single lesion on initial imaging. In these patients with a single lesion, double- and triple-dose gadolinium may reveal additional lesions. However, the

■ **FIGURE 5-14** T1W gadolinium-enhanced MR images of acute cerebellar PICA infarction. Sagittal (**A**) and axial (**B**, **C**) images show linear enhancement of the cerebellar folia in the right posterior inferior cerebellar artery territory. *Note:* In **C**, the lesion has ring enhancement.

same dosing scheme may also reveal single lesions in patients whose standard MR is negative. We should also remember that diffusely infiltrating astrocytomas may present as multifocal lesions in about 15% of cases. One point helpful in differential diagnosis: multifocal glioma lesions are usually not localized to the gray matter/white matter junction, whereas hematogenous metastases usually are. Thus, metastatic disease is often a solitary lesion and primary tumor can be multiple.

Deep and Periventricular Enhancement

Lesions that are localized deeper within the cerebral hemispheres are usually not caused by hematogenous dissemination. The most common exception is for lesions in the basal ganglia. Subcortical white matter and deeper lesions that involve the gray nuclei (e.g., basal ganglia and thalamus) are usually primary processes within the CNS and may be non-neoplastic. Because of the cellular physiology of neurons, metabolic disease and both endogenous and exogenous toxins may preferentially affect the deep gray matter. The majority of diseases that affect myelin production or repair primarily damage the white matter and are called "leukoencephalopathies." Most leukoencephalopathies become destructive at some time during their natural evolution and will lead to a decreased volume ("atrophy") of the affected white matter. These changes may produce imaging changes from a loss of myelin lipids and an increased signal intensity from water on T2W and fluid-attenuated inversion recovery (FLAIR) MR images with correspondingly decreased attenuation on CT images. Many pathologic processes have inflammation that will produce enhancement localization similar to the location of the increased water signal. We look for these clear-cut distinctions between deep white matter lesions and deep gray matter lesions as a guide to differential diagnosis. However, many diseases affect both the deep gray matter and the white matter in the periventricular regions; and, some of these processes occur commonly in immunocompromised patients, such as toxoplasmosis and primary CNS lymphoma.

■ **FIGURE 5-15** This patient presented with an acute right middle cerebral artery infarction. Initial imaging noted a previously asymptomatic subependymoma. Postoperative imaging shows subacute middle cerebral artery cortical infarct enhancement, as well as postoperative dura-arachnoid enhancement.

Deep Ring-Enhancing Lesions

Ring-enhancing lesions are uncommonly superficial. They are most commonly found either subcortical or deeper in the hemisphere (Fig. 5-17). In a review of 221 MR-enhancing ring lesions, Schwartz and colleagues[27] reported that 40% were gliomas, 30% were metastases, 8% were abscesses, and 6% were caused by demyelinating diseases. They also noted that almost one half (45%) of metastatic deposits were solitary whereas the majority (77%) of gliomas were single lesions. In contrast, both abscesses (75%) and multiple sclerosis lesions (85%) were multiple.[27] Because both necrotic metastases and hematogenous abscesses will be cortical or subcortical lesions with central cavitation, we must differentiate them by other means. Metastatic deposits are more often solid nodular lesions that may become ring enhancing because of necrosis (e.g., after chemotherapy or irradiation) (see Fig. 5-16). A history of known primary tumor would suggest metastasis. Additionally, fever, recent dental work, right-to-left shunt, bronchitis/bronchiectasis, intravenous drug use, subacute bacterial endocarditis, and indwelling catheters or other implanted devices such as cardiac valves would support ring-enhancing lesions with an infectious etiology (i.e., they

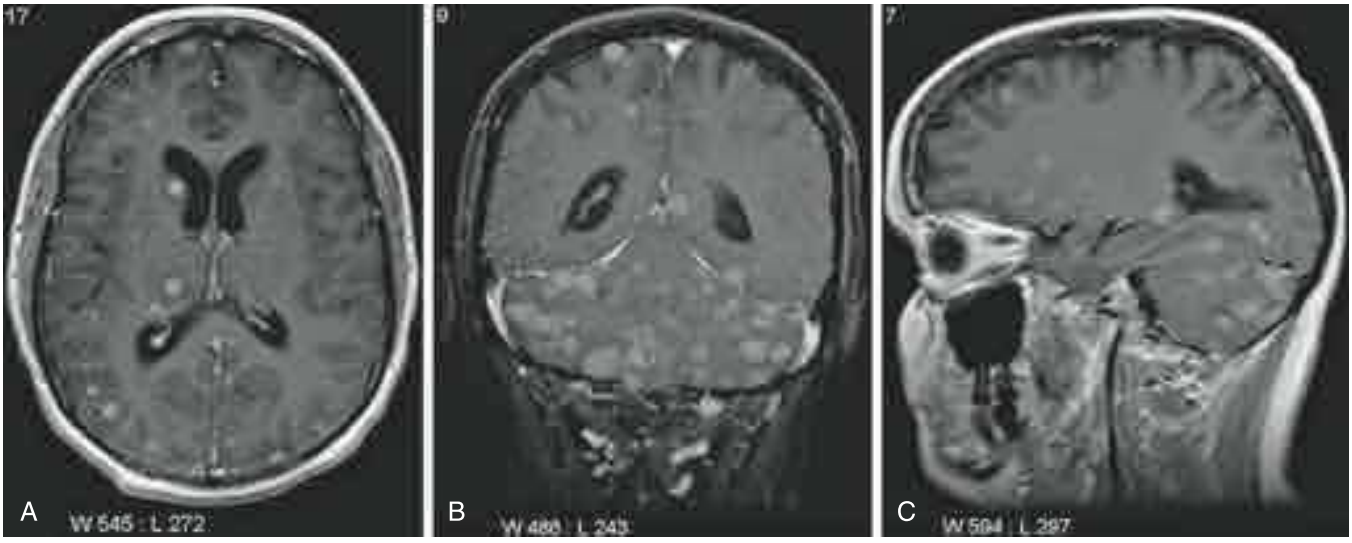

■ **FIGURE 5-16** T1W gadolinium-enhanced images of metastatic breast cancer. Axial (**A**), coronal (**B**), and sagittal (**C**) images all show multiple well-demarcated subcortical enhancing lesions.

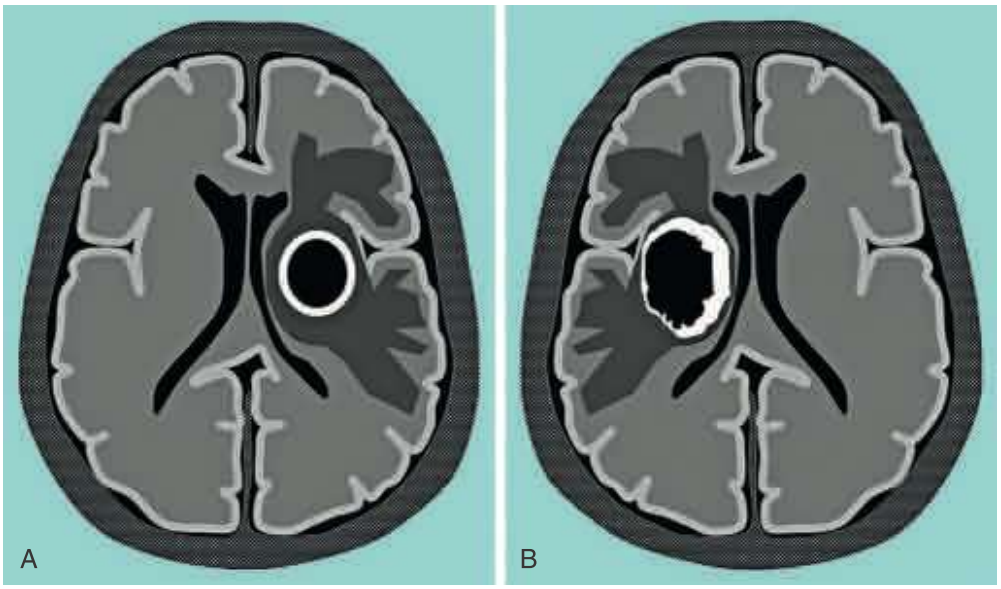

■ **FIGURE 5-17** Diagrams of ring lesions. **A,** Smooth ring suggesting abscess. **B,** Irregular ring with a "shaggy" inner margin suggestive of necrosis in a high-grade neoplasm (e.g., glioblastoma). Both of these lesions may have surrounding interstitial vasogenic edema that spreads away in a "finger-like" manner.

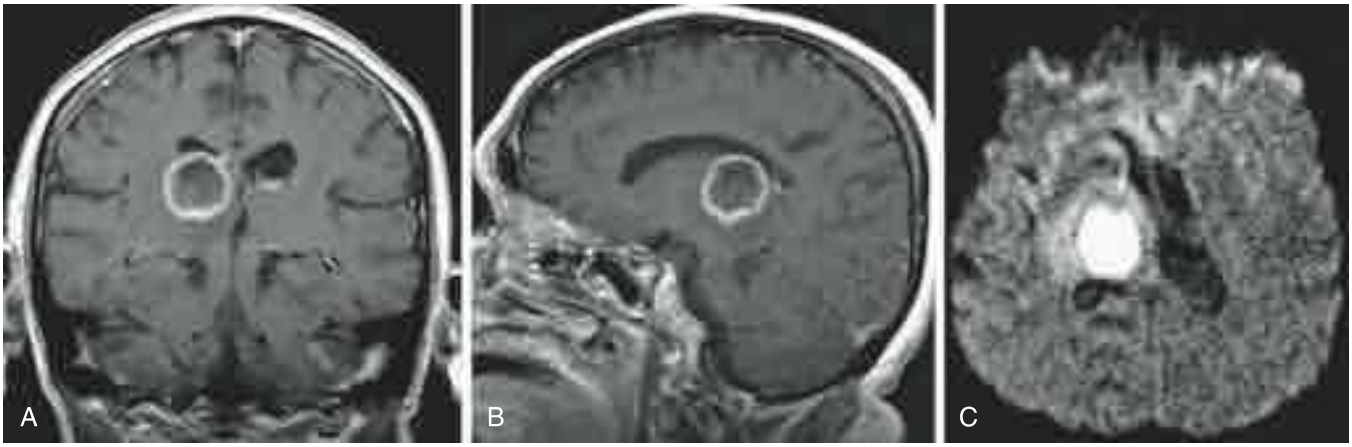

■ **FIGURE 5-18** Abscess. Coronal (**A**) and sagittal (**B**) T1W gadolinium-enhanced MR images and axial diffusion-weighted MR image (**C**). This ring-enhancing lesion has a thin, yet slightly irregular rim. The differential diagnosis would include a glioblastoma. However, the diffusion-weighted image shows hyperintensity from restricted diffusion, most characteristic for pus in an abscess. *(Case courtesy of J. Keith Smith.)*

represent brain abscesses). Deep white matter ring-enhancing lesions, especially those with mass effect and surrounding vasogenic edema, are most often either primary neoplasms (e.g., glioblastoma multiforme) or abscesses (Figs. 5-18 and 5-19; see also Fig. 5-17).

CNS Infections: Cerebritis and Abscess

Most pyogenic infections of the CNS develop from hematogenous septic emboli. Direct extension from adjacent sinus infections (sphenoidal, ethmoidal, frontal, and mastoid air cells) is also possible but requires transgression of the dura. Cerebritis is an acute inflammatory reaction with altered permeability of the native vessels but without angiogenesis or neovascularity. Brain inflammation or cerebritis begins with relatively poorly marginated hyperemia and breakdown of the blood-brain barrier. These reactive changes allow inflammatory white cells, such as neutrophils, and plasma proteins (antibodies and complement) to exit the intravascular space so they can reach the infected parenchyma. Before angiogenesis, the signal intensity and attenuation changes are directly caused by the inflammatory process. The perilesional vasogenic edema is variable and may be minimal. Proliferation of the infecting organisms and necrosis of brain parenchyma create a zone of devitalized and avascular material. In the immunocompetent patient, cerebritis progresses to form an organized abscess with the formation of a capsule of granulation tissue (Figs. 5-20 and 5-21). The lesion now becomes more circumscribed by vascular changes (recruitment and neovascularity) along with a collagenous rim developing from vascular fibroblasts, thus creating a wall around the pus and dead brain, forming a classic abscess. Collagen in the wall reinforces it to localize and confine the infected brain and pus. Just outside the granulation tissue there is a layer of proliferating reactive astrocytes (astrogliosis) (see Figs. 5-20 and 5-21).[28,29]

The imaging appearance will change, just as the reaction and organization about the infection evolves. The enhancement in cerebritis is often diffuse and faint, whereas an organized abscess has a well-marginated rim of discrete enhancement (see Figs. 5-17 and 5-18). The peripheral rim enhancement in an abscess localizes the granulation tissue with its increased capillary permeability and increased perfusion/vascularity. An intermediate stage of transition from cerebritis to an organized abscess may be suspected when the lesion does not have a sharp margin or

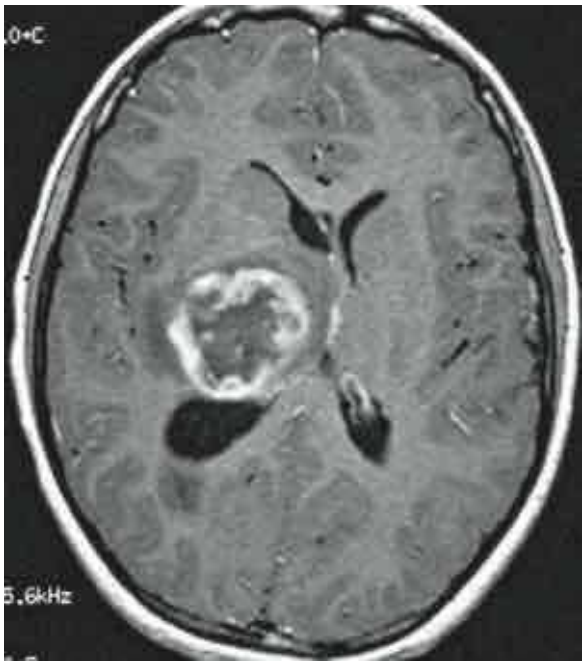

■ **FIGURE 5-19** Necrotic ring pattern of high-grade neoplasm (glioblastoma multiforme— WHO grade 4). Axial gadolinium enhanced T1W MR image shows a large heterogeneous mass that displaces the frontal horn of the lateral ventricle. There is irregular and heterogeneous ring enhancement. The ring has a characteristically undulating or wavy margin, and its inner aspect is shaggy and irregular, all suggesting necrosis in a neoplasm.

■ **FIGURE 5-20** Cerebral abscess in a patient with AIDS who died of multiple brain abscesses from *Toxoplasma gondii*. Axially sectioned gross specimen shows an abscess in the thalamus with three macroscopic zones: a reddish region of neovascularity (*arrowheads*), a white region of extravascular white cells and pus (*asterisk*), and an inner zone of liquefaction necrosis (N). Liquefaction necrosis occurs in lipid-rich organs (e.g., the brain), when an exuberant leukocytic reaction brings lytic enzymes into the infected region. Scale is in centimeters. *(From Smirniotopoulos JG, Murphy FM, Rushing EJ, et al. Patterns of contrast enhancement in the brain and meninges. RadioGraphics 2007; 27:525-551.)*

has a wall that is less discrete. On initial CT and MR images, cerebritis will appear as a ring-enhancing lesion (see Fig. 5-18). In cerebritis without a collagen capsule, images obtained over 20 to 40 minutes may show "fill in" of the ring center.[30] This "filling in" does not occur in a well-organized abscess and suggests cerebritis.[30] Cerebritis is often treated nonsurgically with high doses of antibiotics.

It typically takes 2 to 4 weeks to create a well-formed abscess wall that separates the infection and necrosis from the relatively uninvolved surrounding brain. Pathologically, an organizing infection will develop concentric zones or layers: (1) necrotic brain in the innermost layer, (2) reactive white cells (macrophages, monocytes) and fibroblasts, (3) capillary vascular proliferation and collagen capsule formation, (4) neovascularity and active cerebritis, and (5) reactive astrogliosis and vasogenic edema in the outer margin (see Figs. 5-20 and 5-21).[28-30]

The classic abscess ring usually has both a smooth inner and outer margin and is typically less than 1 cm (usually about 5 mm) thick. During the transition from the diffuse inflammation of cerebritis to the organized wall of an abscess, the outer rim of enhancement may fade into the adjacent brain, like the corona of a solar eclipse (see Fig. 5-18B). On T2W MR images, the abscess wall is usually hypointense, contrasting to the bright necrotic center and the surrounding brain with vasogenic edema. Schwartz and colleagues reported that almost 90% of abscesses demonstrate a hypointense rim and 75% form a continuous hypointense rim.[27] Multiple theories have been proposed, including dense collagen, blood products (hemosiderin), and paramagnetic free radicals (e.g., atomic oxygen produced by leukocytes that are attacking the bacteria).[31] An abscess wall often appears thicker on the gray matter or "oxygen side" of the ring and thinner along the white matter or ventricular side. The tendency for an abscess to "point" toward the ventricular, deep, or medial aspect is a direct consequence of the thinner inner margin. Rupture into the ventricle (pyocephalus) is usually devastating to the patient and often fatal.

We have seen that late stage cerebritis may produce ring enhancement. In addition, as organization progresses, the outer abscess rim may be thick or irregular. Extravascular enhancement (interstitial—from increased capillary permeability) localizes within millimeters of the abnormal vessels. Although extravascular, the contrast material cannot diffuse into the center of an organized abscess cavity, even on delayed images, owing to the viscosity of the pus and liquefaction necrosis. These same physical properties produce the high signal intensity on diffusion-weighted images (see Fig. 5-18C) and have a corresponding reduced apparent diffusion coefficient (ADC) and therefore are of low signal intensity on the maps of ADC values. Lastly, amino acids on proton MR spectroscopy (discussed in detail elsewhere) are seen in 80% of abscesses.[32]

Necrotic High-Grade Primary Neoplasms

Central necrosis within a neoplasm will also produce a ring-enhancing lesion. Remaining residual living tissue surrounds a central zone of necrotic tumor tissue. In general, rapidly growing tumors that become necrotic are usually, but not exclusively, malignant, either primary gliomas or metastases. Multilocular and complex ring patterns—lesions with a thick irregular rim (especially if > 10 mm) and those with an irregular or "shaggy" inner margin—usually represent necrotic high-grade neoplasms rather than abscess or cerebritis (Fig. 5-22; see also Fig. 5-19).

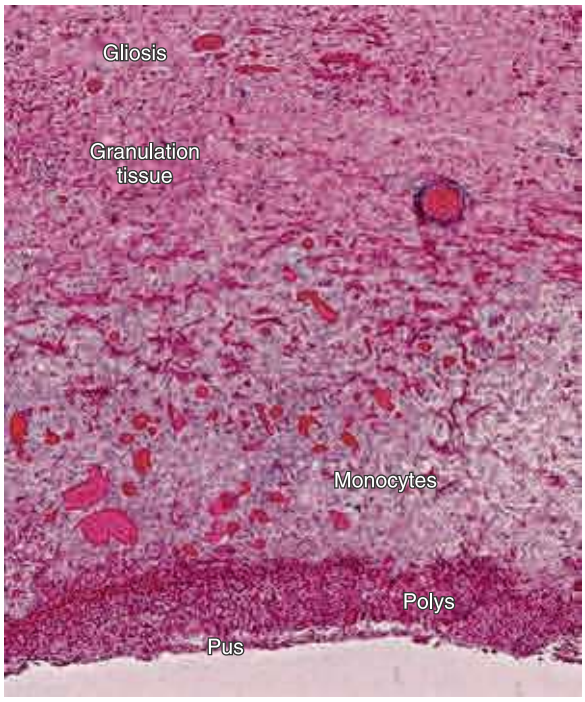

■ **FIGURE 5-21** Brain abscess. Photomicrograph (H&E, original magnification, ×250) shows the microscopic layers from top to bottom: reactive gliosis and the brain margin, vascular proliferation with collagen formation (granulation tissue), migrating white blood cells (monocytes), and pus. polys, polymorphonuclear leukocytes. *(Courtesy of Joseph Parisi, MD, Mayo Clinic, Rochester, MN; from Smirniotopoulos JG, Murphy FM, Rushing EJ, et al. Patterns of contrast enhancement in the brain and meninges. RadioGraphics 2007; 27:525-551.)*

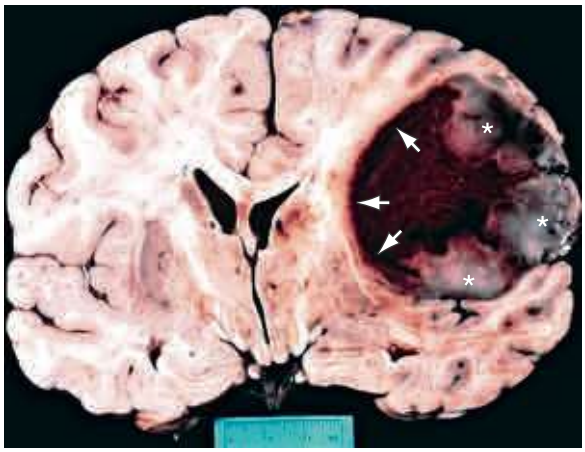

■ **FIGURE 5-22** Glioblastoma multiforme. Coronally sectioned gross specimen shows the outer cortical region of the tumor with the more typical, thick irregular rim (*asterisk*) and shaggy inner margin, and the relatively smooth, thin, deep inner margin (*arrows*). Within the neoplasm is a region of hemorrhagic necrosis. Scale is in centimeters. *(From Smirniotopoulos JG, Murphy FM, Rushing EJ, et al. Patterns of contrast enhancement in the brain and meninges. RadioGraphics 2007; 27:525-551.)*

When these lesions are in the corpus callosum and thalamus, brain stem, or other deep parts of the brain, glioblastoma (diffuse astrocytoma, WHO grade 4) is more likely.

Histologically, grade 4 diffuse astrocytoma is characterized by aggressive features, including microscopic foci of necrosis with pseudopalisading. Larger lesions will have irregular geographic regions of necrotic cavitation.[33,34] These necrotic regions may have increased diffusion rather than restricted diffusion, owing to the lysis of cell membranes and dissolution of boundaries. Glioblastomas vary from smaller unilocular rings to larger and more complex lobulated and multilocular rings, with thick rims of enhancement. They usually show angiographic and macroscopic neovascularity. This abnormal vascularity produces an increased regional cerebral blood volume and increased regional cerebral blood flow that combine to produce a short mean transit time. These findings are measurable on perfusion imaging, whether by MRI, CT, or even catheter angiography. The residual/remaining living tumor in the outer rim survives because it maintains a rich blood supply. This hypervascular rim can be several centimeters thick, may be irregular both outside and toward the central necrosis, and is often thicker toward the cortical gray matter or basal ganglia. The tumor is more likely to grow faster and thicker near the normally more vascular gray matter (see Fig. 5-22). Quite different from an abscess, delayed imaging in a necrotic neoplasm may show progression of enhancement toward the center, from islands of viable tumor that surround remaining patent vessels. Vascular endothelial growth factor has been implicated in the angiogenesis for most high-grade gliomas.[35] The high cellular density, rapid growth, and mitotic activity all require increased metabolism and corresponding increased perfusion. The newly recruited and co-opted vessels develop capillary endothelium with intercellular gaps, and they do not have a continuous basement membrane.

Fluid-Secreting Low-Grade Primary Neoplasms

Necrosis is a common feature of high-grade neoplasms, but all neoplastic "holes" are not formed by necrosis. Low-grade primary neoplasms may become heterogeneous not from necrosis but through accumulation of serous fluid. In addition, because fluid-secreting gliomas have well-defined "pushing margins," they may be resected completely, offering a cure. Because of features of slow growth, possible resection, and well-differentiated histology, most fluid-secreting brain neoplasms are WHO grade 1. The fluid must come from somewhere, so the periphery of the fluid spaces includes neoplastic tissue. Almost all "fluid-secreting" gliomas enhance on both MRI and CT. The two most familiar partially fluid brain tumors are the pilocytic astrocytoma and the hemangioblastoma. They are both most frequently located in the cerebellum (Fig. 5-23). Supratentorially, the differential diagnosis for "fluid-secreting" lesions includes pilocytic astrocytoma, pleomorphic xanthoastrocytoma, ganglioglioma, and extraventricular ependymoma. These lesions are not truly "cystic" because the fluid cavity is not lined by an epithelium. In the majority of cases, the neoplastic tissue is much smaller in volume compared with the fluid component, and either it forms a lump ("mural nodule") or comprises part of the rim. The remaining margin is normal, compressed, or gliotic brain tissue.

The fluid secreted in these low-grade neoplasms is not identical to tissue fluid or serum. It may have a high protein concentration and show increased signal compared with cerebrospinal fluid on T1W MRI and on CT but have lower signal intensity on T2W MR images. These low-grade lesions may have abnormal capillaries but usually do not show increased blood flow. There are limited (if any) changes in arteries and veins. With the exception of hemangioblastoma, these lesions are avascular on angiography. Although lacking increased perfusion, increased metabolism has been reported on metabolic studies.[36] Most authors believe that the abnormal capillaries in these lesions do not form a blood-brain barrier and that the increased permeability is related somehow to both fluid production and contrast material.[37] Histologically, the fluid is seen as microcysts within the "solid" tumor nodule. They may have high signal on FLAIR imaging and low attenuation on CT. The "cyst-with-nodule" appearance (Fig. 5-24; see also Fig. 5-23) is attributed to progressive fluid secretion that accumulates exophytically between the

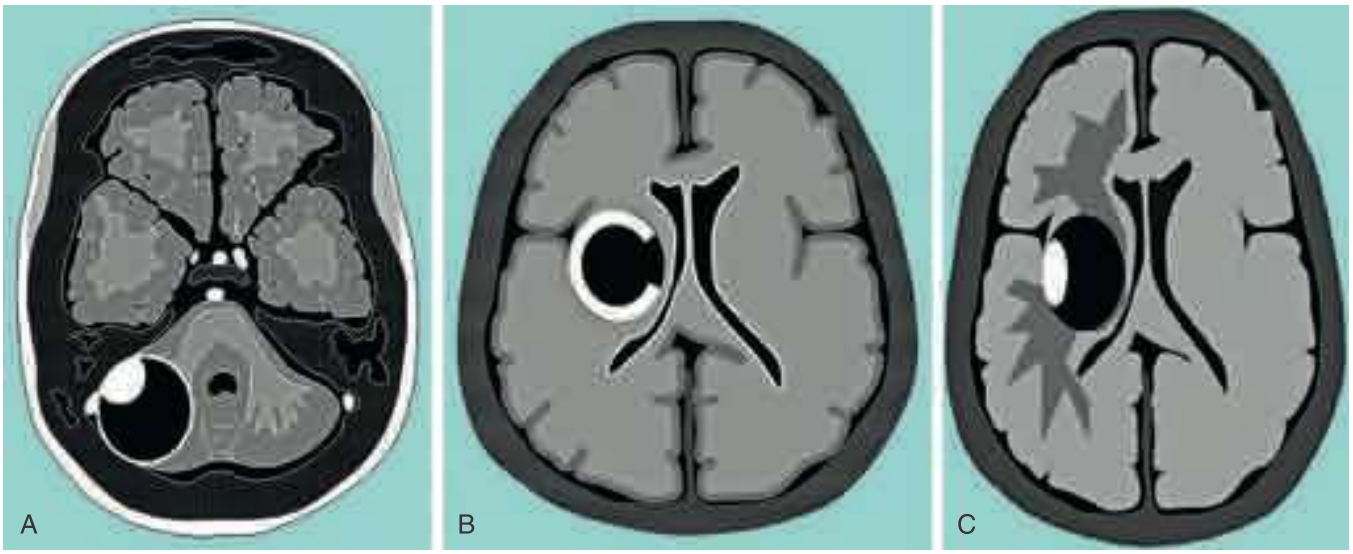

■ **FIGURE 5-23** Schematic fluid-secreting neoplasms and demyelination. **A,** Typical cerebellar "cyst with nodule" appearance for pilocytic astrocytoma and hemangioblastoma. **B,** Classic "open-ring" sign for tumefactive demyelinating lesions. **C,** Fluid secreting "cyst with nodule" neoplasms may produce interstitial vasogenic edema in the cerebral hemispheres. See also Figure 5-24.

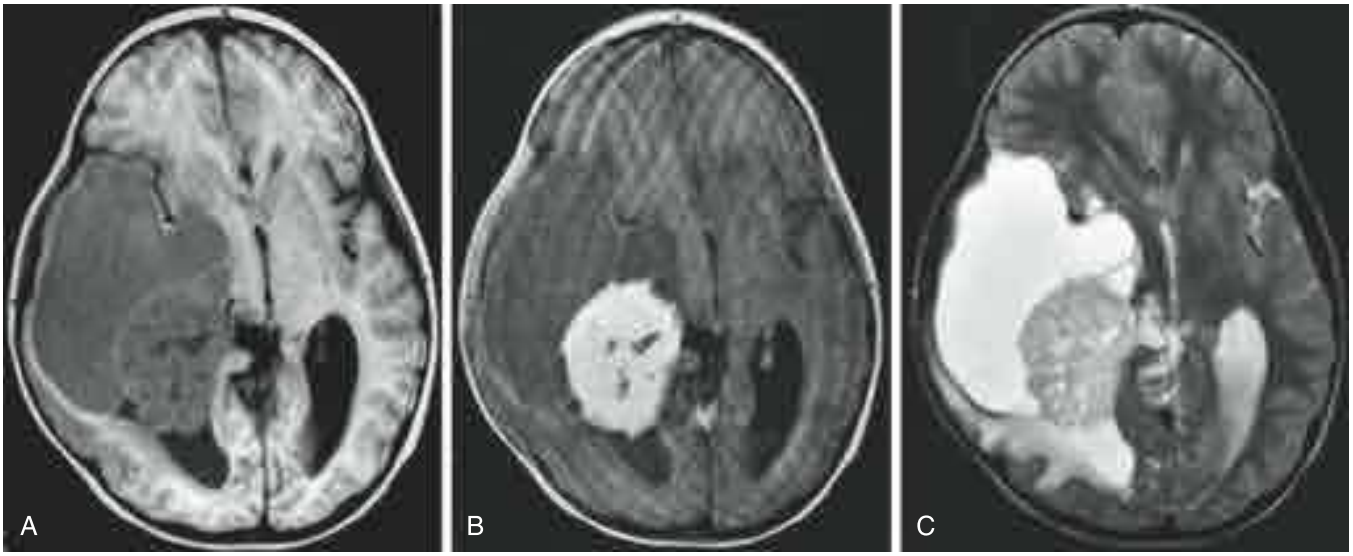

■ **FIGURE 5-24** Pilocytic astrocytoma—cerebral hemisphere. Axial MR images: T1W (**A**), T1W gadolinium-enhanced (**B**), and T2W (**C**). There is a large complex right hemispheric mass. Part of this is solid neoplasm (enhancing on **B**). Part of this is fluid secreted by the neoplasm. There is interstitial vasogenic edema surrounding the mass and extending into the posterior temporal and occipital lobes.

neoplastic nodule and the normal brain. Many fluid-secreting tumors have a more complex shape that cannot be simply described as a biphasic "cyst-with-nodule" shape. Roughly one third of hemangioblastomas show the classic unilocular fluid space with a single mural nodule.[38] The remaining two thirds vary in shape from almost completely solid to a large fluid space with only a tiny nodule. In pilocytic astrocytoma, with thinner slice thickness (<4 mm), MRI and CT frequently demonstrate that even the "solid" mural nodule is often heterogeneous with small fluid "lacunae" within the nodule itself, in addition to the larger fluid "cyst" (Fig. 5-25; see also Fig. 5-24). Reactive gliosis, which by conventional wisdom does not enhance, may nonetheless show contrast enhancement around the fluid in some pilocytic astrocytomas.[39] Enhancement of gliosis is variable and depends on the time delay between injection and imaging, the contrast dose, and probably on the molecular weight of the contrast material. Lastly, the varying morphology of fluid-secreting neoplasms can produce the "open-ring sign," an incomplete rim of enhancement that is also a feature of some other benign lesions, such as demyelination.

White Matter Enhancement: Demyelination

The most common cause of neurologic disability in midlife is the leukoencephalopathy of multiple sclerosis. The demyelination is caused by a failure of the normal myelin physiology. Active destruction of myelin as well as faulty metabolism and repair by the oligodendrocytes will lead to denuded axons—the histologic hallmark of these diseases. There is gray matter involvement in many, if not most, patients, and axon destruction and neuronal loss occur in many cases. Multiple sclerosis is usually character-

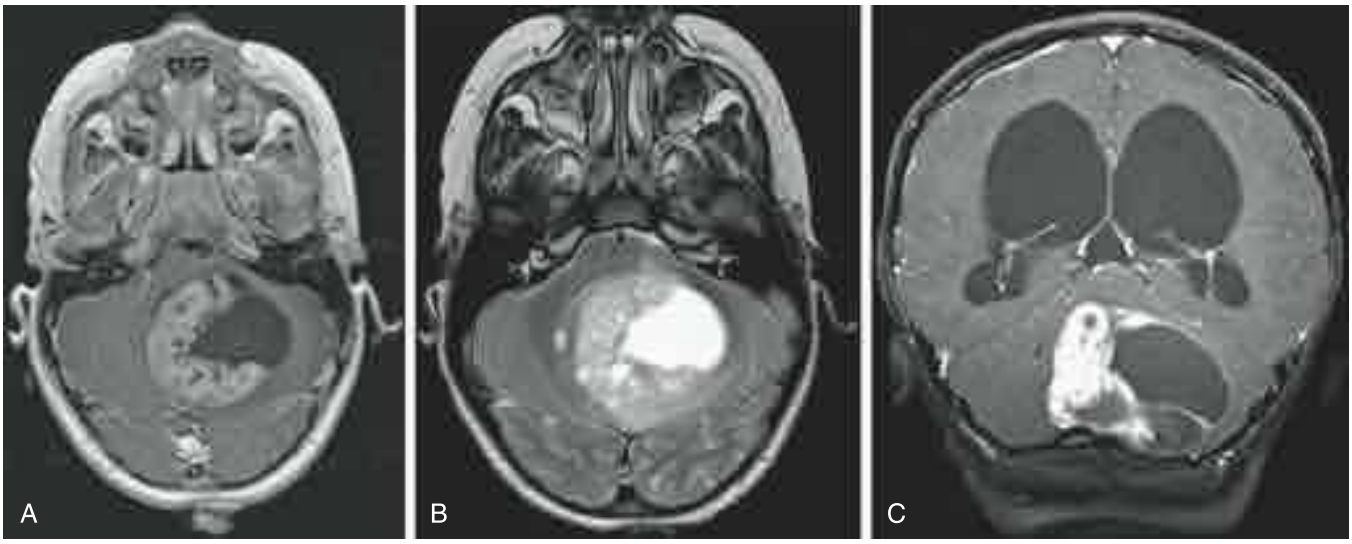

■ **FIGURE 5-25** Pilocytic astrocytoma. **A,** Axial T1W gadolinium-enhanced MR image. There is a heterogeneous C-shaped mass in the fourth ventricle. The right lateral wall enhances with a thick rim. However, the left margin does not. **B,** The axial T2W image shows the macroscopic fluid on the patient's left and heterogeneity from smaller fluid pockets within the mural mass. A fluid-secreting mass in the cerebellum is a classic indicator of a pilocytic astrocytoma in a child but would suggest a hemangioblastoma in an adult patient. **C,** Coronal gadolinium-enhanced T1W MR image shows intense thick enhancement of the right rim, but the left margin shows only very thin linear enhancement. The thin rim of enhancement was not neoplastic tissue; rather, it was reactive astrogliosis and that is why it showed only delayed enhancement on the coronal images.

ized by lesions separated in space and time, and the diagnosis (by the McDonald criteria) may now include imaging as well as clinical findings. Pathologically, the classic lesions of multiple sclerosis begin as a perivenular inflammatory reaction—"Dawson's fingers"—that produce a characteristic pattern of elongated lesions that are adjacent and perpendicular to the lateral ventricular margin. These are bright on T2W and FLAIR images because the normal myelin lipid has been destroyed and replaced by inflammation with macrophages and increased water. Contrast enhancement occurs in "active" demyelination and may be modulated by corticosteroids and other therapies. It may or may not be associated with correlating neurologic findings. Most active plaques will enhance for 2 to 6 weeks and only rarely longer.[40] Although we commonly think that the cause of the enhancement in demyelination is inflammation, it may be that the breakdown of the blood-brain barrier is a actually a necessary requirement and precursor for the self-destructive immune reaction that causes demyelination.

Classic demyelination does not cause angiogenesis nor necrosis. The blood-brain barrier changes are not associated with increased perfusion so that, unlike neoplasms and infection, the plaques usually do not show vasogenic edema beyond the rim of enhancement. The enhancing rim about an active zone may be discontinuous or "incomplete"[27,41] (Fig. 5-26), which may allow differentiation from necrotic neoplasm (which has a thick rim) or an abscess, both of which have surrounding vasogenic edema. Masdeu and associates[41] reported that an "open ring sign" is less common in abscess and neoplasm and may indicate demyelination. An "incomplete ring" or "open ring" may produce a "tumefactive demyelinating lesion" pattern[41] in multiple sclerosis, as well as other leukoencephalopathies, such as acute disseminated encephalomyelitis. The diagnosis of multiple sclerosis may be bolstered when MRI also demonstrates lesions in the spinal cord and/or optic nerve.[42]

Acute disseminated encephalomyelitis typically presents in children and younger patients (often < 13 years of age) within days of an immunologic event (infection or vaccination). The disease is monophasic with larger lesions that are more round and may be juxtacortical. There may be multiple ring-enhancing lesions with minimal mass effect and usually without spreading vasogenic edema. Once again, imaging the spinal cord may help narrow the differential diagnosis.

Periventricular Enhancement: Infection and Neoplasm

Periventricular enhancement may occur with inflammatory white matter disease, as described earlier. But, there may be true infection of the ventricle (ventriculitis) or its lining (ependymitis). Ependymitis may be caused by cytomegalovirus, a member of the herpesvirus family (herpesvirus type 5). Cytomegaloviral ependymitis often produces a thin (<2 mm, more often 1 mm) continuous linear enhancement of the ventricular lining on CT and MRI (Figs. 5-27 and 5-28). On coronal images, this will appear as thin linear enhancement along the ventricular (inferior) surface of the corpus callosum. Cytomegaloviral ependymitis is seen most often in immunocompromised patients, especially those with human immunodeficiency virus infection (see Fig. 5-28). Patients with infected ventricular diversion (shunt catheters) may also develop ventriculitis or meningitis. Some patients will also have a choroid plexitis, and a parenchymal abscess may "point" and drain into the ventricle, causing pyocephalus.

Primary glial neoplasms, usually astrocytoma grade 4 (glioblastoma), often infiltrate the corpus callosum, producing periventricular enhancement. However, they can also spread in the subependymal space or seed the ventricle directly from the surrounding white matter. Primary CNS lymphoma is also likely to both infiltrate the periventricular white matter and seed the ventricle. Almost all primary CNS lymphomas are malignant B-cell lymphomas. Previously a rare tumor, called "reticulum cell sarcoma" in the older literature, this lesion has become very common because of immune suppression for transplantation, treatment of immune-mediated diseases, and human immunodeficiency virus infection and acquired immunodeficiency syndrome. Periventricular CNS lymphomas may be multifocal or present as a lumpy periventricular mass, often with only mild to moderate surrounding cerebral edema. Because they are highly cellular "small round blue cell tumors," they usually have a characteristically "woolly" or "fluffy" high attenuation on

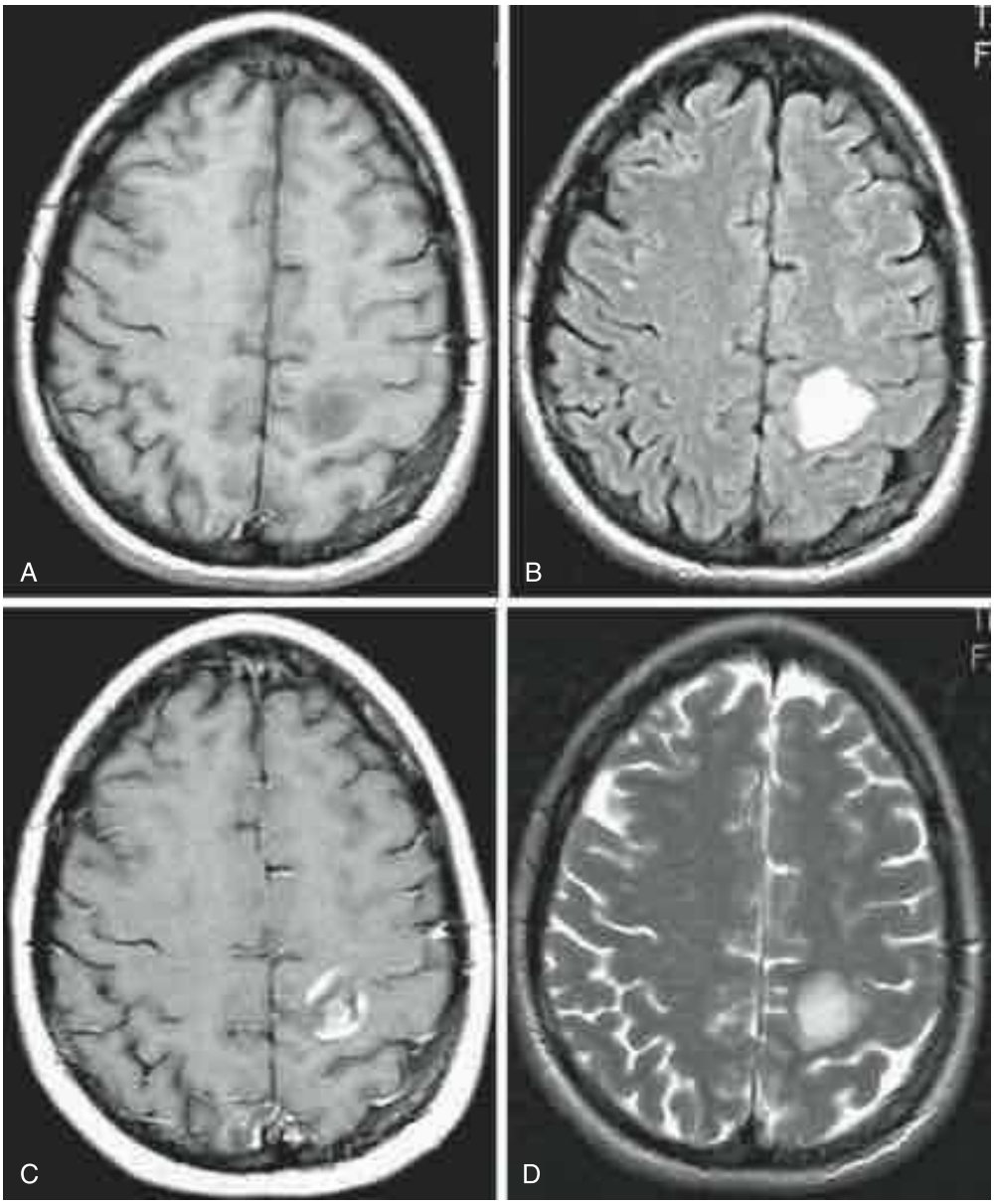

■ **FIGURE 5-26** Tumefactive demyelination. Axial MR images: noncontrast T1W (**A**), T2W FLAIR (**B**), T1W gadolinium-enhanced (**C**), and T2W (**D**). The enhancement is both discontinuous ("open ring") as well internal. Most significantly, the enhancing rim is at the exact margin of the lesion's signal abnormality, that is, there is no perilesional white matter change. There is no vasogenic edema to suggest an abscess or a neoplasm.

noncontrast CT. There is correspondingly low signal on FLAIR and T2W images, which contrasts to the high signal of perilesional vasogenic edema (Fig. 5-29). Periventricular CNS lymphomas may have restricted diffusion with low signal on ADC map images. They almost invariably enhance, unless pretreated with corticosteroids or radiation. This periventricular pattern of enhancement is typical but not pathognomonic of the disease, with most cases of primary CNS lymphoma involving the corpus callosum, periventricular white matter, thalamus, or basal ganglia. Overall, the most common causes of tumefactive lesions of the corpus callosum are tumors with infiltrating cells: primary CNS lymphoma or astrocytomas.[33,43] Unlike primary CNS lymphoma, secondary CNS lymphoma is usually extra-axial, commonly affecting the dura and subarachnoid space.[43,44]

KEY POINTS

- Contrast enhancement may indicate increased blood volume and/or increased blood flow.
- Increased volume/flow can be physiologic (e.g., "luxury perfusion"), neoplastic (e.g., glioblastoma, metastasis), or reactive (abscess).
- Contrast enhancement may reflect altered permeability (i.e., blood-brain barrier breakdown).
- Altered permeability can be neoplastic (e.g., glioblastoma, metastasis) or inflammatory (e.g., infection, demyelination).
- Patterns of enhancement and surrounding edema may limit the differential diagnosis.

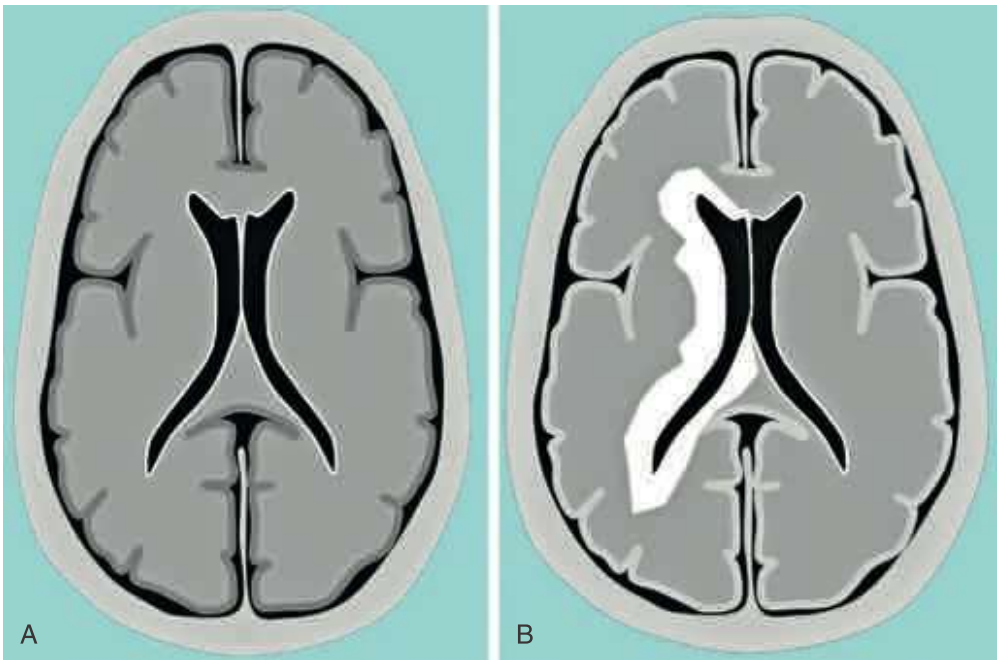

■ **FIGURE 5-27** Schematic periventricular enhancement. **A,** Ependymitis (e.g., from cytomegalovirus infection) usually produces only a very thin linear rim of enhancement. **B,** In contrast, periventricular lymphoma (usually primary B cell lymphoma) most often forms a mass or a thick irregular rind about the ventricle.

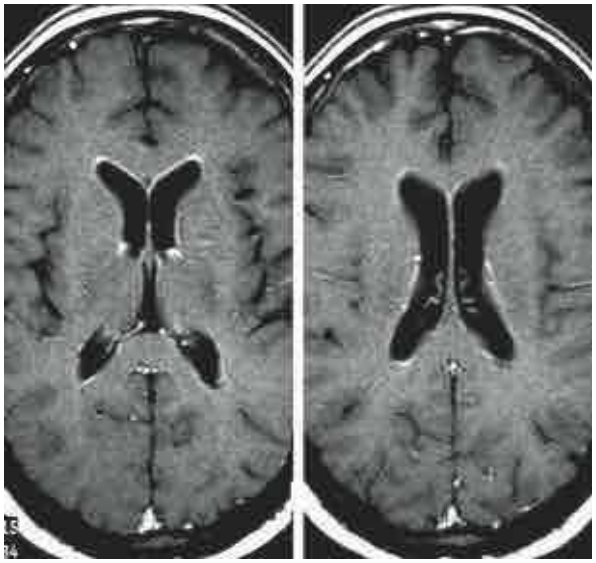

■ **FIGURE 5-28** Thin periventricular enhancement in cytomegaloviral ependymitis. Two axial gadolinium-enhanced T1W MR images show abnormal enhancement completely surrounding both lateral ventricles. The enhancement is thin and very uniform. Cytomegalovirus causes an inflammation of the ventricular lining and produces ependymitis. *(Courtesy of Vince Mathews, MD, University of Indiana, Indianapolis, IN; from Smirniotopoulos JG, Murphy FM, Rushing EJ, et al. Patterns of contrast enhancement in the brain and meninges. RadioGraphics 2007; 27:525-551.)*

■ **FIGURE 5-29** Primary CNS lymphoma. Axial T2W (*left*) and T1W gadolinium-enhanced (*right*) MR images. The lesion is expansile and involves the corpus callosum. In this location, infiltrating gliomas (astrocytomas) and primary CNS lymphoma are the most common lesions. The low signal intensity on the T2W image (*left*) is highly consistent and also suggestive of lymphoma.